



UNIVERSIDADE DA CORUÑA

**Efficient and accurate methods for
computational simulation of netting
structures with mesh resistance
to opening**

Amelia de la Prada Arquer

DOCTORAL THESIS

Advisor: Manuel González Castro

Programa Oficial de Doctorado en Ingeniería Industrial

Ferrol, July 2014

A mi familia:

Florian, Amelia y Manuel

To my family:

Florian, Amelia y Manuel

Aknowledgements

This Ph.D. thesis has been conducted at the Mechanical Engineering Laboratory of University of A Coruña, headed by Prof. Javier Cuadrado. This research was motivated by the project *PSE-REDES, Subproject 3, Simulation, experimentation and design of fishing gears*, supported by the Spanish Ministry of Science and Innovation.

First, I wish to express my special gratitude to Prof. Manuel González, my advisor, for his excellent advice, dedication, patience, and the passion for research and well-finished work he has transmitted to me. Also, I would like to thank to Prof. Javier Cuadrado, for giving me such a great opportunity.

I would like to thank my colleagues at the Mechanical Engineering Laboratory: Alberto, Daniel, David, Emilio, Florian, Fran, Miguel, Roland and Urbano. For the fabulous work environment they have provided, their useful advice and the enjoyable hours we have spent together.

During my doctorate, I have made a stay at the IFREMER at Brest, under the supervision of Daniel Priour. I am grateful for his kindness and the very interesting and productive conversations that helped me to better understand the fishing nets' behaviour. Also, many thanks to his research team for welcoming me so warmly.

Finally, I owe my heartfelt thanks to my close people: to my parents, for supporting me despite the distance that separates us; and last but no least to my husband, Florian, for his love and support, which always encourage me to give the best of myself.

Agradecimientos

Esta tesis doctoral ha sido realizada en el Laboratorio de Ingeniería Mecánica de la Universidad de A Coruña, dirigido por el profesor Javier Cuadrado. Esta investigación fue motivada por el proyecto *PSE-REDES, Subproyecto 3, Simulación, experimentación and rediseño de artes y dispositivos de pesca*, financiado por el Ministerio de Ciencia e Innovación de España.

En primer lugar, me gustaría dar las gracias al profesor Manuel González, mi director de tesis, por sus excelentes consejos, dedicación, paciencia y la pasión por la investigación y el trabajo bien hecho que ha sabido trasmitirme. También agradecer al profesor Javier Cuadrado, por haberme brindado esta gran oportunidad.

Quiero dar las gracias a mis compañeros del Laboratorio de Ingeniería Mecánica: Alberto, Daniel, David, Emilio, Florian, Fran, Miguel, Roland and Urbano, por el fabuloso ambiente de trabajo, sus utilísimos consejos y las agradables horas que hemos pasado juntos.

Durante mi doctorado he realizado una estancia en el IFREMER en Brest, bajo la supervisión de Daniel Priour. Le estoy muy agradecida por su amabilidad y las interesantes conversaciones que me ayudaron a entender mejor el comportamiento de las redes de pesca. Me gustaría agradecer también a su equipo de investigación, por haberme proporcionado una acogida tan cálida.

Finalmente, me gustaría dar las gracias a aquellas personas que siempre han estado a mi lado, a mis padres, por su cariño y apoyo a pesar de la distancia que nos separa y, por último, a mi esposo Florian, por su amor y apoyo que siempre me impulsan a dar lo mejor de mí.

Abstract

Current research in computational simulation of fishing gears focuses on efficient numerical models that accurately predict the behaviour of the netting structure. This thesis is collection of four papers related to the development of a new model that includes the mesh resistance to opening.

Firstly, several nonlinear stiffness models of a net twine are developed. The net twine is modelled as a double-clamped beam and its force-displacement response is calculated by finite element analysis and approximated with three different models. The proposed models overcome the drawbacks of previous models. The twine model is based on the bending stiffness and other geometrical properties of the netting material, so, a procedure to quantify them is presented. Although the methodology is similar to the previous studies, several original contributions are introduced, like a simpler experimental set-up. This procedure is also used to validate the presented twine models with experimental data.

Regarding the simulation, the performance of a fishing gear is mainly determined by its equilibrium shape. In this thesis, the robustness and efficiency of gradient-based energy minimization methods and Newton iteration are compared by applying them to a set of benchmark problems.

Finally, a lumped mass formulation for netting structures is developed. The lumped mass formulation is widely used to model netting structures, but in this thesis the linear springs that traditionally connect the nodes are replaced by the developed twine model. Besides, the knots are modeled as spheres instead of point masses. Although the expressions of the presented model are more complex than those of the spring model, it has been demonstrated that both models have a similar computational overhead. To validate the model, a netting panel is simulated and compared with experimental results.

Resumen

La investigación actual en simulación computacional de artes de pesca se centra en modelos numéricos eficientes capaces de predecir con precisión el comportamiento del material de la red. Esta tesis es un compendio de artículos relativos al desarrollo de un nuevo modelo que incluye la resistencia a la apertura.

En primer lugar, se desarrollan varios modelos de rigidez no lineal para un hilo de red. El hilo es modelado como una viga biempotrada y su respuesta fuerza-desplazamiento es calculada mediante análisis por elementos finitos y aproximada por tres modelos diferentes. Se obtienen diferentes variantes en función de la expresión utilizada para aproximar dicha respuesta. El modelo propuesto supera las desventajas de los modelos previos. El modelo está basado en la rigidez a flexión, por tanto, se presenta también un procedimiento para cuantificarla. Aunque la metodología es similar a la de estudios previos, en esta tesis se aportan nuevas contribuciones, como un montaje experimental más simple.

En cuanto a la simulación, el funcionamiento de un arte de pesca viene determinado principalmente por su posición de equilibrio. En esta tesis se comparan la robustez y eficiencia de los métodos de minimización de energía basados en el gradiente y del método de Newton-Raphson, aplicándolos a un conjunto de problemas representativos.

Finalmente, se desarrolla una formulación basada en masas suspendidas para modelar la red. La formulación de masas suspendidas es ampliamente utilizada para modelar la red, pero en esta tesis los muelles que tradicionalmente conectan los nodos son remplazados por el modelo de hilo propuesto. Además, los nudos de la red son modelados como esferas en lugar de masas puntuales. Aunque las expresiones del modelo propuesto son más complejas que las de los muelles, se demuestra que ambos modelos tienen un coste computacional similar. Para validar el modelo, un paño de red es simulado y comparado con resultados experimentales.

Resumo

A investigación actual en simulación computacional de redes de pesca céntrase en modelos numéricos eficientes, capaces de prever con precisión o comportamento da estrutura da rede. Esta tese é un compendio de artigos sobre o desenvolvemento dun novo modelo que inclúe a resistencia á abertura.

En primeiro lugar, desenvólvense varios modelos de rixidez non lineal para fíos de redes. O fío é modelado como unha viga biempotrada e a súa resposta de forza-desprazamento foi calculada mediante análise de elementos finitos e aproximada mediante diferentes modelos. O modelo proposto supera as desvantaxes dos modelos anteriores. O modelo baséase na rixidez a flexión, e polo tanto, tamén se presenta un novo método para cuantificala. Aínda que a metodoloxía é semellante á de estudos anteriores, o novo método ten importantes vantaxas, como por exemplo unha configuración experimental máis simple.

Con respecto á simulación, compárase a robustez e eficiencia de dúas familias de métodos para calcular a posición de equilibrio: métodos de minimización baseados no gradiente e método de Newton-Raphson, aplicándose a un conxunto de problemas representativos.

Por último, desenvólvese unha nova formulación de masas suspendidas para estruturas de rede. A formulación de masa suspendida é amplamente utilizada para modelar a rede, pero nesta tese os resortes que tradicionalmente conectando os nodos son reemplazados polo modelo desenvolvido nesta tese. Ademais, os nós da rede son modelados como esferas, en vez de masas puntuais. Aínda que as ecuacións do modelo proposto son máis complexas do que as resortes, móstrase que ambos modelos posúen un custo computacional similar. Para validar o modelo, un pano de rede é simulado e comparado cos resultados experimentais.

Resumen extendido

Motivación

La conservación de los recursos marinos es fundamental para suministrar alimentos a la población mundial y garantizar la sostenibilidad del sector pesquero como un medio de vida. La FAO (Food and Agriculture Organization of the United Nations) estima que unos 3 mil millones de personas dependen del pescado como su principal fuente de proteína animal (FAO, 2012). Sin embargo, la contaminación, la sobreexplotación y la destrucción de los hábitats marinos están amenazando el futuro de este sector. Por ello, la Unión Europea está haciendo grandes esfuerzos políticos para garantizar su continuidad.

Una de las estrategias a seguir es mejorar el diseño de artes de pesca para reducir su impacto medioambiental e incrementar su eficiencia energética. Estos objetivos están directamente relacionados con la forma que toma la red ante un flujo de corriente, esto es, su comportamiento estructural e hidrodinámico (Suuronen, 2005). Dicho comportamiento depende de muchos factores: la geometría de la red (forma, tamaño y configuración de las mallas, presencia de elementos rígidos y flexibles, cables, etc.), condiciones de trabajo (velocidad de arrastre, tipo de suelo marino, olas, condiciones climáticas, etc.) y peso y volumen de la captura. Entender y predecir la influencia de estos factores es crítico para mejorar los nuevos diseños.

El método tradicional para comprobar el funcionamiento de un arte de pesca consiste en campañas experimentales, que son enormemente costosas y lentas. Como alternativa más barata, se utilizan los ensayos en canal hidrodinámico, aun así, estos ensayos siguen siendo lentos y caros porque, además del coste de alquiler de las instalaciones, los ensayos se realizan con prototipos escalados del arte. Además, no permiten reproducir las condiciones de trabajo reales (olas, corrientes variables, suelo marino, etc.). Los inconvenientes de estos ensayos han impulsado el desarrollo de modelos numéricos para predecir la forma del arte, no obstante, la validación de éstos modelos con ensayos experimentales es siempre necesaria.

La presente tesis doctoral es un compendio de cuatro artículos enfocados al modelado y simulación de redes, con el objetivo de desarrollar un modelo numérico robusto y eficiente computacionalmente, capaz de predecir con exactitud el comportamiento real de la red, pudiendo resolver algunos de los inconvenientes de los modelos previos.

Resistencia a la apertura de mallas

En un paño de red, el hilo se anuda formando un conjunto de mallas, cuya configuración puede ser tipo diamante (la más común), hexagonal o cuadrada. Uno de los rasgos más relevantes de las mallas es la resistencia a la apertura, puesto que ésta es crucial para alcanzar uno de los objetivos relativos a reducir el impacto medioambiental de un arte de pesca, la selectividad.

La selectividad se define como la capacidad para capturar especies objetivo y dejar a las otras escapar. Se ha demostrado que la selectividad depende principalmente de la resistencia a la apertura debido a que ésta limita la apertura de las mallas en el copo, impidiendo que los peces de talla pequeña escapen (Herrmann, B., 2006; Sala, A., 2007b). La mayoría de los modelos numéricos para redes ignoran la resistencia a la apertura porque asumen que los hilos son completamente flexibles y flectan sin resistencia. Sin embargo, en los últimos años crece la tendencia a utilizar hilos más gruesos y fuertes en la fabricación de copos de red ya que así aumenta su durabilidad, afectando negativamente a la selectividad al incrementar la resistencia a la apertura de las mallas. Por lo tanto, la incorporación de la resistencia a la apertura a los modelos numéricos es esencial para poder predecir con precisión el comportamiento de la red.

En mallas tipo diamante, la resistencia a la apertura se caracteriza por la rigidez a flexión EI del hilo (Herrmann, B., 2006; O'Neill, 2004). Entonces, el principal reto es el desarrollo de un modelo de resistencia a la apertura que esté basado en esta propiedad. La investigación más relevante sobre rigidez a flexión ha sido desarrollada por O'Neill (2002); él describió las ecuaciones que gobiernan la flexión en un hilo basándose en la teoría de vigas, encontrando dos soluciones analíticas para ellas (una solución exacta y una solución asintótica aproximada). Aunque estas soluciones analíticas son muy apropiadas para describir la flexión en el

hilo (O'Neill and Priour, 2009; Sala et al., 2007a), presentan dos inconvenientes importantes a la hora de aplicarlas a la simulación numérica de redes: su alto coste computacional y que no tienen en cuenta los esfuerzos axiales, al considerar el hilo inextensible.

Puesto que los modelos presentados dependen de la rigidez a flexión, la medida de esta propiedad mecánica es indispensable. La investigación más relevante ha sido desarrollada por Sala (2007a), pero ésta requiere un instrumento de medida especialmente diseñado para medir deformaciones en un paño de red, que no está disponible en el mercado. Además, los autores remarcaron la falta de ajuste entre los datos experimentales y el modelo numérico (utilizaron la solución asintótica de O'Neill (2002)).

Por lo tanto, los objetivos de la presente tesis, en cuanto a la resistencia a la apertura son:

- 1) Desarrollar un modelo de hilo que supere las desventajas explicadas anteriormente. El modelo debe representar de forma correcta el comportamiento a flexión de un hilo, y ser robusto y eficiente desde el punto de vista computacional, puesto que va orientado a la simulación de artes de pesca reales, que pueden estar formados por un gran número de variables.
- 2) Desarrollar un montaje experimental que permita analizar datos para estimar la resistencia a la apertura de forma más simple y precisa que el método propuesto por Sala et al. (2007a).

Los artículos asociados a esta investigación son los artículos No.1 y No. 2:

El artículo No.1 comprende el primer objetivo de esta tesis. En él, se presenta un nuevo modelo de hilo a flexión, el cual trata de resolver los inconvenientes de los modelos desarrollados por O'Neill (2002). El segundo artículo corresponde al segundo objetivo, donde se describe un procedimiento experimental para medir la rigidez a flexión y otros parámetros geométricos para diferentes materiales de red.

Equilibrio estático de redes

En lo que respecta a la simulación, en la mayoría de aplicaciones marítimas, el funcionamiento de un arte de pesca viene determinado, principalmente por su posición de equilibrio bajo condiciones estáticas o quasi-estáticas, esto es, su posición de equilibrio sometido a una corriente de agua constante (Priour, 1999; Priour et al., 2009; O'Neill and Priour, 2009). Se trata de resolver el sistema de ecuaciones formado por todas las fuerzas que actúan en el arte de pesca, por ejemplo, las fuerzas elásticas, derivadas de los modelos de la red (como los descritos anteriormente) y cables, las fuerzas hidrodinámicas, contacto con el fondo marino, peso y flotación, etc. Algunas de estas fuerzas introducen ecuaciones altamente no lineales en el sistema, esto hace la aplicación de algoritmos iterativos necesaria para resolver el problema.

Uno de los métodos más comunes para resolver sistemas de ecuaciones no lineales es el método de Newton-Raphson, aunque ha sido ya utilizado con éxito, presenta dos desventajas principales: la primera es la dificultad de implementación del método, puesto que requiere la matriz Jacobiana de las fuerzas descritas anteriormente; la segunda es que la matriz Jacobiana puede presentar problemas de mal condicionamiento a lo largo de las iteraciones. Como alternativa al método de Newton-Raphson, en esta tesis se propone el uso de métodos de minimización de energía basados en el gradiente.

En cuanto a la implementación del modelo, es necesaria una formulación basada en el modelo de hilo mencionado anteriormente. Una de las formulaciones más utilizadas es la formulación basada en masas suspendidas (Bessoneau, J.S. and Marichal, D. 1998; Le Dret et al. 2004; Lee et al., 2005; Li et al., 2006; Takagi et al., 2004; Theret, F., 1993), ésta consiste en una serie de masas puntuales (que representan los nudos de la red) interconectadas por muelles lineales (que representan los hilos). Las formulaciones de masas suspendidas desarrolladas hasta ahora presentan dos inconvenientes principales: (i) la aproximación de los hilos como muelles lineales y (ii) no tienen en cuenta el tamaño de los nudos de red. Además, como los muelles no representan el comportamiento real del muelle, se suelen añadir nudos intermedios para mejorar la precisión del modelo, lo cual incrementa el coste computacional.

Por tanto, los objetivos de la tesis son:

- 3) Encontrar el método más apropiado para resolver la posición de equilibrio de la red con el objetivo de solventar las desventajas del método de Newton-Raphson.
- 4) Desarrollar un modelo de red basado en la formulación de masas suspendidas y el modelo de hilo del artículo No. 1, teniendo en cuenta el tamaño de los nudos. El modelo debe ser validado comparando los resultados numéricos con datos experimentales.

Los artículos de esta tesis relacionados con estos objetivos son los artículos No. 3 y No. 4:

Aunque encontrar el método más apropiado para simular la red (el tercer objetivo de esta tesis) es una tarea intermedia para simular el modelo propuesto, el artículo No. 3 consiste en un estudio detallado sobre éste objetivo. Es un análisis de la robustez y la eficiencia computacional de dos familias de métodos: el método de Newton-Raphson (NR) y métodos de minimización de energía basados en el gradiente, con el objetivo de analizar sus ventajas e inconvenientes y cómo les afectan distintas características de la red.

El artículo No. 4 comprende el cuarto objetivo, usando los artículos mencionados anteriormente para alcanzarlo: el modelo de hilo del artículo No. 1 es incorporado a la formulación de masas suspendidas. Para encontrar su posición de equilibrio, se utiliza el método basado en el gradiente propuesto en el artículo No. 3. Finalmente, se utiliza el experimento presentado en el artículo No. 2 para validar el modelo.

Resultados

Los modelos de hilo propuestos (modelo de ajuste polinómico de las fuerzas, y modelo de ajuste por splines de la energía potencial del artículo No.1) cumplen con éxito los objetivos planteados. Los modelos coinciden con la solución obtenida mediante análisis por elementos de una viga a flexión en el artículo No. 1. Aunque los modelos no son igualmente precisos, los errores relativos a la solución de referencia son aceptables, ajustándose perfectamente a los resultados experimentales,

tanto en la validación experimental del modelo en el artículo No. 1 como en las estimaciones de la rigidez a flexión en el artículo No. 2, con un coeficiente de determinación comprendido entre 0.97 y 0.99 para todas las muestras de paños de red ensayadas.

Además, se han implementado también las soluciones asintótica y exacta desarrolladas por O'Neill (2002), para compararlas con los modelos propuestos. Sus diferencias pueden apreciarse en el test del artículo No. 1 mencionado anteriormente. La solución exacta coincide con la referencia hasta que la deformación vertical es muy alta, lo mismo ocurre con la solución asintótica la explicación para este fenómeno es que O'Neill no tuvo en cuenta la deformación axial. Además, la solución asintótica presenta diferencias más pronunciadas respecto a la solución de elementos finitos. Estas diferencias tienen un impacto negativo en el ajuste con los datos experimentales; el peor ajuste en el artículo No. 1 se corresponde con el de la solución asintótica y en el artículo No. 2 generó problemas en la estimación de parámetros, coincidiendo con las observaciones de Sala et al. (2007a). Por el contrario, la solución exacta generó ajustes muy precisos en ambos artículos. La solución exacta representa con éxito el comportamiento del hilo, sin embargo, lo hace bajo un alto coste computacional y una difícil implementación. Los nuevos modelos propuestos son una alternativa a la solución exacta, puesto que sus ecuaciones son mucho más simples y eficientes pero la calidad del ajuste con los datos experimentales es muy similar.

En cuanto al montaje experimental, en este trabajo se propone una alternativa más simple que el utilizado por Sala et al. (2007a). Aunque el montaje se describe en detalle en el artículo No. 2, los resultados experimentales se utilizan en más artículos con diferentes propósitos: en el artículo No.1 se utilizan para validar el modelo de hilo, y en el artículo No. 4 para validar el modelo de red, particularizado para las dimensiones de la muestra de red.

El procedimiento propuesto en el artículo No. 2 proporciona estimaciones para la rigidez a flexión y otros parámetros geométricos a partir de datos experimentales. Se han analizado dos modelos de hilo desarrollados en (O'Neill, 2002) y otros dos modelos de hilo ya estudiados en el artículo No. 1 combinados con cuatro estrategias diferentes de restricción de parámetros. Se ha demostrado que el

método propuesto es una forma simple y eficiente para estimar la resistencia a la apertura de redes. No obstante, hay que tener en cuenta que las estimaciones no son valores reales absolutos de las propiedades de la red, sino parámetros de calibración de los diferentes modelos. Por tanto, el modelo utilizado para estimar los parámetros debe ser el mismo que el que se aplicará para predecir el comportamiento de la red.

Sin embargo, este método presenta algunas objeciones que requieren investigaciones futuras: en primer lugar, este método no permite estimar la altura del nodo; segundo, no tiene en cuenta la flexión fuera del plano de la red, la cual puede influir en la resistencia a la apertura. Además, en el artículo No. 2, se ha demostrado que la resistencia a la apertura es diferente en los ciclos de carga y descarga, probablemente causada por deformaciones plásticas en el material debido a que estuvo expuesto a altas tensiones durante largo tiempo. Estos resultados sugieren que son necesarias investigaciones futuras para analizar cómo el historial de carga afecta a la resistencia a la apertura durante el uso de los artes de pesca.

En lo que respecta al análisis de métodos para la simulación de redes, los resultados muestran que el método de minimización de energía basado en el gradiente más adecuado es el método de memoria limitada BFGS (LBFGS). Por otro lado, la mejor variante de la familia de NR es el método NR de paso limitado (propuesto por los autores). Ambos métodos tienen sus ventajas e inconvenientes y el uso de uno u otro viene indicado por la situación. Por un lado LBFGS es más robusto y eficiente en problemas donde la posición inicial está lejos de la solución, por ejemplo, cuando ésta es muy difícil de estimar, como en redes compuestas por paneles diferentes. Por otro lado NR es más rápido cuando la posición inicial está muy cerca de la posición de equilibrio, por ejemplo, cuando las condiciones de simulación son levemente modificadas respecto a la situación anterior, como en las aplicaciones de optimización automática de la topología de la red (Khaled et al., 2012; Priour, 2009). De hecho, ambos métodos pueden incluso combinarse, utilizando LBFGS en las primeras iteraciones para acercar la posición inicial al equilibrio y después aplicar NR para aumentar la precisión de los resultados. En cuanto a la implementación de los métodos, LBFGS es mucho más fácil de implementar, puesto que no requiere la matriz Jacobiana.

En el artículo No. 4, el método LBFGS es utilizado para calcular la posición de equilibrio de una red modelada con una formulación que incluye la resistencia a la apertura. El modelo propuesto se basa en la formulación de masas suspendidas, pero los muelles lineales que tradicionalmente conectan los nodos son reemplazados por el modelo de hilo de ajuste polinómico de la fuerza descrito en el artículo No. 1. Además, los nodos de la red son aproximados como esferas en lugar de masas puntuales. Para validar el modelo, los datos experimentales del artículo No. 2 son analizados con el modelo propuesto como función modelo en la regresión, particularizado para el paño de red utilizado en los experimentos. La bondad del ajuste confirma que el modelo es capaz de predecir la resistencia a la apertura. Dado que el modelo de hilo ya ha sido validado en el artículo No. 1, en este caso los sujetos de validación son: la aproximación de la geometría del paño de red mediante la formulación de masas suspendidas y la hipótesis de nodos esféricos. En cuanto a la eficiencia computacional, aunque pueda parecer que la incorporación del modelo de hilo a la red incrementa su coste computacional porque requiere la evaluación de raíces y funciones trigonométricas, se ha demostrado lo contrario. Un experimento numérico se ha llevado a cabo para comparar su eficiencia computacional con el modelo tradicional de masas suspendidas, los resultados muestran que aunque el tiempo por evaluación de función por nodo del modelo propuesto es más alto, no es necesario incluir los nodos intermedios del modelo tradicional, resultando en un coste computacional total similar.

Conclusiones

Esta tesis aspira a desarrollar nuevos modelos de hilo eficientes y precisos para simulación numérica de redes, incluyendo la resistencia a la apertura. Los modelos propuestos alcanzan con éxito los objetivos planteados en esta tesis.

- 1) Los modelos de hilo propuestos están basados en la aproximación de la respuesta obtenida mediante análisis por elementos finitos de una viga a flexión. Trabajos experimentales confirman que los modelos propuestos son muy precisos. Además son más eficientes que los modelos previos puesto que expresan las fuerzas del hilo como función explícita de su deformación
- 2) El montaje experimental propuesto es más simple y barato que el prototipo construido por Sala et al. (2007a). La combinación de los nuevos modelos de

hilo presentados en el artículo No. 1 con las estrategias de restricción de parámetros resulta en un método simple y preciso para estimar la resistencia a la apertura de mallas.

- 3) De los métodos comprobados en la tesis, los más robustos y eficientes para simular redes han sido LBFGS y Newton-Raphson de paso limitado, pero los resultados demuestran que el método más apropiado depende de la situación. LBFGS es más robusto y eficiente cuando la posición inicial está lejos del equilibrio. Por el contrario, Newton-Raphson es más rápido cuando la posición inicial está cerca de la posición de equilibrio. Además LBFGS es mucho más sencillo de implementar.
- 4) El modelo de hilo propuesto se ha incorporado con éxito a la formulación de masas suspendidas. El modelo es más preciso que los modelos previos puesto que tiene en cuenta la flexión en hilos y el tamaño de los nodos. Además su coste computacional no es superior a los modelos previos.
- 5) Finalmente, el modelo de red se ha validado experimentalmente, ajustando los datos experimentales del artículo No. 2 con el modelo propuesto, particularizado para la muestra de red utilizada en los experimentos. Los resultados confirman que la calidad del ajuste es muy buena.

Content

Introduction	1
1. Background	1
2. Aim and motivation	2
2.1 Mesh resistance to opening	2
2.2 Static equilibrium of netting structures	4
3. Results and discussion	7
3.1 Mesh resistance to opening	7
3.2 Static equilibrium of netting structures	9
4. Conclusions	11
5. References	12

Appendix: publications	15
-------------------------------------	----

Article No. 1

Article No. 2

Article No. 3

Article No. 4

Introduction

1. Background

The preservation of marine resources is mandatory to supply food to the world population and to guarantee the sustainability of the fishing sector as a livelihood. The Food and Agriculture Organization of the United Nations (FAO) estimates that about 3.0 billion people depend on fish as their main source of animal protein (FAO, 2012). However, pollution, overfishing and destruction of marine habitats are threatening the future of this sector; in order to overcome these problems, the European Union is making hard political efforts, promoting research in this topic.

One of the pursued goals is to enhance the design of the fishing gears in order to reduce their environmental impact and increase their energy efficiency. These goals are primarily related with the shape that the netting structure takes under the current flow, that is, its structural and hydrodynamic behaviour (Suuronen, 2005). In any case, the structural and hydrodynamic behavior is dependent on many different factors: the geometry of the netting structure (mesh shape, size and configuration, material properties, flexible and rigid bodies, wires etc...); working conditions (towing speed, composition of the seabed, waves, weather conditions...) and catch fish (weight and volume of the catch). Being able to understand and forecast the influence of these factors is critical to improve the new designs.

The traditional method to check the correct performance of a fishing gear is by experimental campaigns, which are very expensive and time-consuming. Although experimental tests in flume tank are used as a cheaper alternative (Priour et al., 2005; O'Neill et al., 2005; Balash, 2012), they are still costly and time-consuming because, in addition to the cost of renting the tank facilities, scaled prototypes of the gear are necessary. Besides, they do not allow the simulation of real working conditions (fishing operations, composition of the seabed, etc.). The drawbacks of the experimental tests have encouraged the development of numerical

models to predict the shape of the netting structure. Even so, experimental validation of the numerical models is always required.

Up to now, different numerical models for the netting structures have been developed, which can be categorized as: (1) 1D finite element models (Bessoneau and Marichal, 1998; Tsukrov and Eroshkin, 2003; Le Dret et al., 2004), (2) 2D finite element models, (Priour, 1999; Priour, 2003; Nicoll et al., 2011), (3) lumped mass models (Takagi et al., 2004; Lee et al., 2005; Li et al., 2006) and (4) differential equation models for axisymmetric structures (O'Neill, 2002; Priour, 2009). Such models have been successfully applied to solve real-life design and optimization problems.

2. Aim and motivation

This Ph.D. thesis is a compendium of four publications regarding the development and validation of an accurate and efficient model of a netting structure. Subsection 2.1 focuses on the development of a numerical model able to represent the real behaviour of a netting twine. It also addresses experimental methods to measure the mechanical and geometrical properties of netting panels. Subsection 2.2 regards the implementation and simulation of the model.

2.1 Mesh resistance to opening

In a netting panel, the twine is knotted making up a set of meshes, which can be diamond (the predominant type), hexagonal or square shaped. One of the most relevant features of the netting structure is the mesh resistance to opening, since it governs one of the major concerns related to reducing the environmental impact of a fishing gear: the selectivity.

The selectivity is defined as the ability to capture the target species and let the others scape. It has been demonstrated that the selectivity depends primarily on the resistance to opening since it hampers the mesh opening in the cod-end, thereby limiting the escapement of small fish (Herrmann, 2006; Sala, 2007b). Most of the numerical models for netting materials ignore mesh resistance to opening because

they assume that twines are completely flexible and easily bent without resistance. However, in recent years, there is a tendency towards thicker and stronger twines in the manufacture of netting materials for the codend of trawls because it increases the durability of the netting, affecting negatively to the selectivity as the mesh resistance to opening increases. This makes the incorporation of the mesh resistance to opening to the numerical models of the netting materials essential to accurately predict the selective performance of fishing gears by simulation.

In diamond mesh panels, the resistance to opening is mainly characterized by the bending stiffness EI of the twine (Herrmann, B., 2006; O'Neill, 2004). Therefore, the main challenge is the development of a model of the netting structure that takes into account this mechanical property. Theoretical models for the mesh resistance to opening are generally based on the beam theory of solid mechanics. The most comprehensive research about twine bending stiffness has been developed by O'Neill (2002). He described the equations of a bending twine assuming that it can be modeled as a double-clamped beam. He found two analytical solutions for these equations (an exact and an approximated asymptotic solution). These analytical solutions are highly valuable to describe bending stiffness (O'Neill and Priour, 2009; Sala et al., 2007a) but they have two major drawbacks when they are incorporated in numerical simulation of flexible net structures: their high computational cost and they do not take into account axial deformations.

As the previous numerical models are based on the bending stiffness EI , the quantification of this mechanical property is necessary. Unfortunately, despite there are some studies about it in the literature, the research about this topic is still scarce (Sala et al., 2007a; Priour and Cognard, 2011; Balash, 2012). The most relevant research was carried out by Sala et al. (2007a), but it required a specially designed measuring instrument which is not commercially available. Besides, the authors reported a systematic lack of fit between the experimental data and the model (they used the asymptotic solution developed by O'Neill (2002)).

Consequently the objectives of this thesis regarding the modelization of the netting material are the following:

- 1) To develop a twine model able to overcome above-mentioned disadvantages. The model has to accurately represent the behaviour of the bending twine, taking into account also the axial deformations. Besides, it must be computationally robust and efficient since the model aims at being used in simulation of real fishing gear, which can have a large number of variables.
- 2) To design a new experimental set-up and procedure to analyse experimental data to quantify the mesh resistance to opening of netting panels in a simpler and more accurate way than the method proposed by Sala et al. (2007a).

The publications related to this research are:

- **Article No. 1:** de la Prada, A. González M., 2014. Nonlinear stiffness models of a net twine to describe mesh resistance to opening of flexible net structures. *Journal of Engineering for the Maritime Environment*. DOI:10.1177/1475090214530876
- **Article No. 2:** de la Prada, A. González M., 2014. Quantifying mesh resistance to opening of netting panels: experimental method, regression models and parameter estimation strategies. *ICES Journal of Marine Science*. DOI 10.1093/icesjms/fsu125

The first article covers the first objective: a new model for the twine bending is developed, which tries to overcome the disadvantages of O'Neill's models. The second publication addresses the second objective. It develops an experimental procedure to measure the bending stiffness and other geometrical parameters of netting materials.

2.2 Static equilibrium of netting structures

Regarding the simulation, in most marine applications the performance of a fishing gear is mainly determined by its equilibrium shape under static or quasi-static conditions (Priour, 1999; Priour et al., 2009; O'Neill and Priour, 2009). It consists in solving the static equilibrium equations taking into account all the forces that act on the netting structure, for example, the elastic forces from the models of the netting structure (like the twine model developed previously) and wires, the hydrodynamic forces, contact with the seabed, weight and buoyancy, etc. Some of these forces are

defined by high non-linear expressions; hence, iterative methods are required to solve the equations.

One of the most popular methods to solve non-linear systems is the Newton-Raphson (NR) iteration. Although it has been already used in netting applications (Priour, 1999), it presents two main disadvantages: the first one is the difficulty of implementation of the method, as it requires the Jacobian matrix of the forces; the second downside is that the Jacobian matrix is often ill-conditioned during the iterations. As an alternative to the NR method, gradient-based energy minimization methods are proposed in this thesis. The only reference in the literature to the use of them to calculate the equilibrium shape of netting structures can be found in (Le Dret et al., 2004), which briefly mentions the use of the Polak-Ribière version of the nonlinear conjugate gradient method. However that work assesses neither the computational performance nor the robustness of the method in comparison to the NR method. This makes the analysis of gradient-based methods and their comparison with NR methods a subject worthy of investigation.

As far as the modelization of the netting of the fishing gear is concerned, it is necessary a formulation based on the above-mentioned twine model. One of the most used formulations is the spring-based lumped mass formulation (Bessoneau, J.S. and Marichal, D. 1998; Le Dret et al. 2004; Lee et al., 2005; Li et al., 2006; Takagi et al., 2004 ; Theret, F., 1993). It consists on a series of point masses (representing netting knots) that are interconnected with linear springs (representing twines). Existing lumped mass formulations have two main drawbacks: (i) the approximation of the net twines as linear springs and (ii) the knot size is not taken into account. Moreover, as linear springs cannot represent the behaviour of a real twine, intermediate knots are introduced to improve the accuracy of the model, which also increase the computational cost.

The objectives of this part of the thesis are:

- 3) To find the most suitable iterative method to solve the equilibrium shape of netting structures, in order to overcome the drawbacks of the classical Newton-Raphson iteration.

- 4) To develop a model of the netting structure based on the lumped mass formulation and the twine model from Article No.1, taking into account the knot size. The model of the netting structure has to be validated by comparing the results from computational simulation with experimental data.

The publications of this thesis related to this research are:

- **Article No. 3:** de la Prada, A. González M., 2014. Assessing the suitability of gradient-based energy minimization methods to calculate the equilibrium shape of netting structures. *Computers and structures*. DOI: 10.1016/j.compstruc.2014.01.021
- **Article No. 4:** de la Prada, A. González M., 2014. An efficient and accurate model for netting structures with mesh resistance to opening. *International Journal of Solids and Structures*. In review.

Although finding the best simulation method (third objective of this thesis) is an intermediate task to simulate the fishing gear, we have reported a detailed study in Article No. 3. It contains a comprehensive analysis of the robustness and computational performance of numerical methods to find the equilibrium position of netting structures. Two families of methods have been tested: Newton iteration and gradient-based energy minimization methods. In order to get insight on the advantages and disadvantages of each method and identify how they are affected by particular characteristics of the netting structure.

Article No. 4 comprises the objective 4, using the previous articles as tools to accomplish it: the model of the netting structure is based on the twine model presented in Article No. 1, which is used in the lumped mass formulation. To find the equilibrium shape, the gradient-based method proposed in Article No. 3 is applied. Finally, the experimental set-up presented in Article No. 2 is used to validate the model.

3. Results and discussion

This section presents a brief combined discussion of the four articles in this thesis. Please refer to the full publications in the Appendix for further details.

3.1 Mesh resistance to opening

The developed twine models (polynomial fitting of the force and the spline fitting of the potential energy from the Article No. 1) have successfully accomplished the objectives of this thesis. The models match up with the finite element solution for a bending beam in Article No. 1. Although the three models are not equally accurate, the relative errors of all of them are acceptable. This results in excellent fittings with the experimental data in Article No. 1 and also when estimating the bending stiffness in Article No. 2, with high values of the coefficient of determination R^2 , ranging between 0.97 and 0.99 for every tested netting panels.

The exact and the asymptotic solution from (O'Neill, 2002) have been also implemented in order to compare them with the proposed models. Their differences can be noticed in the above-mentioned bending beam test presented in Article No. 1. The exact solution matches with the reference finite element solution until the normal deformation of the mesh is high. The same occurs with the asymptotic solution. The explanation for these results is that the models developed by O'Neill (2002) do not take into account the effect of the axial deformation of the twine. Moreover, the asymptotic solution presents more pronounced differences in comparison with the finite element solution. These differences have a negative impact on the goodness of fit when this model is used to analyse experimental data. The worst fits in Article No. 1 and Article No. 2 were given by the asymptotic solution. Moreover, it caused identifiably problems in Article No. 2, also reported by Sala et al. (2007a). On the contrary, the exact solution provided highly accurate fittings in both articles, which suggests that the axial deformation applied in the experiments was not important enough to have an effect that cannot be predicted by the exact solution (the panels were stretched until the normal mesh opening reached an 80% of the nominal mesh size).

Consequently, the exact solution succeeds in representing the twine behaviour. However, this comes at the cost of a high computational overhead and a very difficult computer implementation due to the complexity of the highly non-linear implicit expressions. This is a very important drawback since, as shown in Article No. 3, most simulation methods (e.g. gradient-based and NR) require evaluating the forces as explicit function of the deformation. When using NR the implementation is even more difficult, because it also needs the Jacobian of the forces. Thus, the proposed models are a good alternative to the exact solution, because they provide similar goodness of fit with experimental data but their equations are much simpler and efficient.

Note that the third twine model presented in Article No. 1, the spring-based model, was developed to make the model able to deal with large axial deformations. However, in Article No. 4 it has been proved that this objective can be also accomplished with the polynomial fitting of the force model (which covers small deformations) combined with a linear spring model (which covers large deformations) using a blending function as a transition between both models.

Regarding the experimental methods to measure the mesh resistance to opening of netting panels, this work proposes in Article No. 2 a simpler alternative method to the method proposed by Sala et al. (2007a). The proposed experimental set-up is also used in other articles for different aims: in Article No. 1 it is used to validate the proposed twine models, while in Article No. 4, it is used to validate the presented lumped mass formulation for netting structures model.

The procedure presented in Article No. 2 managed to provide accurate and plausible estimates of the twine bending stiffness and other geometrical parameters of the netting panel. Two of the twine models described in Article No. 1 and the two models developed in (O'Neill, 2002) were used to analyse experimental data, combined with four different parameter estimation strategies. The method proved to be a simple yet accurate way to quantify the mesh resistance to opening of netting panels. Nevertheless, the parameter estimates depend on the twine model used to analyse the experimental data. Hence, they are not absolute measurements of the netting properties, but rather calibration parameters for different theoretical models

of mesh resistance to opening, as observed by Sala et al. (2007a). Therefore, the model used to estimate the parameters should be the same that will be used to make predictions of the netting behaviour.

This method presents some objections that require further research. Firstly, as the experiment is uniaxial, it does not allow estimating the knot height. Secondly, this method does not take into account the out-of-plane bending in netting panels, which can influence the mesh resistance to opening. Besides, in Article No. 2, it has been demonstrated that the mesh resistance to opening is different in the loading and unloading cycles of the experimental set-up. This is probably caused by plastic deformations in the netting material due to long-term exposure to high stress. This result suggests that further research is required to investigate how the loading history affects the mesh resistance to opening of netting during the lifespan of a fishing gear.

3.2 Static equilibrium of netting structures

The motivation of Article No. 3 is to analyse and compare methods to calculate the equilibrium shape of the netting structure. A set of benchmark problems (10 different cases) is solved to better understand the robustness and computational performance of two families of methods: Newton-Raphson iteration and gradient-based methods. The triangular finite element developed by Priour (1999) is used to model the netting structure.

Results show that the most suitable gradient-based method is the limited memory BFGS method (LBFGS). Also, the best NR method is the NR step limit variant (proposed by the authors). Both methods have their advantages and drawbacks. LBFGS is more robust and efficient in problems where the initial position is very different from the equilibrium position. This is useful to calculate the equilibrium position of trawls made up by many different panels that make difficult to estimate a good initial position. On the other hand, NR is faster when the initial position is close to the equilibrium position. For instance, to calculate the equilibrium position of a problem which is slightly modified with respect to the previous equilibrium situation, like in optimization of netting structures (Khaled et al., 2012; Priour, 2009), where only small changes in panel dimensions are applied. Actually,

both methods can be combined, using LBFGS at first iterations to bring the shape of the netting structure closer to the equilibrium and then apply NR to increase the accuracy of the solution. Regarding the implementation of the methods, LBFGS is considerably easier to implement and allows testing new force models as it does not require the Jacobian of the forces.

In addition to the 10 test cases presented in Article No. 3, the LBFGS and NR methods have been used to calculate the equilibrium position of complete trawls under a uniform current flow. These results have not been included in this thesis.

In Article No. 4, the LBFGS method is used to calculate the equilibrium position of a netting structure modelled with a formulation that includes de mesh resistance to opening. The proposed model is based on the lumped mass formulation, but the linear springs that traditionally connect the nodes are replaced by the polynomial fitting of the force twine model presented in Article No. 1. Besides, the knots are approximated as spheres instead of point masses. To validate the model, the experimental data from Article No. 2 are analysed with the proposed model for the netting structure. The goodness of fit confirms that the proposed model accurately predicts the mesh resistance to opening of netting panels. Note that the twine force model has already been validated in Article No. 1; hence in this case the objective is to validate the approximation of the panel geometry with the lumped mass model and the hypothesis of spherical knots. Regarding the computational efficiency, although it may seem that the proposed model is slower than the classical lumped mass model because it requires the evaluation of root and trigonometric functions, it has been demonstrated otherwise. A numerical experiment has been carried out to compare its computational efficiency with the traditional lumped mass formulation based on linear springs. The results show that, although the time per evaluation of the force model is higher, it avoids the inclusion of intermediate nodes, resulting in a similar computational overhead. The proposed model does not affect to the number of iterations.

Remark that gradient-based methods from Article No. 3 require that the forces are conservative. If it is not the case (like the polynomial fitting model and the spring-based model from Article No. 1), the energy required by the gradient-based

method is approximated, which increases the number of iterations necessary for the convergence. Although it has been proved that this method is still competitive (as shown in Articles No. 3 and No. 4), the spline fitting of the potential energy model presented in Article No. 1 has been specially developed to preserve the condition of conservative forces. This model has already been successfully implemented in the same way as in article No. 4, but the results are not included in this thesis.

4. Conclusions

This thesis aims to develop new efficient and accurate methods for numerical simulation of netting structures with mesh resistance to opening. The models and methods presented in this thesis successfully accomplish the proposed objectives.

The first objective of this thesis was to develop new twine models that are more accurate and more efficient than the models from the literature (Article No. 1). The proposed models are based on the approximation of the response obtained by a finite element analysis of a bending double clamped beam. Experimental work confirms that the proposed models are highly accurate. They are also more efficient than the previous models since they express the twine forces as an explicit function of its deformation.

The second objective was to develop a new experimental method to quantify the mesh resistance to opening of netting panels (Article No. 2). The proposed uniaxial experimental set-up is simpler than the biaxial set-up developed by Sala et al. (2007a). The combination of the new twine models presented in Article No. 1 with suitable estimation strategies results in a method that proved to be a simple yet accurate way to quantify the mesh resistance to opening of netting panels.

The third objective was to investigate methods to calculate the equilibrium position of the netting structure (Article No. 3). Two families of methods have been evaluated: gradient-based energy minimization methods and Newton-Raphson methods. The most robust and efficient methods are the gradient-based LBFGS method and the variant step limit Newton Raphson method. Results show that the most suitable one depends on the application. LBFGS is more robust and faster when

the initial position is far from the equilibrium. On the contrary, Newton-Raphson performs better when it is very close to the equilibrium. LBFGS is considerable simpler to implement.

The fourth objective of this thesis was to develop a new model for netting structures with mesh resistance to opening (Article No. 4). This has been achieved by incorporating the twine model developed in Article No. 1 into a lumped mass formulation. Finally, the model is validated by fitting the experimental data from Article No. 2 with the numerical results obtained by simulation of the proposed model. The goodness of fit confirms that the proposed model accurately predicts the mesh resistance to opening. In addition, it is as efficient as previous models that do not take into account the mesh resistance to opening.

5. References

- Balash, C., 2012. Prawn Trawl Shape Due to Flexural Rigidity and Hydrodynamic Forces. University of Tasmania.
- Bessoneau, J.S., Marichal, D., 1998. Study of the dynamics of submerged supple nets (applications to trawls). *Ocean Engineering* 563–583. doi:10.1016/S0029-8018(97)00035-8
- FAO Fisheries and Aquaculture Department, 2012. The state of world fisheries and aquaculture.
- Herrmann, B., O., FG, 2006. Theoretical study of the influence of twine thickness on haddock selectivity in diamond mesh cod-ends. *Fisheries Research* 80, 221–229. doi:10.1016/j.fishres.2006.04.008
- Khaled, R., Priour, D., Billard, J.-Y., 2012. Numerical optimization of trawl energy efficiency taking into account fish distribution. *Ocean Engineering* 54, 34–45.
- LeDret, H., Lewandowski, R., Priour, D., Chagneau, F., 2004. Numerical simulation of a cod end net part 1: Equilibrium in a uniform flow. *Journal of Elasticity* 76, 139–162.
- Lee, C.-W., Lee, J.-H., Cha, B.-J., Kim, H.-Y., Lee, J.-H., 2005. Physical modeling for underwater flexible systems dynamic simulation. *Ocean Engineering* 32, 331–347.
- Li, Y.-C., Zhao, Y.-P., Gui, F.-K., Teng, B., 2006. Numerical simulation of the hydrodynamic behaviour of submerged plane nets in current. *Ocean Engineering* 33, 2352–2368.
- O’Neill, 2002. Bending of twines and fibres under tension. *Journal of the Textile Institute*. 93, 1–8.
- O’Neill, F.G., 2004. The Influence of Bending Stiffness on the Deformation of Axisymmetric Networks 749–754. doi:10.1115/OMAE2004-51421

- O'Neill, F.G., Priour, D., 2009. Comparison and validation of two models of netting deformation. *Journal of Applied Mechanics, Transactions ASME* 76, 1–7. doi:10.1115/1.3112737
- Petri Suuronen, 2005. Mortality of fish scaping trawl gears. *FAO Fisheries technical paper* 478.
- Priour, D., 1999. Calculation of net shapes by the finite element method with triangular elements. *Communications in Numerical Methods in Engineering* 15, 755–763.
- Priour, D., 2009. Numerical optimisation of trawls design to improve their energy efficiency. *Fisheries Research* 98, 40–50.
- Priour, D., Herrmann, B., O'Neill, F.G., 2009. Modelling axisymmetric cod-ends made of different mesh types. *Proceedings of the Institution of Mechanical Engineers, Part M: Journal of Engineering for the Maritime Environment* 223, 137–144. doi:10.1243/14750902JEME120
- Priour, D., J.-Y, C., 2011. Investigation of Methods for the Assessment of the 472 Flexural Stiffness of Netting Panels. Presented at the Proceedings of the 10th DEMaT 473 Workshop, October 26th-29th. Split.
- Sala, A., O'Neill, F.G., Buglioni, G., Lucchetti, A., Palumbo, V., Fryer, R.J., 2007. Experimental method for quantifying resistance to the opening of netting panels. *ICES Journal of Marine Science* 64, 1573–1578.
- Sala, A., L., A., 2007. The influence of twine thickness on the size selectivity of polyamide codends in a Mediterranean bottom trawl. *Fisheries Research* 192–203. doi:10.1016/j.fishres.2006.09.013
- Takagi, T., Shimizu, T., Suzuki, K., Hiraishi, T., Yamamoto, K., 2004. Validity and layout of “NaLA”: A net configuration and loading analysis system. *Fisheries Research* 66, 235–243.
- Theret, F., 1993. Etude de l'équilibre de surfaces réticulées placées dans le courant uniforme. Application aux chaluts.

Appendix: publications

Article No. 1

Nonlinear stiffness models of a net twine to describe mesh resistance to opening of flexible net structures

Amelia de la Prada, Manuel González

Submitted to the *Journal of Engineering for the Maritime Environment*
on 16th October 2013

Revised version submitted on 15th January 2014

Revised version submitted on 21st February 2014

Accepted for publication on 3rd March 2014

Published online on 9th June 2014

Proceedings of the Institution of Mechanical Engineers, Part M: Journal of Engineering for the Maritime Environment

<http://pim.sagepub.com/>

Nonlinear stiffness models of a net twine to describe mesh resistance to opening of flexible net structures

Amelia de la Prada and Manuel González

Proceedings of the Institution of Mechanical Engineers, Part M: Journal of Engineering for the Maritime Environment

published online 9 June 2014

DOI: 10.1177/1475090214530876

The online version of this article can be found at:

<http://pim.sagepub.com/content/early/2014/05/20/1475090214530876>

Published by:



<http://www.sagepublications.com>

On behalf of:



[Institution of Mechanical Engineers](http://www.institutionofmechanicalengineers.org)

Additional services and information for *Proceedings of the Institution of Mechanical Engineers, Part M: Journal of Engineering for the Maritime Environment* can be found at:

Email Alerts: <http://pim.sagepub.com/cgi/alerts>

Subscriptions: <http://pim.sagepub.com/subscriptions>

Reprints: <http://www.sagepub.com/journalsReprints.nav>


Permissions: <http://www.sagepub.com/journalsPermissions.nav>

Citations: <http://pim.sagepub.com/content/early/2014/05/20/1475090214530876.refs.html>

>> [OnlineFirst Version of Record](#) - Jun 9, 2014

[What is This?](#)

Nonlinear stiffness models of a net twine to describe mesh resistance to opening of flexible net structures

Proc IMechE Part M:
J Engineering for the Maritime Environment
 1–12
 © IMechE 2014
 Reprints and permissions:
sagepub.co.uk/journalsPermissions.nav
 DOI: 10.1177/1475090214530876
pim.sagepub.com


Amelia de la Prada and Manuel González

Abstract

Numerical simulation of marine flexible net structures allows predicting the behavior of fishing gears and aquaculture cages. In recent years, the tendency toward the use of thicker and stronger twines in netting materials has made its resistance to opening a key factor in the performance of such structures. To accurately describe the mesh resistance to opening, a net twine was modeled as a double-clamped beam and its force–displacement response was calculated by finite element analysis. Fitting techniques were used to develop three different dimensionless stiffness models that express elastic forces in the twine as an explicit nonlinear function of its deformation: (1) a polynomial fitting of the force, (2) a spline fitting of the potential energy, and (3) a spring-based model able to deal with large axial deformations. Each model has different characteristics and advantages. Numerical and experimental tests were used to assess and compare them with previous models described in the literature. The results show that the presented models have very good accuracy and high computational efficiency. They will allow introducing accurate simulation of mesh resistance to opening in numerical simulations of marine netting structures without a high impact in the computational performance.

Keywords

Netting, mesh resistance to opening, flexural rigidity, bending stiffness, finite element

Date received: 15 October 2013; accepted: 3 March 2014

Introduction

Flexible net structures are extensively used in marine applications such as fishing and aquaculture. Several numerical models and simulation methods have been specially developed for this kind of marine structures,^{1–9} and they have been successfully applied to real-life design problems.^{10–15}

A major concern in the fishing industry is fishing gear selectivity, which is mainly affected by the size and shape of netting meshes during the fishing operation.¹⁶ In recent years, the tendency toward the use of thicker and stronger twines in the manufacture of fishing netting materials has caused a reduction in the selective performance. This reduction in selectivity is related to the increasing bending stiffness of the twines that hampers mesh opening and the release of small fish.^{16–19} An increasing twine bending stiffness also changes the overall shape of the netting structure during fishing operations.^{19,20} This makes the mesh resistance to opening of net panels a key factor in the performance of fishing gears. In panels of diamond-oriented mesh, the predominant netting in towed fishing gears, the resistance to

opening is mainly characterized by the bending stiffness of the netting twine, also known as flexural rigidity (*EI*). Therefore, methods to measure bending stiffness and to incorporate this mechanical property in numerical simulations of flexible net structures are subjects worthy of investigation.

The most comprehensive research about twine bending stiffness has been developed by O'Neill:²¹ he described the equations governing the bending stiffness of a twine assuming that (1) the slope angle between the twine and the knot at the insertion point remains fixed, (2) the bending moment is proportional to the curvature of the twine, and (3) there is no twine

Laboratorio de Ingeniería Mecánica, Departamento de Ingeniería Industrial II, Escuela Politécnica Superior, Universidade da Coruña, Campus de Ferrol, Ferrol, Spain

Corresponding author:

Manuel González, Laboratorio de Ingeniería Mecánica, Universidade da Coruña, Escuela Politécnica Superior, C/Mendizábal s/n, 15403 Ferrol, Spain.
 Email: manuel.gonzalez@udc.es

extension. He found two analytical solutions: (1) an exact solution, expressed as a set of implicit highly nonlinear equations involving elliptic integrals and (2) a simpler asymptotic solution that expresses the coordinates of the end point of the twine as an explicit function of the tensile forces acting on it. Both solutions were used to study the factors influencing the measurement of netting mesh size,²² and the asymptotic solution was used to develop an experimental method for measuring bending stiffness in netting panels.²³ Although these analytical solutions are highly valuable to describe bending stiffness, they have two major drawbacks when they are incorporated into numerical simulations of flexible net structures:

1. Numerical formulations often need to evaluate elastic forces in twines as a function of mesh deformation.^{3,4,6,7} The asymptotic solution provides the opposite expression, and therefore, it needs to be numerically inverted for every mesh element in the model at every simulation iteration, causing a significant computational overhead compared with current formulations that do not consider bending stiffness. The overhead of the exact solution is even higher.
2. Both solutions can only be numerically inverted for twine deformations that are compatible with bending without axial deformation. This is a downside because mesh twines also experience moderate extension. A workaround would be the use of separate solutions for bending and axial deformations, but this approach would ignore the probable coupling between both deformations due to tension stiffening.²⁴

Priour²⁵ proposed a model based on the assumption that the couple created by the twines on the knot varies linearly with the angle between twines. Although this model can be easily included in numerical formulations, it is not derived from any physical law and the twine bending stiffness EI is not a parameter of the model. Nevertheless, it has been demonstrated that for large-deformation bending, this model can be modified to approximate the above-mentioned asymptotic solution.²⁶ The textile sector has also developed models for characterizing the bending stiffness of fabrics,^{27–29} but they have similar drawbacks as the models developed by O'Neill.²¹

The goal of this work is to develop accurate and efficient force models to describe the bending behavior of a twine, which can be easily incorporated into existing numerical formulations to simulate marine net structures. These models should meet the following two requirements:

1. To achieve high computational efficiency, they should express elastic forces in a twine as *explicit* functions of the twine deformation. This will allow including mesh resistance to opening in numerical simulations without a noticeable increase in

computer time, which is already high in some applications.^{3,4,7,12}

2. They should allow evaluating elastic forces for twine deformations that include moderate axial elongation.

This work is focused on the modeling of mesh resistance to opening of flexible net structures, that is, the stiffness of the structure. It is not aimed at developing a complete model for static or dynamic analysis of marine flexible net structures. Therefore, mass, damping, and hydrodynamic forces on the net structure are out of the scope of this article. Examples of complete static and dynamic models for marine flexible net structures are available in the literature.^{3,4,7,8,15}

The proposed approach is to use a finite element model (FEM) of the twine and to calculate its force–displacement response using finite element analysis. Then fitting techniques are used to develop three approximate force models that fit the force–displacement response of the twine FEM. Each of the three force models has different features and advantages. A numerical test problem and experimental data are used to evaluate and compare the three approximated force models and the two analytical solutions proposed by O'Neill.²¹

Description of the twine FEM

The twine was modeled as a two-dimensional (2D) double-clamped beam between knots represented as points \mathbf{P}_0 and \mathbf{P}_1 , as shown in Figure 1. The slope angle φ_0 between the twine and the knots at the insertion points remains fixed. The coordinate system has its x -axis aligned with the undeformed beam to make the obtained results independent from φ_0 . Point \mathbf{P}_0 is fixed and \mathbf{P}_1 is free to move under an applied force \mathbf{F} or a prescribed displacement $\mathbf{U} = (U_x, U_y)$ with respect to its undeformed position.

The force–displacement response of the beam was obtained using the finite element method. The beam was discretized with 20 quadratic three-dimensional beam elements based on Timoshenko beam theory; this element is well-suited for large rotation and/or large strain nonlinear applications. It was verified that this mesh discretization size achieves good convergence in all the performed analyses. Since a tridimensional beam element was used, additional boundary conditions were applied to make the model to behave as the 2D model, as shown in Figure 1.

Dimensional analysis was applied to make the results from the finite element analysis applicable to twines of different properties. Let us select as independent variables of the model the properties of the twine (unstretched beam length L , flexural rigidity EI and axial rigidity EA) and the polar coordinates (R, φ) of \mathbf{P}_1 , which are directly related to a prescribed displacement $\mathbf{U} = (U_x, U_y)$. The dependent variables are the two components of the force \mathbf{F} at \mathbf{P}_1 . Therefore, any of these two force components F can be expressed as

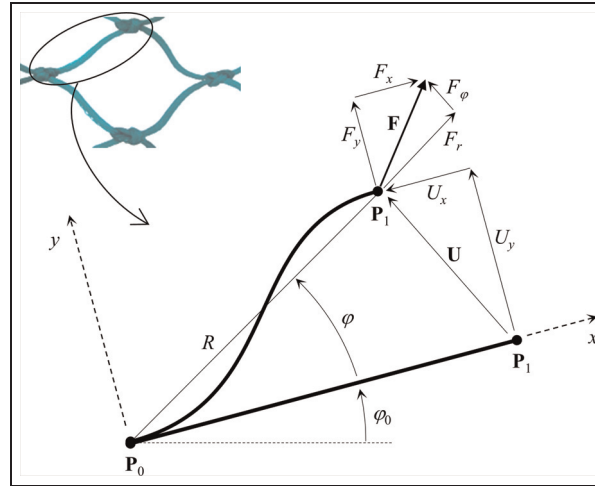


Figure 1. Finite element model of a twine, represented in undeformed and deformed shapes.

$$F = F(L, EA, EI, R, \varphi) \quad (1)$$

Dimensional analysis leads to four dimensionless similarity parameters (Π_0 , Π_1 , Π_2 , and Π_3) which are selected as follows: dimensionless force component f , dimensionless radial coordinate r , angle φ , and parameter γ

$$\Pi_0 = f = F \frac{L^2}{EI} \quad (2)$$

$$\Pi_1 = r = \frac{R}{L} \quad (3)$$

$$\Pi_2 = \varphi \quad (4)$$

$$\Pi_3 = \gamma = L^2 \frac{EA}{EI} \quad (5)$$

Hence, the nondimensionalized version of equation (1) can be expressed as

$$f = f(r, \varphi, \gamma) \quad (6)$$

Dimensionless Cartesian coordinates (x , y) and displacements (u) are obtained in a similar way

$$x = \frac{X}{L}, \quad y = \frac{Y}{L}, \quad u = \frac{U}{L} \quad (7)$$

According to equation (6), forces depend on three parameters, which makes extremely difficult to graphically represent the force–displacement response of the model and to fit approximate expressions to it. Since parameter γ represents the ratio between axial and bending forces, the authors decided to simplify the analysis by studying the force–displacement response as a set of continuous functions of the first two parameters (r , φ) for discrete values of the twine axial rigidity EA

$$f^{EA_i} = f^{EA_i}(r, \varphi) \quad (8)$$

The results from this work will demonstrate that this decision is correct since the effect of EA on f is small compared with r and φ . Representative values of twine

axial rigidity EA in netting panels range from 500 to 3000 N,^{3,30,31} although some authors have reported values for aquaculture net cages as low as 80 N³² or as high as 4000 N.⁸ In this work, the authors studied the force–displacement response of the twine for four values of EA : 500, 1000, 2000, and 3000 N.

Force–displacement response

To obtain the force–displacement response of the FEM, a series of geometric nonlinear static analyses were performed applying an enforced displacement constraint (u_x , u_y) at point P_1 to calculate the reaction force \mathbf{F} at that point. The magnitude of (u_x , u_y) in each analysis corresponds to the position of each of the vertices of the regular curvilinear grid, as shown in Figure 2. In this grid, the dimensionless radial coordinate r takes N_r linearly equally spaced values in the interval $[r_{min}, r_{max}] = [0.92, 1.05]$, and the angular coordinate φ takes N_φ linearly equally spaced values in the interval $[0, \Pi/2]$. This grid size spans most of the deformed positions that a twine can undergo in bending and moderate compression/tension. The grid discretization size was adjusted to $N_r \times N_\varphi = 27 \times 27$ (729 static analyses) in order to obtain a smooth results grid. Four series of analyses were performed, one for each value of EA (500, 1000, 2000, and 3000 N).

The clearest view of the results is provided by a grid surface representation of the polar components (f_r , f_φ) of the dimensionless force \mathbf{f} obtained for each discrete value of axial rigidity EA . In addition, replacing the angular coordinate φ by $\cos \varphi$ results in smoother surfaces that simplify the data fitting. Figure 3 shows this representation for a twine with $EA = 500$ N. For higher values of EA , the surfaces have the same overall shape but with a higher slope with respect to r .

Missing points in the surfaces represent failed analyses. Most of them are concentrated in two regions: the very large-deformation bending region of $\cos \varphi < 0.35$

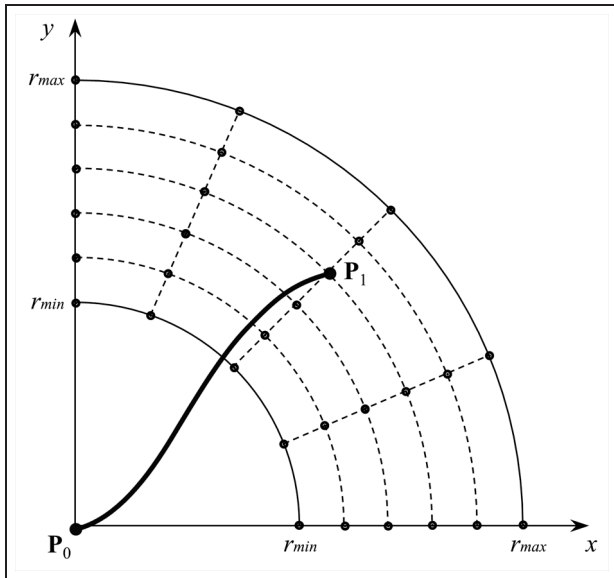


Figure 2. Regular curvilinear grid used to calculate the force–displacement response of the twine.

($\varphi > 70^\circ$) and the high-compression, small-bending region delimited by $\cos \varphi > 0.9$ ($\varphi < 26^\circ$) and $r < 0.95$. When point \mathbf{P}_1 moves into these regions, the FEM becomes very ill-conditioned and the static analysis fails or provides meaningless results. The series of static analyses were run again increasing the finite element discretization in a factor of 4 (80 elements instead of 20) with similar results. The percentage of failed analyses (and the area of the two ill-conditioned regions) increased with the axial rigidity: 19% ($EA = 500$ N), 29% ($EA = 1000$ N), and 40% ($EA = 2000$ N). For $EA = 3000$ N, 58% of the analyses failed and the authors excluded this data set from the research. In any case, the two regions with failed analyses represent

extreme and unusual cases of twine deformation. For example, most of the first region ($\varphi > 70^\circ$) is often not physically meaningful because the maximum physical value for φ is $\Pi/2 - \varphi_0$ (Figure 1), and representative values for φ_0 in diamond-shaped meshes range from 5° to 15° .

Cutting the f_r surface in Figure 3(a) with plane $f_r = 0$ generates the trajectory of \mathbf{P}_1 along the path of 0 radial force that defines the limit between twine tension and compression. This trajectory is a line $r = a \cos(\varphi) + b$ in the selected coordinate space and it is virtually independent of EA (see Table 1).

Approximate force models

Force model No. 1: polynomial surface fitting

The first force model consists of a polynomial surface fitting of the force–displacement response: two polynomial surfaces of degree $m \times n$ were fitted to the surfaces of the force components f_r and f_φ , as shown in Figure 3

$$f(r, \cos \varphi) = \sum_{0 < i + j < m + n} c_{ij} r^i (\cos \varphi)^j \quad (9)$$

The surface fitting was calculated using weighted linear least squares regression since the data set has negligible scatter and no outlier points. Weights were adjusted to give more significance to points near the path $f_r = 0$, as shown in Table 1, because forces are small in this region and residuals cause high relative errors. Constraints were applied to the coefficients c_{ij} in order to generate polynomial expressions with the same zeros as the original FEM: $f_r(r = 1, \cos \varphi = 1) = 0$ and $f_\varphi(r, \cos \varphi = 1) = 0$. Two additional constraints were tested and rejected because they proved to be too restrictive and impeded a good fit: $f_r(r = a \cos \varphi + b, \cos \varphi) = 0$, which represents the path $f_r = 0$ shown in

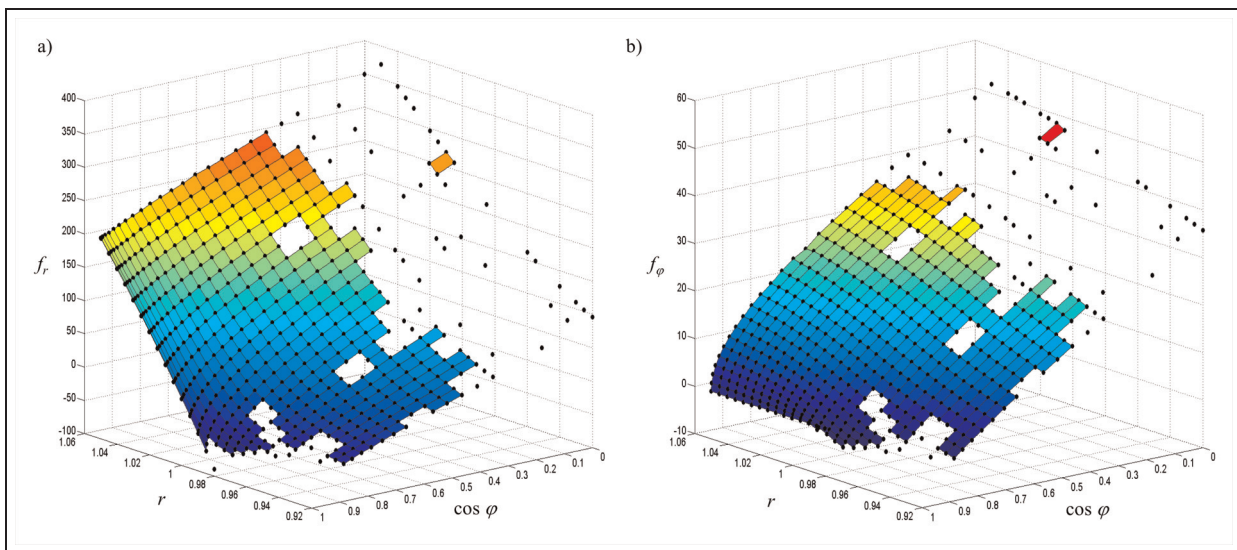


Figure 3. Dimensionless force–displacement response of a twine with axial rigidity $EA = 500$ N, as a function of the position of its end point \mathbf{P}_1 ($r, \cos \varphi$): (a) radial component f_r and (b) tangential component f_φ .

Table 1. Path of 0 radial force ($f_r = 0$): coefficient values and coefficient of determination R^2 for the simple linear regression $r = a \cos(\varphi) + b$.

Axial rigidity (EA) (N)	a	b	R^2
500	0.2018	0.7984	0.99993
1000	0.2023	0.7979	0.99994
2000	0.2018	0.7981	0.99992

Table 2. Polynomial surface fitting of the dimensionless radial force f_r : coefficient values and coefficient of determination R^2 .

c_{ij}	Twine axial rigidity (EA)		
	500 N	1000 N	2000 N
c_{00}	-6.58×10^3	-8.58×10^3	-2.02×10^4
c_{10}	1.18×10^4	1.36×10^4	2.90×10^4
c_{01}	2.74×10^4	5.55×10^4	1.34×10^5
c_{20}	-4.92×10^3	-4.59×10^3	-7.42×10^3
c_{11}	-5.65×10^4	-1.12×10^5	-2.60×10^5
c_{02}	4.34×10^2	-5.95×10^2	-6.67×10^3
c_{21}	2.88×10^4	5.59×10^4	1.22×10^5
c_{12}	-1.63×10^1	1.59×10^3	1.23×10^4
c_{03}	-3.16×10^2	-7.04×10^2	-3.04×10^3
R^2	0.994	0.992	0.990

Table 1, and $f_r(r, \cos \varphi = 1) \propto (r - 1)$, which represents the behavior of the beam under axial loads at $\varphi = 0$; nevertheless, the obtained fitted expressions are very close to satisfy these constraints.

The best fit was obtained with a polynomial degree (m, n) of (2, 3) for f_r and (1, 4) for f_φ . Coefficient values and the coefficient of determination R^2 for the fitting are provided in Table 2 (radial force) and Table 3 (tangential force). A visual inspection of the residuals confirmed the excellent quality of the fitting indicated by the high value of R^2 .

Force model No. 2: spline surface fitting

The beam model described in Figure 1 is a conservative system, and preserving this characteristic is essential when energy minimization methods are applied to find the equilibrium position of netting structures.^{2,33} But force model No. 1 described in the previous subsection is not a gradient field, and therefore, it does not preserve this property.

A conservative force model can be obtained by fitting the potential energy of the system instead of the force–displacement response and then evaluating forces as the gradient of the fitted expression. However, a polynomial fitting of the potential energy cannot generate an accurate gradient force field because even small fitting errors in the energy can generate high errors in its gradient due to the differentiation process. Consequently, a spline interpolation was used because it provides much better fittings than polynomials.

Table 3. Polynomial surface fitting of the dimensionless tangential force f_φ : coefficient values and coefficient of determination R^2 .

c_{ij}	Twine axial rigidity (EA)		
	500 N	1000 N	2000 N
c_{00}	-1.28×10^2	-1.12×10^2	-9.35×10^2
c_{10}	1.76×10^2	1.73×10^2	1.06×10^3
c_{01}	6.80×10^2	4.05×10^2	4.03×10^3
c_{11}	-7.31×10^2	-4.49×10^2	-4.35×10^3
c_{02}	-2.06×10^3	-2.04×10^3	-7.86×10^3
c_{12}	2.09×10^3	1.96×10^3	8.36×10^3
c_{03}	1.54×10^3	1.85×10^3	4.70×10^3
c_{13}	-1.53×10^3	-1.68×10^3	-5.06×10^3
c_{04}	-2.50×10^1	-1.05×10^2	6.55×10^1
R^2	0.985	0.983	0.977

A dimensionless potential elastic energy v is defined as function of the potential elastic energy V of the beam as

$$v = V \frac{L}{EI} \tag{10}$$

The procedure followed to obtain the force–displacement response also provides the dimensionless potential elastic energy v , which is represented in Figure 4 for a twine with $EA = 500$ N; for higher values of EA , the surfaces have the same overall shape but a higher slope.

The surface of dimensionless potential energy $v = v(r, \varphi)$ was approximated using bicubic spline 2D interpolation. This procedure computes $(N_r - 1) \times (N_\varphi - 1)$ bicubic spline patches, where each patch (i, j) spans the rectangular region $[r_i, r_{i+1}] \times [\varphi_j, \varphi_{j+1}]$. Then, v at each patch (i, j) is calculated as

$$v_{ij}(r, \varphi) = \sum_{k=0}^3 \sum_{l=0}^3 c_{kl}^{ij} (r - r_i)^k (\varphi - \varphi_j)^l \tag{11}$$

and the polar components of the force are evaluated as

$$f_r^{ij}(r, \varphi) = \frac{\partial v_{ij}}{\partial r} \tag{12}$$

$$f_\varphi^{ij}(r, \varphi) = \frac{1}{r} \frac{\partial v_{ij}}{\partial \varphi} \tag{13}$$

Spline patches are twice continuously differentiable across patch limits, and therefore, the continuity of forces is ensured. This method calculates the $16 \times (N_r - 1) \times (N_\varphi - 1)$ coefficients needed to define the interpolation; in the followed procedure, $N_r = N_\varphi = 27$, resulting in 676 patches and 10,816 coefficients. Coefficient values are provided in a machine-readable supplementary file.

Force model No. 3: spring-based model for vertical forces

Mesh twines can experience large, unrealistic axial deformations in the numerical simulation of net

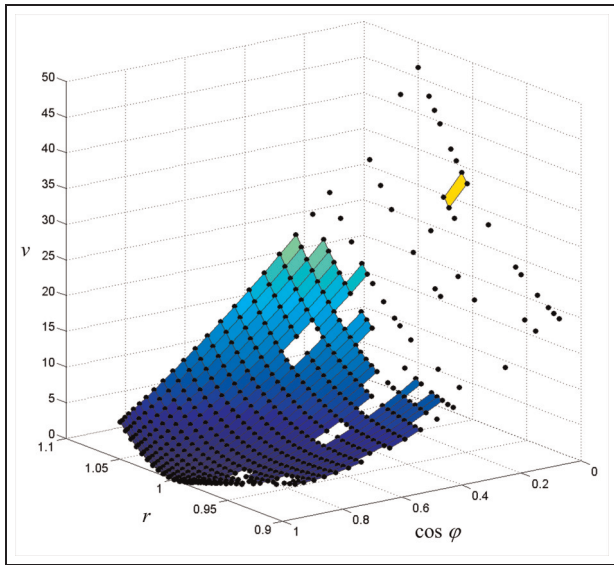


Figure 4. Dimensionless potential elastic energy v of a twine with axial rigidity $EA = 500$ N, as a function of the position of its end point \mathbf{P}_1 ($r, \cos \varphi$).

structures, and twine force models must be able to deal with these situations. For example, the model usually goes through positions far from the equilibrium in static equilibrium analysis based on Newton iteration⁶ or iterative optimization.²

A twine force model based on linear springs, which is the most common for numerical simulation of marine netting structures,^{3,4,6,7} can deal easily with extreme axial deformations and reach the equilibrium position in few iterations. However, force models developed in the previous subsections do not have this capability: the polynomial surface fitting generates erroneous force values when r is far from the interval $[r_{min}, r_{max}]$, and the spline surface fitting cannot be evaluated outside this interval. Therefore, they cannot be used as stand-alone models, but they need to be combined with a classic spring-based force model for large axial deformations.

The force model developed here aims at dealing with large axial deformations, and at the same time, achieving good accuracy in situations where the normal forces applied to the twine are small compared with the transverse forces ($F_y \gg F_x$ in Figure 1 when $\varphi_0 = 0$). This situation is often present in some applications, for example, in T90 netting panels placed in cod-ends of fishing trawls,³⁴ where the force component in the direction of the water flow is much higher than other components.

The twine FEM was used to calculate the force–displacement response of a twine when a vertical force ($F_y > 0, F_x = 0$) is applied to \mathbf{P}_1 . Note that this force distribution ($F_x = 0$) only matches exactly with a 0 transverse force if $\varphi_0 = 0$; nevertheless, φ_0 is usually below 15° in diamond-shaped meshes. A series of static analyses were run with increasing values of F_y , for twine axial rigidity EA of 500, 1000, and 2000 N. The trajectory of \mathbf{P}_1 is represented in Figure 5 and was adjusted

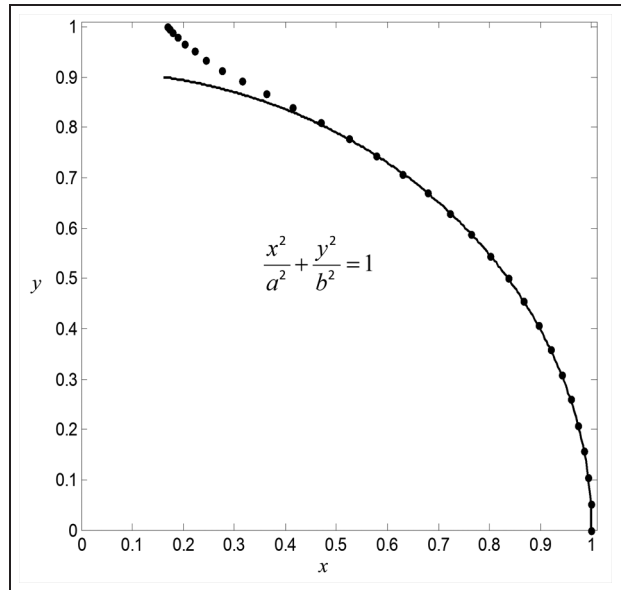


Figure 5. Trajectory of twine end point \mathbf{P}_1 when a vertical force F_y is applied to it, for twine axial rigidity $EA = 500$ N.

Table 4. Coefficient values and coefficient of determination R^2 for the elliptical regression of the trajectory shown in Figure 5.

Axial rigidity (EA) (N)	a	b	R^2
500	1	0.9118	0.99998994
1000	1	0.9086	0.99998196
2000	1	0.9069	0.99997217

to an ellipse using nonlinear regression. Points with $x < 0.5$ ($\varphi > 60^\circ$) were removed from the regression since in this region the axial deformation of the twine becomes noticeable and the points separate from an elliptical path. Regression results (Table 4) confirm that the fitting is virtually exact for $\varphi < 60^\circ$ and nearly independent of EA .

The proposed force model approximates the radial force f_r as a linear spring with variable-length r_{eq}

$$f_r(r, \cos \varphi) = EA \left(\frac{L^2}{EI} \right) (r - r_{eq}(\cos \varphi)) \quad (14)$$

With this expression, iterative methods can converge to the equilibrium position in few iterations even if the axial deformation is large. The length function $r_{eq}(\cos \varphi)$ is calculated to generate the same radial force as the FEM when point \mathbf{P}_1 moves along the elliptical trajectory, as shown in Figure 5

$$r_{eq}(\cos \varphi) = r(\cos \varphi) - \left(\frac{1}{EA} \right) \left(\frac{EI}{L^2} \right) f_r^{FEM}(\cos \varphi) \quad (15)$$

This expression generates a set of points $(r_{eq}, \cos \varphi)$, which are approximated by a fifth-degree polynomial using linear regression

Table 5. Coefficient values and coefficient of determination R^2 for the polynomial curve fitting of r_{eq} .

c_i	Twine axial rigidity (EA)		
	500 N	1000 N	2000 N
c_0	1.032	1.017	1.009
c_1	-0.6585	-0.5551	-0.4872
c_2	1.427	1.115	0.8789
c_3	-1.398	-0.9335	-0.5363
c_4	0.7955	0.4606	0.1427
c_5	-0.1979	-0.1042	-0.006747
R^2	0.99854	0.99996	0.99976

$$r_{eq}(\cos \varphi) = \sum_{i=0}^5 c_i (\cos \varphi)^i \quad (16)$$

Coefficients are provided in Table 5; $c_0 \rightarrow 1$ and $\sum_{i=1}^5 c_i \rightarrow 0$ as $EA \rightarrow \infty$, as expected. The tangential force component f_φ is calculated as a function of φ by substituting in the tangential force model of the polynomial surface interpolation (equation (9)) the radius $r = r(\varphi)$ of the elliptical trajectory shown in Figure 5.

Test problem and results

To evaluate the accuracy of different models of mesh resistance to opening, they have been used to calculate the force–displacement response of a twine with $\varphi_0 = 0$ when a vertical force ($F_y > 0$, $F_x = 0$ in Figure 1) is applied to \mathbf{P}_1 . This test problem represents the force distribution used to develop force model No. 3.

Force–displacement response

The test problem was solved using three different approaches, as follows:

1. The twine FEM, which calculates the displacement (u_x , u_y) of \mathbf{P}_1 as a function of f_y ; this solution was considered the reference solution.
2. The exact and the asymptotic analytical solutions described by O'Neill,²¹ which provide the position (x , y) of \mathbf{P}_1 as a function of the force magnitude and force angle ($\Pi/2$ in this case).
3. The three approximate force models developed in this work. Since they provide explicit expressions for the force as a function of the position, the following set of nonlinear equations was solved to find the equilibrium position (r , $\cos \varphi$) for a vertical force f_y

$$\begin{cases} f_x(r, \cos \varphi) = f_r \cos \varphi - f_\varphi \sin \varphi = 0 \\ f_y(r, \cos \varphi) = f_r \sin \varphi + f_\varphi \cos \varphi \end{cases} \quad (17)$$

The bending force model developed by Priour²⁵ was not included in this comparison because it has been already demonstrated²⁶ that it is very similar to the asymptotic solution.²¹ The following figures show the results for a twine with axial rigidity $EA = 500$ N. For

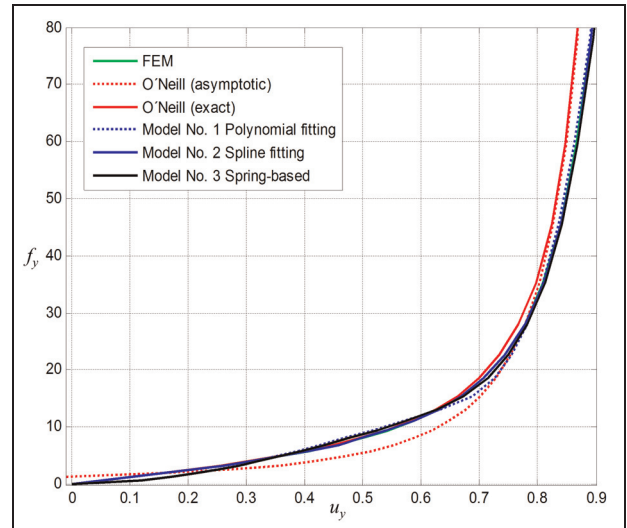


Figure 6. Vertical force f_y as a function of the vertical displacement u_y for twine axial rigidity $EA = 500$ N. FEM: finite element model.

higher values of EA (1000 and 2000 N), figures are very similar for $u_y < 0.7$, the interval where axial deformation is negligible. Figure 6 plots the vertical force f_y as a function of the vertical displacement u_y . Figure 7 represents the trajectory of point \mathbf{P}_1 as the vertical force f_y increases from 0 to 250. Figure 8 compares the different solution methods to the FEM, showing absolute and relative errors in force and position calculated from Figure 6.

The exact analytical solution is virtually identical to the FEM solution in the region where axial deformation is negligible ($u_y < 0.7$, $\varphi < 48^\circ$), with relative errors below 4% (force) and 1% (position). For higher vertical deformations, axial deformation becomes noticeable and the relative error in force increases exponentially.

The asymptotic analytical solution has the highest deviation from the FEM. It generates a positive force for 0 vertical deformation, which results in high relative errors for $u_y < 0.1$ ($\varphi < 6^\circ$); in the interval $0.2 < u_y < 0.7$ ($12^\circ < \varphi < 48^\circ$), the relative errors also surpass 30% in force and position. The generated trajectory of \mathbf{P}_1 follows a line instead of an ellipse and deviates significantly from the FEM for $\varphi < 48^\circ$. For higher vertical deformations, the asymptotic solution converges to the exact analytical solution.

Force model No. 2 (spline fitting) is virtually identical to the FEM solution for all the range of vertical deformations, with relative errors below 2% (force) and 1% (position). Force models No. 1 (polynomial fitting) and No. 3 (spring-based model) have a similar behavior: although both of them generate a 0 force for $u_y = 0$, the force is slightly lower than the FEM force in the interval $0.05 < u_y < 0.35$ ($3^\circ < \varphi < 20^\circ$), generating high relative errors in force and position due to the small absolute value of the FEM forces. For

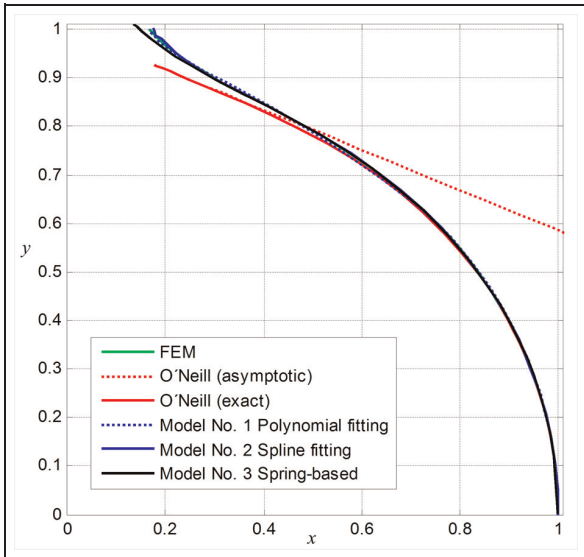


Figure 7. Trajectory of point P_1 for twine axial rigidity $EA = 500$ N.
FEM: finite element model.

higher deformations, both models are closer to the FEM, with relative errors below 8% (force) and 5% (position) for the spring-based model, and below 12% (force) and 7% (position) for the polynomial surface fitting. In the interval where the axial deformation becomes noticeable ($u_y > 0.7$, $\varphi > 48^\circ$), the position error is below 2%. Both methods generate a trajectory of P_1 almost identical to the FEM.

Effect of twine axial rigidity

The test problem was solved using the FEM for different values of twine axial rigidity EA in order to evaluate the effect of this parameter. Figure 9 plots the vertical force f_y as a function of the vertical displacement u_y , and Figure 10 plots f_y as a function of EA for different values of u_y .

The approximated force models developed in this work were calculated for a set of discrete values $\{EA_1, EA_2, EA_3\} = \{500, 1000, 2000$ N}. For moderate vertical deformations ($u_y < 0.7$, $\varphi < 48^\circ$), the effect of EA

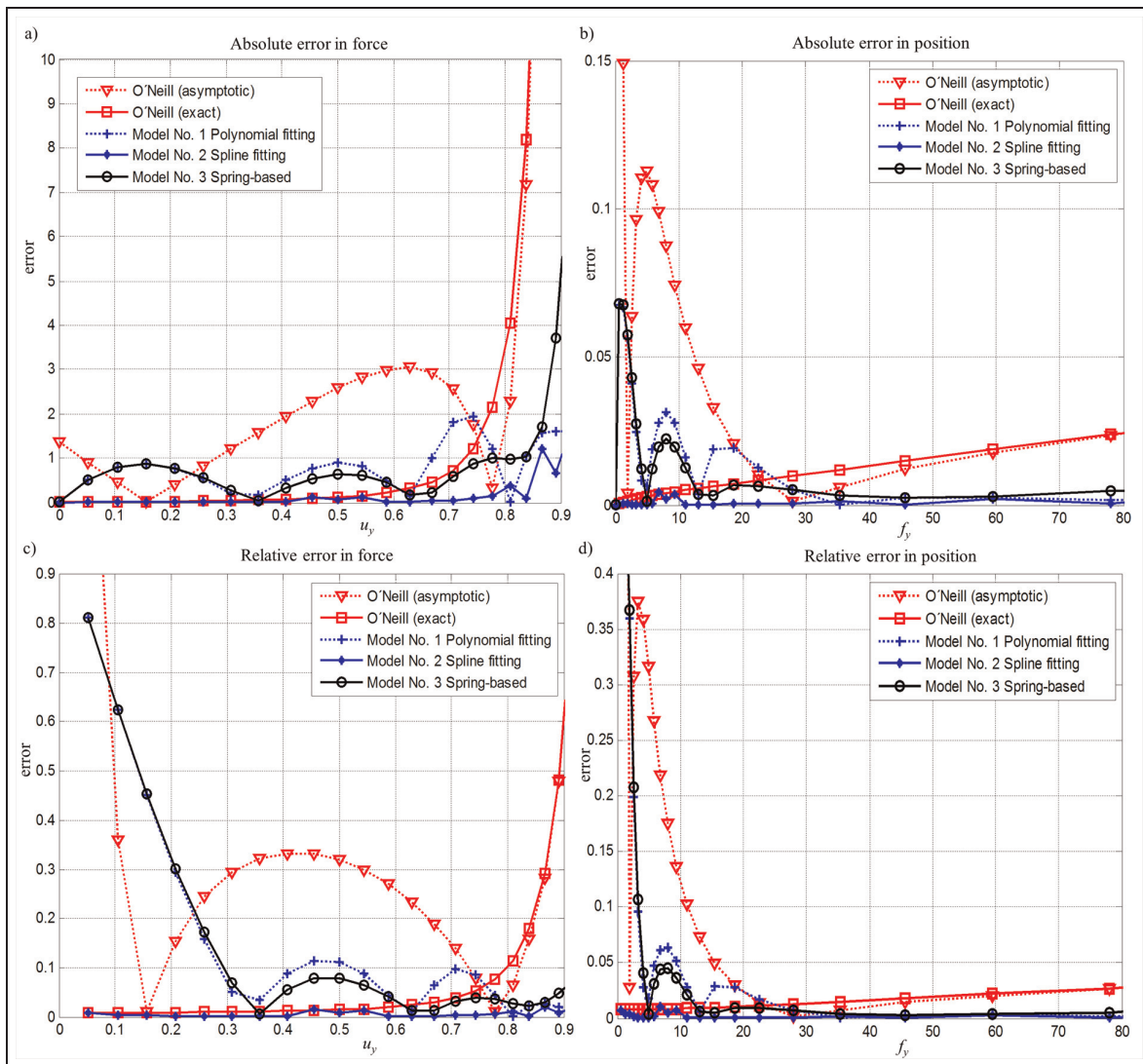


Figure 8. Comparison of the different solution methods with the finite element method, for twine axial rigidity $EA = 500$ N: (a) absolute error in force, (b) absolute error in position, (c) relative error in force, and (d) relative error in position.

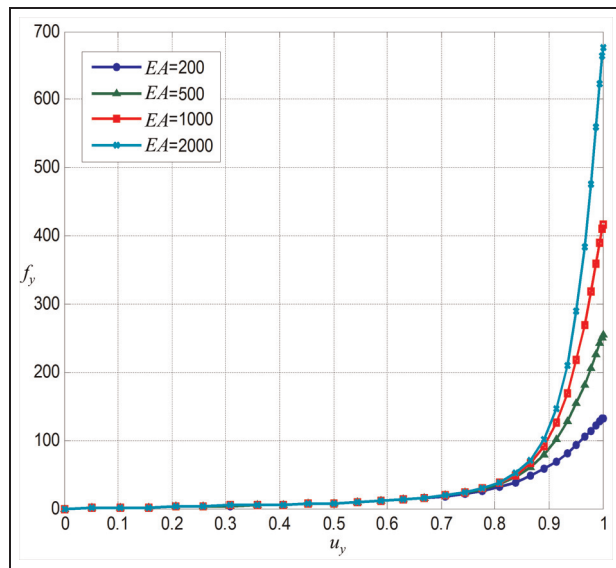


Figure 9. Vertical force f_y as a function of the vertical displacement u_y for different values of twine axial rigidity EA , calculated with the finite element method.

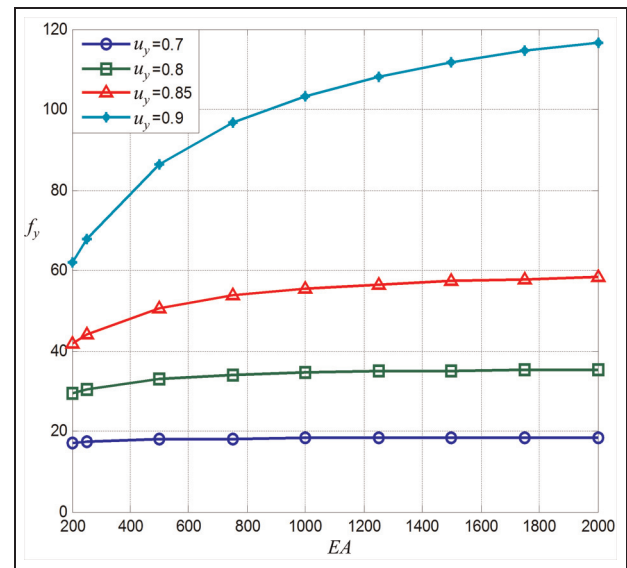


Figure 10. Vertical force f_y as a function of the twine axial rigidity EA for different values of vertical displacement u_y , calculated with the finite element method.

is negligible since axial deformation is imperceptible. For higher deformations, Figure 10 suggests that the force–displacement response for a particular value of EA can be calculated using three-point parabolic interpolation/extrapolation from the force models calculated for $\{EA_1, EA_2, EA_3\}$.

Experimental validation

An alternative version of the experiment carried out by Sala et al.²³ was used to verify that the presented models can predict the mesh resistance to opening of real netting. A polyethylene netting panel with a nominal mesh size of 80 mm and a twine diameter of 4 mm (a common material in European commercial fishing nets) was mounted between a fixed bar and a free bar, as shown in Figure 11. A growing force F_{panel} was applied to the free bar to open the netting meshes, and the resulting length of the panel L_{panel} was measured. The experimental data were analyzed with the method proposed by Sala et al.:²³ the twine bending stiffness EI was estimated using nonlinear least squares regression to fit a force model for mesh resistance to opening to the experimental data. This method also allows evaluating how well the model can predict the results of the experiment. Figure 12 compares the experimental data with the predictions provided by different models of mesh resistance to opening, including the three models presented in this work. The legend shows the estimate of EI and the coefficient of determination R^2 for each model. The model by Priour²⁵ could not be used because it does not take into account the bending stiffness EI .

The results show that the exact model by O’Neill²¹ and model No. 2 have an excellent agreement with

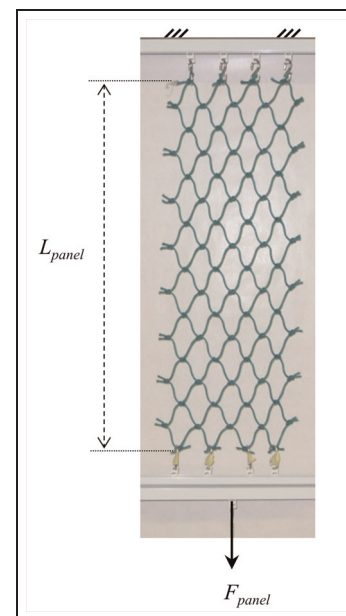


Figure 11. Experimental setup for measuring mesh resistance to opening of a netting panel.

experimental data ($R^2 > 0.99$) and similar estimates of EI . Models No. 1 and No. 3 give a slightly worse, but still very satisfactory fitting. The asymptotic model by O’Neill²¹ gives the worst results, with appreciable deviations from experimental data in the region of small and moderate forces. Note that this was the model used by Sala et al.²³ to measure the mesh resistance to opening of a wide range of netting materials, and the results indicated that the model can predict the behavior of such materials with enough accuracy.

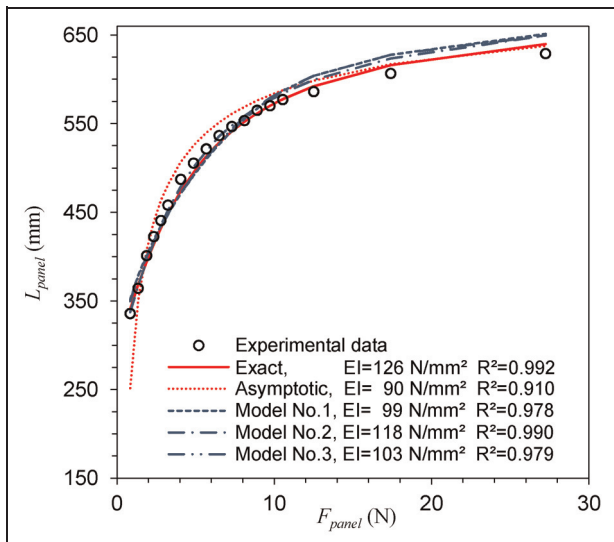


Figure 12. Length of the netting panel in normal mesh direction L_{panel} as a function of the applied force F_{panel} . Fittings obtained with different models of mesh resistance to opening are shown: the exact and asymptotic models by O'Neill²¹ and the three models presented in this work. Model No. 1 refers to the polynomial fitting of the force, Model No. 2 refers to the spline fitting of the potential energy, and Model No. 3 refers to the spring-based model. The legend also provides the estimates for twine bending stiffness EI and the coefficient of determination R^2 for each model.

Discussion

The FEM used in this work assumes that the twine behavior follows the Timoshenko beam theory, and that the slope angle φ_0 between the twine and the knots at the insertion points remains fixed. These assumptions are unlikely to hold exactly for all kinds of netting materials due to the complex structure of the constituent fibers of fishing netting, and more experimental work will be needed to evaluate their validity. In addition, the beam theory is often not valid to represent the behavior of twines in moderate or high compression. In spite of this the FEM makes less assumptions about twine behavior than previously existing models,²¹ since it takes into account axial deformations and geometric nonlinearities caused by large rotations.

The results from the test problem support the select size $[r_{min}, r_{max}] = [0.92, 1.05]$ for the regular curvilinear grid used to calculate the force–displacement response of the twine FEM (Figure 2): the dimensionless radial coordinate r was bounded to this interval for $\varphi < 80^\circ$ (Figure 7), and higher values of φ are often impracticable due to physical limitations ($\varphi_{max} = \Pi/2 - \varphi_0$). For situations different from the test problem, that is, $F_x > 0$ and $F_y > 0$, then $\varphi_{max} = \tan^{-1}(F_y/F_x)$ and the behavior in Figures 7 and 9 indicates that r will not exceed $r_{max} = 1.05$ for the usual values of EA , unless extremely high forces are applied.

The results also support the decision of studying the force–displacement response of the beam model as a set of continuous functions of (r, φ) for discrete values of

the twine axial rigidity EA . This decision was based on the assumption that the effect of EA on the dimensionless forces is small compared with r and φ . According to Figures 9 and 10, the effect of EA is insignificant for moderate vertical deformations of the mesh ($u_y < 0.7$, $\varphi < 48^\circ$). The effect of EA is only noticeable for very large vertical deformations ($u_y > 0.8$, $\varphi > 60^\circ$), but such deformations hardly happen in real marine net structures because the applied forces are not so high. In any case, the presented approach is able to take into account the small effect of EA using the aforementioned three-point parabolic interpolation from the force models calculated for $\{EA_1, EA_2, EA_3\}$.

The behavior of the asymptotic analytical solution agrees with the results reported by O'Neill,²¹ which shows that it is very accurate in comparison to the exact analytical solution for $f > 25$. On the other hand, this solution has significant errors in force and position for smaller values of the dimensionless force f (equivalent to $\varphi < 50^\circ$ in the test problem), especially in the trajectory of the twine end point, and this fact could partially explain the lack of fit with experimental results reported by Sala et al.²³

Another interesting matter is related to the fact that most numerical formulations for flexible net structures model the axial behavior of the twine as a linear spring, and therefore assume that its natural length remains constant during mesh opening.^{3,4,6,7} Table 1 reveals that this assumption is not correct since the length corresponding to a 0 axial force decreases as the bending angle increases. The same conclusion could be achieved using the exact analytical solution,²¹ which generates a similar shape for a bending twine (Figure 7). As a result, the mesh shape and dimensions calculated by such formulations will differ from the actual values, and this fact has an impact on the accuracy of selectivity of fishing gears calculated with those methods. Conversely, the three developed force models take into account the coupling between axial and bending deformations, and therefore, it is expected that they can generate more precise mesh shapes.

Regarding computational efficiency of the evaluation of forces as a function of twine deformation, the three approximate force models are extremely efficient due to their explicit and simple expressions, even for force model No. 2 (spline surface fitting). Conversely, the computational cost of the asymptotic analytical solution is notably higher, and the exact analytical solution proved to be extremely inefficient.

The numerical and experimental validations carried out in this work are based on static analysis. Hence, this work does not demonstrate that the presented models are efficient and accurate for dynamic analysis. But the results show that they are better (i.e. significantly faster with similar or even better accuracy) than existing models developed by Priour²⁵ and O'Neill²¹ when applied to static analysis. Therefore, it is reasonable to suppose that they will also perform better than such existing

Table 6. Comparison of the presented force models (De la Prada and González) with previous models of mesh resistance to opening by Priour²⁵ and O'Neill²¹

Features	Priour ²⁵	O'Neill ²¹		De la Prada and González		
		Exact	Asymptotic	No. 1	No. 2	No. 3
Takes into account twine bending stiffness (EI)	–	✓	✓	✓	✓	✓
Takes into account twine axial stiffness (EA)	–	–	–	✓	✓	✓
Force as explicit function of position (i.e. fast evaluation of forces)	✓	–	–	✓	✓	✓
Highly accurate	–	✓	–	✓	✓	✓
Very easy to implement in existing formulations	✓	–	–	✓	–	✓
Conservative force field	✓	–	–	–	✓	–
Compatible with large twine axial deformations	–	–	–	–	–	✓
Compatible with high transversal forces	✓	✓	✓	✓	✓	–

Model No. 1 refers to the polynomial fitting of the force, Model No. 2 refers to the spline fitting of the potential energy, and Model No. 3 refers to the spring-based model.

models when applied to dynamic analysis. Further research must be carried out to verify this hypothesis.

Finally, Table 6 summarizes the differences between the three presented force models and previous models for mesh resistance to opening. The comparison shows that the models developed in this work have strong advantages over previous models. The comparison also helps to choose which one of the three presented force models is best suited for a particular application.

Conclusion

A FEM of a twine has been used to develop three dimensionless approximate force models of mesh resistance to opening, which express elastic forces in a twine as explicit functions of twine deformation. Each force model has different features, and researchers can choose which one better fits the requirements of a particular application:

1. A polynomial fitting of the force components, with good accuracy and extremely easy to implement.
2. A spline fitting of the potential energy, which generates a highly accurate, conservative force field suitable to energy optimization methods, at the cost of a slightly more complex implementation.
3. A spring-based model able to deal with large axial deformations, designed for situations where the normal forces applied to the twine are small compared with the transverse forces.

The developed force models have good accuracy and high computational efficiency. They will allow introducing accurate simulation of mesh opening resistance in existing numerical formulations for marine netting structures without a high impact in their computational performance. In the future, the authors will apply these models to the static and dynamic analysis of such structures under hydrodynamic loads. Furthermore, they may also be useful to analyze data from experimental work to measure mesh resistance to opening, with the

intention of achieving a better goodness of fit with previous force models. However, several questions remain open and require further research, such as the behavior of force models No. 1 and No. 2 under large axial deformations.

Declaration of conflicting interests

The authors declare that there is no conflict of interest.

Funding

This research received no specific grant from any funding agency in the public, commercial, or not-for-profit sectors.

References

1. Ito S, Kinoshita T and Bao W. Hydrodynamic behaviours of elastic net sheets in waves. *Proc IMechE, Part M: J Engineering for the Maritime Environment* 2012; 226(2): 156–169.
2. Le Dret H, Lewandowski R, Priour D, et al. Numerical simulation of a cod end net part 1: equilibrium in a uniform flow. *J Elasticity* 2004; 76(2): 139–162.
3. Lee C-W, Lee J-H, Cha B-J, et al. Physical modeling for underwater flexible systems dynamic simulation. *Ocean Eng* 2005; 32(3–4): 331–347.
4. Li Y-C, Zhao Y-P, Gui F-K, et al. Numerical simulation of the hydrodynamic behaviour of submerged plane nets in current. *Ocean Eng* 2006; 33(17–18): 2352–2368.
5. O'Neill FG. Axisymmetric trawl cod-ends made from netting of a generalized mesh shape. *IMA J Appl Math* 1999; 62(3): 245–262.
6. Priour D. Calculation of net shapes by the finite element method with triangular elements. *Commun Numer Meth Eng* 1999; 15(10): 755–763.
7. Takagi T, Shimizu T, Suzuki K, et al. Validity and layout of “NaLA”: a net configuration and loading analysis system. *Fish Res* 2004; 66(2–3): 235–243.
8. Tsukrov I, Eroshkin O, Fredriksson D, et al. Finite element modeling of net panels using a consistent net element. *Ocean Eng* 2003; 30(2): 251–270.
9. Priour D, Herrmann B and O'Neill FG. Modelling axisymmetric cod-ends made of different mesh types. *Proc*

- IMechE, Part M: J Engineering for the Maritime Environment* 2009; 223(1): 137–144.
10. DeCew J, Tsukrov I, Risso A, et al. Modeling of dynamic behavior of a single-point moored submersible fish cage under currents. *Aquac Eng* 2010; 43(2): 38–45.
 11. Herrmann B, Priour D and Krag LA. Theoretical study of the effect of round straps on the selectivity in a diamond mesh cod-end. *Fish Res* 2006; 80(2–3): 148–157.
 12. Khaled R, Priour D and Billard J-Y. Numerical optimization of trawl energy efficiency taking into account fish distribution. *Ocean Eng* 2012; 54: 34–45.
 13. Lee J, Lee C-W, Choe M-Y, et al. Applying fishing-gear simulation software to better estimate fished space as fishing effort. *Fish Aquat Sci* 2011; 14(2): 138–147.
 14. Shimizu T, Takagi T, Korte H, et al. Application of NaLA, a fishing net configuration and loading analysis system, to bottom gill nets. *Fish Sci* 2007; 73(3): 489–499.
 15. Xu T-J, Dong G-H, Zhao Y-P, et al. Analysis of hydrodynamic behaviors of gravity net cage in irregular waves. *Ocean Eng* 2011; 38(13): 1545–1554.
 16. Herrmann B. Effect of catch size and shape on the selectivity of diamond mesh cod-ends: I. Model development. *Fish Res* 2005; 71(1): 1–13.
 17. Herrmann B and O'Neill FG. Theoretical study of the influence of twine thickness on haddock selectivity in diamond mesh cod-ends. *Fish Res* 2006; 80(2–3): 221–229.
 18. Sala A, Lucchetti A and Buglioni G. The influence of twine thickness on the size selectivity of polyamide codends in a Mediterranean bottom trawl. *Fish Res* 2007; 83(2–3): 192–203.
 19. O'Neill FG. The influence of bending stiffness on the deformation of axisymmetric networks. In: *Proceedings of the international conference on offshore mechanics and arctic engineering—OMAE*, Vancouver, BC, Canada, 20–25 June 2004, pp.749–754. New York: ASME.
 20. O'Neill FG and Xu L. Twine flexural rigidity and mesh resistance to opening. In: *ICES CM (1994/B:31)*, International Council for the Exploration of the Sea (ICES), Copenhagen, Denmark: 25–26 April 1994.
 21. O'Neill FG. Bending of twines and fibres under tension. *J Textil Inst* 2002; 93(1): 1–8.
 22. O'Neill FG. A theoretical study of the factors which influence the measurement of fishing netting mesh size. *Ocean Eng* 2003; 30(16): 2053–2063.
 23. Sala A, O'Neill FG, Buglioni G, et al. Experimental method for quantifying resistance to the opening of netting panels. *ICES J Marine Sci* 2007; 64(8): 1573–1578.
 24. Behbahani-Nejad M and Perkins NC. Hydrodynamic and geometric stiffening effects on the out-of-plane waves of submerged cables. *Nonlinear Dynam* 1997; 13(3): 243–257.
 25. Priour D. Introduction of mesh resistance to opening in a triangular element for calculation of nets by the finite element method. *Commun Numer Meth Eng* 2001; 17(4): 229–237.
 26. O'Neill FG and Priour D. Comparison and validation of two models of netting deformation. *J Appl Mech: T ASME* 2009; 76(5): 1–7.
 27. Peirce FT. The “Handle” of cloth as a measurable quantity. *J Textil Inst Trans* 1930; 21(9): T377–T416.
 28. Abbott GM. Yarn-bending and the weighted-ring stiffness test. *J Textil Inst* 1983; 74(5): 281–286.
 29. Du Z-Q, Zhou T, Yan N, et al. Measurement and characterization of bending stiffness for fabrics. *Fiber Polym* 2011; 12(1): 104–110.
 30. Lee C-W, Kim Y-B, Lee G-H, et al. Dynamic simulation of a fish cage system subjected to currents and waves. *Ocean Eng* 2008; 35(14–15): 1521–1532.
 31. Sala A, Lucchetti A and Buglioni G. The change in physical properties of some nylon (PA) netting samples before and after use. *Fish Res* 2004; 69(2): 181–188.
 32. Moe H, Olsen A, Hopperstad OS, et al. Tensile properties for netting materials used in aquaculture net cages. *Aquac Eng* 2007; 37(3): 252–265.
 33. De la Prada A and González M. Assessing the suitability of gradient-based energy minimization methods to calculate the equilibrium shape of netting structures. *Comput Struct* 2014; 135: 128–140.
 34. Herrmann B, Priour D and Krag LA. Simulation-based study of the combined effect on cod-end size selection of turning meshes by 90° and reducing the number of meshes in the circumference for round fish. *Fish Res* 2007; 84(2): 222–232.

Article No. 2

Quantifying mesh resistance to opening of netting panels: experimental method, regression models and parameter estimation strategies

Amelia de la Prada, Manuel González

Submitted to the *ICES Journal of Marine Science* on 10th April 2014

Revised version submitted on 30th May 2014

Revised version submitted on 17th June 2014

Accepted for publication on 23rd June 2014

Quantifying mesh resistance to opening of netting panels: experimental method, regression models and parameter estimation strategies

Amelia de la Prada, Manuel González*

Laboratorio de Ingeniería Mecánica — Universidade da Coruña
Escuela Politécnica Superior, Mendizábal s/n, 15403 Ferrol, Spain

E-mail address: amelia.delaprada@udc.es, manuel.gonzalez@udc.es

* Corresponding author. E-mail address: manuel.gonzalez@udc.es

Tel.: (+34) 981337400 fax: (+34) 981337410

Abstract

The increased mesh resistance to opening of netting panels manufactured with thick and stiff twines has a notable impact in the structural response and selective performance of the fishing gears. The only available method to quantify the mesh resistance to opening of netting panels was described in (Sala *et al.*, 2007b). We present an alternative method with a similar methodology: we attempt to estimate the mechanical and geometrical properties of a netting material that best fits the experimental measurements of a netting panel. We introduce three major contributions: (i) a considerably simpler uniaxial experimental setup, which stretches a netting sample in the normal direction of the meshes while leaving free its deformation in the transverse direction; (ii) more accurate theoretical models for mesh resistance to opening; (iii) new strategies to estimate the parameters of the models. We present the results of the analysis of polyethylene (PE), compacted polyethylene (CPE), single-twine and double-twine netting. Some of the assessed combinations of estimation strategies and theoretical models have an excellent goodness of fit with experimental data. The method proved to be a simple yet accurate way to quantify the mesh resistance to opening of netting panels.

Keywords: bending stiffness; flexural rigidity; mesh resistance to opening; twine; regression

Introduction

In recent years, there is a tendency in some sectors of the fishing industry towards the use of thicker and stiffer twines in the manufacture of netting materials for the codend of trawls. The increased mesh resistance to opening of such materials has a notable impact in the structural response and performance of the fishing gears. For example, an increased mesh resistance to opening hinders mesh opening in the cod-end (O'Neill, 2004), which affects the escapement of small fish. Theoretical and experimental studies demonstrate that mesh resistance to opening plays as major role in the reduction of selective performance of trawls (Herrmann and O'Neill, 2006; Herrmann *et al.*, 2013; Lowry and Robertson, 1996; Sala *et al.*, 2007a). Theoretical models for mesh resistance to opening are generally based on the beam theory of solid mechanics. In diamond mesh panels, the predominant netting in towed fishing gears, the resistance to opening is mainly characterized by the bending stiffness of the netting twine. An increased twine bending stiffness also changes the overall shape of the fishing gear during fishing operations (O'Neill, 2004; Priour, 2001). Therefore, methods to quantify the mesh resistance to opening and to incorporate this property in theoretical models of netting materials are necessary to accurately predict the selective performance of fishing gears by simulation. Despite this, research about this topic is still scarce (Priour and Cognard, 2011).

The only available method to quantify mesh resistance to opening of netting panels is described in (Sala *et al.*, 2007b). The method uses a specially designed instrument that applies normal and transversal displacements to a netting sample and measures the generated reaction forces. Then, twine bending stiffness and geometric parameters of the netting are estimated through nonlinear regression analysis of the obtained experimental data. The asymptotic solution for a bending twine proposed in (O'Neill,

2002) is used as model in the regression analysis. Although the method proved to be robust and useful to estimate mesh resistance to opening, the authors reported several problems: inconsistencies between normal and transversal forces and displacements, occasional unrealistic estimates of geometrical parameter values and systematic lack of fit of the model to the experimental data. Another concern is that the authors carried out the regression analysis using the force as independent variable and the displacement as dependent variable, despite the force was an effect caused by an applied displacement in the experimental setup. The complexity of the experimental setup required by this method is another important drawback.

A method to estimate twine bending stiffness was proposed by (Priour and Cognard, 2011). The method measures the out-of-plane bending deformation of a netting sample and then adjusts a theoretical model of a cantilever beam to the experimental data, in order to estimate the twine bending stiffness EI . The method is very simple, but it has some drawbacks. It does not take into account the knot size, which can have an important effect on the shape of the codends (*PREMECS: Development of predictive model of cod-end selectivity*, 2000). In addition, and it cannot estimate the slope angle between twines and knots at the insertion points.

The goal of this article is to describe a simple but accurate experimental method to quantify the mesh resistance to opening of netting panels. We follow a methodology similar to (Sala *et al.*, 2007b), that is, we attempt to estimate the mechanical and geometrical properties of a netting material that best fit the experimental measurements of a netting panel. This research introduces three original contributions:

(i) The biaxial experimental setup used in (Sala *et al.*, 2007b) requires a very complex measurement instrument which is not commercially available. In contrast, this work

proposes a new uniaxial experimental setup that notably simplifies the required measurement instrument.

(ii) The regression model used in (Sala *et al.*, 2007b) is the asymptotic model for a bending twine described in (O'Neill, 2002). This model is an approximate solution. This work uses more accurate models to describe mesh resistance to opening: the exact model described in (O'Neill, 2002) and two recently developed models based on finite element analysis (de la Prada and González, 2014a).

(iii) The parameter estimation strategy used in (Sala *et al.*, 2007b) fixed one of the geometrical properties of the netting (the slope angle between the twine and the knots) and leaved the remaining parameters unconstrained. As results, the estimates were sometimes out of physical limits. This work assesses other estimation strategies that avoid that problem.

Material and Methods

Theoretical models for mesh resistance to opening

Priour proposed a theoretical model for mesh resistance to opening based on the assumption that the couple created by mesh twines on the knot varies linearly with the angle between twines (Priour, 2001). Although this model can be easily introduced in numerical formulations for netting structures, it does not involve parameters with specific physical interpretation, and therefore it is not suited to identify the mechanical properties of the netting (e.g. twine bending stiffness) from experimental data.

O'Neill proposed a physically-oriented approach to the problem (O'Neill, 2002) by modelling the twine as a bi-dimensional double-clamped beam (Figure 1) and describing the equations governing its bending assuming that: (i) the slope angle θ

between the twine and the knots at the insertion points remains fixed, (ii) the bending moment is proportional to the curvature of the twine, (iii) there is no twine extension. He found two analytical solutions: the exact solution and an asymptotic solution. The exact solution expresses the coordinates of the end point of the twine \mathbf{p}_1 (Figure 1) as a set of implicit non-linear equations. To overcome the high complexity of the exact solution, the asymptotic solution expresses the coordinates of \mathbf{p}_1 as an explicit function of the tensile forces acting on it:

$$x_{twine} = L_{twine} \cos \beta + 4\sqrt{\frac{EI}{F}} \left\{ \cos\left(\frac{\theta + \beta}{2}\right) - \cos \beta \right\} \quad (1)$$

$$y_{twine} = L_{twine} \sin \beta + 4\sqrt{\frac{EI}{F}} \left\{ \sin\left(\frac{\theta + \beta}{2}\right) - \sin \beta \right\} \quad (2)$$

where θ is the slope angle between the twines and the knots at the insertion points, L_{twine} is the twine length, EI is the twine bending stiffness, $F = (F_x^2 + F_y^2)^{0.5}$,

$\beta = \tan^{-1}(F_y/F_x)$ and F_x and F_y are the tensile forces that act at the end of the twine.

This approximation is very close to the exact solution when $\varepsilon^2 = EI/(FL_{twine}^2) < 0.04$.

Both analytical solutions were used in (O'Neill, 2003) to study the factors influencing the measurement of netting mesh size. The asymptotic solution was used in (Sala *et al.*, 2007b) to develop an experimental method for quantifying mesh resistance to opening. It has been demonstrated that the model proposed in (Priour, 2001) can be modified to approximate the asymptotic solution for small values of ε^2 (O'Neill and Priour, 2009).

In (de la Prada and González, 2014a) a different approach was followed aiming at development of models that enable a fast and accurate evaluation of elastic forces in the twine as a function of its deformation. The mesh twine was also modelled as a double-clamped beam (Figure 1), but its force-displacement response was calculated by finite

element analysis (Zienkiewicz, 2000). Then, fitting techniques were used to develop two dimensionless models. The first model, named the polynomial model, fits a polynomial of the radial and tangential force components F_r and F_φ that act at the end of the twine. This results in a polynomial degree (m,n) of $(2,3)$ for F_r and $(1,4)$ for F_φ :

$$F_r(r, \varphi) = \left(\frac{EI}{L_{twine}^2} \right) \sum_{0 < i+j < m+n} c_{ij} r^i (\cos \varphi)^j \quad (3)$$

$$F_\varphi(r, \varphi) = \left(\frac{EI}{L_{twine}^2} \right) \sum_{0 < i+j < m+n} c_{ij} r^i (\cos \varphi)^j \quad (4)$$

where $r = (x_{twine}^2 + y_{twine}^2)^{0.5} / L_{twine}$, $\psi = \tan^{-1}(y_{twine}/x_{twine})$ and $\varphi = \psi - \theta$.

The second model, called the spline model, calculates F_r and F_φ as the gradient of the potential elastic energy V of the twine. V was interpolated with $(N_r - 1) \times (N_\varphi - 1)$ bicubic spline patches, where each patch (i, j) spans the rectangular region $[r_i, r_{i+1}] \times [\varphi_j, \varphi_{j+1}]$ and expresses V as:

$$V_{ij}(r, \varphi) = \left(\frac{EI}{L_{twine}} \right) \sum_{k=0}^3 \sum_{l=0}^3 c_{kl}^{ij} (r - r_i)^k (\varphi - \varphi_j)^l \quad (5)$$

A comprehensive description of the polynomial and spline models is provided in (de la Prada and González, 2014a), with comparisons to the abovementioned exact and asymptotic models described in (O'Neill, 2002). The spline model is very accurate and it is well suited for simulation methods based on energy minimization (de la Prada and González, 2014b). The polynomial model has a simpler mathematical form at the cost of a slightly lower accuracy (5% – 10% of deviation), as reported in (de la Prada and González, 2014a).

Experimental setup

The experimental setup is portrayed in Figure 2. A rectangular netting sample is attached between an upper fixed bar and a bottom free bar, with the normal direction of the meshes aligned to the vertical axis of the figure (i.e. perpendicular to the bars). The free bar can move in the normal direction of the netting while keeping its orientation parallel to the fixed bar. The attachment system between the netting sample and the bars allows the netting knots to freely move in the transverse direction of the netting when the sample is stretched. In this way, the force applied to meshes and twines in the transverse direction of the netting is zero. The panel has m_n and m_t netting meshes in normal and transverse direction respectively. During the experiment, the sample is stretched in the normal direction of the netting to open the meshes.

The sample is stretched by applying a force F_{panel} to the free bar. The normal length of the panel L_{panel} , defined as the distance between centres of the upper and bottom knots, is calculated as $L_{panel} = D_0 - (D_R + D_L)/2 - D_1 - D_2$, where distances D_0 , D_1 and D_2 are measured at the beginning of the experiment and distances D_R and D_L are measured for each value of F_{panel} (both distances should be equal in theory, but in practice slight differences can appear due to misalignment of the free bar). F_{panel} is generated by applying calibrated weights to the free bar. The weight of the free bar (0.68 N) and mounting hooks (0.04 N each) is also included in F_{panel} . Distances D_1 and D_2 are measured with a Vernier calliper, while distances D_0 , D_R and D_L are measured with digital laser rangefinders with an accuracy of ± 0.5 mm. Other measuring procedures are also compatible with the experimental setup described in Figure 2: for example, L_{panel} could be prescribed and the required F_{panel} could be measured.

The objective of this work is not to quantify the mesh resistance to opening for a wide range of netting materials, but rather to investigate different combinations of regression models and parameter estimation strategies for the proposed uniaxial experimental setup. Hence, a number of new and unused netting samples were tested. All of them are used in commercial North Sea trawls. Their main characteristics are given in Table 1: materials are sorted according to the perceived mesh resistance to opening from manual manipulation of the netting, from low (PE 80×2.5) to high (CPE2 80×4) stiffness.

The following steps were performed for each netting sample:

- i. The netting is attached to the bars and distances D_1 and D_2 are measured. At this moment F_{panel} is equal to the weight of the bottom free bar and hooks (0.7 N).
- ii. F_{panel} is increased. Load increments start with 0.5 N and increase up to a maximum value of 9.8 N as L_{panel} increases.
- iii. Distances D_R and D_L are measured at every minute to monitor netting twine relaxation (Sala *et al.*, 2007b); when they get stabilized, the final values are recorded.
- iv. Steps (ii) and (iii) are repeated until L_{panel} reaches 80% of $m_n \cdot L_{mesh}$, where L_{mesh} is the nominal mesh size. Above this value, the main characteristic contributing to mesh resistance to opening is twine axial stiffness EA rather than twine bending stiffness EI (de la Prada and González, 2014a).

Netting materials used in fishing gears may experience high tensile forces able to generate permanent plastic deformations in twines and knots. To simulate such situation in the experimental setup, the maximum value of F_{panel} reached in step (iv) is applied for one hour to the netting. Then steps (ii) and (iii) are repeated with decreasing values of

F_{panel} in step (ii). In this way two sets of data are obtained: a loading cycle and an unloading cycle.

Data analysis

To analyse the experimental data it is necessary to make the same assumptions as in (Sala *et al.*, 2007b), which define the idealized panel represented in Figure 3: (i) the netting is homogeneous, so all the meshes experience the same deformation, (ii) knots can be represented as rectangles of size $a \times b$, and (iii) twines emerge from knots at the corners of the rectangles. Note that the knot size $a \times b$ is smaller than the measured outer knot size $a_{ext} \times b_{ext}$ given in Table 1. The mechanical and geometrical parameters of this idealized netting panel are estimated by fitting theoretical models for mesh resistance to opening to experimental data. The observed variable in the experiment is the distance between twine knots in the normal direction of the netting

$$y_{knots} = L_{panel} / 2m_n \quad (6)$$

and the explanatory variable is the vertical force applied to the twines

$$F_y = F_{panel} / 2m_t \quad (7)$$

The predicted values for the distance between knots can be expressed as

$$\hat{y}_{knots} = b + y_{twine}(EI, L_{twine}, \theta) \quad (8)$$

where y_{twine} can be calculated with any theoretical model for mesh resistance to opening. Therefore, four parameters can be estimated: EI , L_{twine} , b and θ . Notice that the knot dimension a cannot be estimated with the proposed experimental setup because the transversal length of the panel is not measured. Preliminary analysis show that there are not outlier points in the experimental data. For simplicity, the observed and the

explanatory variables are assumed to be distributed with constant variance. Therefore, nonlinear least squares regression is used (Seber, 1989).

With respect to the regression model $y_{twine}(EI, L_{twine}, \theta)$ in Eq. (8), the four models for mesh resistance to opening described in Section 2 were assessed: the exact model, the asymptotic model, the polynomial model and spline model. The use of the asymptotic model is straightforward, since it provides y_{twine} as an explicit function of the explanatory variable F_y . The other models need to be numerically solved for every evaluation in the regression analysis.

A remark must be made regarding the use of the asymptotic model in this experimental setup, where $F_x = 0 \Rightarrow \beta = \tan^{-1}(F_y/F_x) = \Pi/2$ in Eq. 1 and 2. The asymptotic approximation is very close to the exact solution when $\varepsilon^2 < 0.04$ (O'Neill, 2002), but ε^2 usually ranges from 0.4 and 0.1 in most part of the loading and unloading cycles of our experiments. This is explained in Figure 4, which shows the dimensionless vertical displacement of the twine calculated with Eq. 2 for $\beta = \Pi/2$, as a function of the parameter $\varepsilon^2 = EI/(FL_{twine}^2)$ and the slope angle θ . Since $F_x = 0$, the mesh can be opened in normal direction with a relatively small force. Hence, the condition $\varepsilon^2 < 0.04$ can only be achieved provided that θ is small and the mesh is nearly completely opened ($y_{twine}/L_{twine} \geq 0.75$). The only way to achieve $\varepsilon^2 < 0.04$ without completely opening the mesh is to apply a transversal force $F_x > 0$ to reduce β as in the experimental setup used in (Sala *et al.*, 2007b). Nevertheless, (de la Prada and González, 2014a) shows that the vertical position of the twine y_{twine} predicted by the asymptotic model is close to the exact model even if $\beta = \Pi/2$ (relative error below 10% in most of the range of displacement), because most of the error in this model is in the horizontal position x_{twine} .

As a result, the asymptotic solution can still be used as model in this experimental setup, but caution should be taken to interpret its goodness of fit.

Parameter estimation strategies

Regression analysis can generate parameter estimates that are out of physical limits. For example, (Sala *et al.*, 2007b) reported that the estimates for θ were often negative, which is physically impossible. To circumvent this problem, constraints can be applied to the parameters. Table 2 summarizes the two types of parameter constraints considered in this work.

A fixed constraint means to remove the parameter from the regression analysis, which greatly reduces the required computational effort. For example, (Sala *et al.*, 2007b) fixed θ to 0° to avoid negative estimates, and this constraint was also considered in this work. Fixed constraints for L_{twine} and b are obtained by assuming that the knot size $a \times b$ matches $2D_{twine}^* \times D_{twine}^*$, with $D_{twine}^* = D_{twine}$ for single twine netting and $D_{twine}^* = 2D_{twine}$ for double twine netting. This is a plausible assumption after a visual inspection of several netting samples (see Figure 3).

Another approach is to constrain parameters between minimum and maximum physical limits. The limits for L_{twine} and b are obtained by assuming that the knot size $a \times b$ can be neither negative nor greater than $a_{ext} \times b_{ext}$. A minimum value of 5° for θ seems reasonable to avoid knot overlapping when no forces are applied to the netting, and it is also consistent with visual observations in the netting samples.

Finally, the different constraints listed in Table 2 were combined to form the four parameter estimation strategies summarized in Table 3. All of them were assessed in this work.

Results

Figure 5 shows an example of the data sets obtained in the loading cycle and in the unloading cycle. The number of recorded measurements in every netting panel and cycle ranged between 17 and 21. The two data sets are quite different. The length of the panel L_{panel}^{end} at the end of the unloading cycle is higher than the length L_{panel}^{start} at the beginning of the loading cycle. The ratio $L_{panel}^{end} / L_{panel}^{start}$ is higher in PE netting samples (1.52 on average) than in the CPE sample (1.23) or the CPE2 sample (1.37). The two data sets were analysed separately to quantify the mesh resistance to opening.

Loading cycle

Table 4 shows the results of the nonlinear regression with unconstrained parameters (parameter estimation strategy No. 1). Confidence intervals for estimates of EI are represented as a percentage; confidence intervals for other parameters are omitted because they are of the same order of magnitude as confidence intervals for estimates of EI . The goodness of fit is measured with the coefficient of determination R^2 . Results indicate that all models can fit a diverse variety of experimental data sets, as represented by their ability to achieve very high R^2 values at the cost of providing estimates of L_{twine} , b and θ that are often out of their physical limits. Estimates of EI are inconsistent in some cases. For example, the estimates for PE 80×4 and PE 100×4 are very different, despite their stiffness seems very similar when they are manipulated by hand.

This unconstrained regression analysis exposed the degree of correlation in the parameters of two models. The exact model generates several solutions with $R^2 > 0.99$, showing some degree of correlation between parameters: Figure 6 reveals a nonlinear correlation between EI and θ , and a linear correlation between b and L_{twine} .

Nevertheless, it is easy to select the best solution, since most of them have unrealistic parameter estimates: among the solutions with plausible estimates, the one with highest R^2 is listed in Table 4. The asymptotic model exhibits a very strong correlation between EI and θ , and between b and L_{twine} (Figure 6). It generates multiple solutions with identical R^2 , most of them with plausible estimates, so it is not possible to identify the best solution. Hence, results for this model are not listed in Table 4. An analysis of Eq. (2) and Eq. (8) reveals that parameters are not identifiable for this regression model because its basis functions are not orthogonal when β is constant (Seber, 1989).

Table 5 shows the results of the regression with min/max constraints on all the parameters (parameter estimation strategy No. 2). Despite the constraints on the parameters, R^2 values are almost as high as in Table 4. Confidence intervals for the spline model are unusually high. Table 6 shows the results for the parameter estimation strategy No. 3, which applies fixed constraints on L_{twine} and b and min/max constraints on θ . In this strategy, the fixed values for L_{twine} and b correlate with visual observations of the netting. Furthermore, the computational effort of the regression analysis is reduced by about one order of magnitude with respect to the previous estimation strategies (e.g. from 10 minutes to 20 seconds for the polynomial and the spline models). R^2 values are still very high, confidence intervals are reduced and the estimates of EI obtained with the three models are closer to each other than in Table 4 and Table 5. Notice that the constraint on θ was activated in only one netting sample (PE 80×3). Regarding the asymptotic model, the strong correlation between EI and θ is still present in this analysis.

Finally, Table 7 shows the results with a fixed constraint on θ and leaving the remaining parameters unconstrained (parameter estimation strategy No. 4), as in the

analysis carried out in (Sala *et al.*, 2007b). With this estimation strategy, the asymptotic model can only estimate EI , and therefore L_{twine} and b are not listed for this model. R^2 values are high except when the asymptotic model is applied to very stiff materials (CPE 80×5 and CPE2 80×4). However, estimates of EI are inconsistent for all models: estimates for stiff materials (PE 80×4 and PE 100×4) are very similar to estimates for very soft materials (PE 80×2.5 and PE 100×2.5), which seems abnormal. In addition, estimates of L_{twine} and b are often out of physical limits.

A visual inspection of the residual plots of all the analysis confirm that the models have a very good fit when $R^2 > 0.98$. R^2 values between 0.9 and 0.98 often under-predict the experimental data, and values below 0.9 correspond to inaccurate fits. Results from the parameter estimation strategies No. 2 (Table 5) and No. 3 (Table 6) are summarized in Figure 7 and Figure 8. Figure 7 shows a box plot of the R^2 values for different combinations of estimation strategies and regression models. Figure 8 plots the estimates of EI against the linear density of the netting (kRtex).

Unloading cycle

Parameter estimation strategies No. 1 and 4 have not been used for the unloading cycle due to the disadvantages exposed in the loading cycle. Table 8 shows the results with the strategy No 2: min/max constraints on all the parameters (compare to the loading cycle in Table 5). R^2 values are very good for stiff materials and acceptable for soft materials. Estimates of θ are considerably increased in all materials compared with the loading cycle. Visual observations of the netting samples after the experiment also show an increased θ , but it is not as high as the estimated values. Average estimates of EI are slightly lower than in the loading cycle. The polynomial and spline models exhibit very wide confidence intervals in some cases.

Table 9 shows the results with fixed constraints on L_{twine} and b , and min/max constraints on θ (compare to the loading cycle in Table 6). Fittings for PE netting samples have $R^2 < 0.9$, which indicates a poor fit. This fact is confirmed by a visual inspection of the residual plots. Conversely, CPE 80×5 shows acceptable R^2 values and CPE2 80×4 shows very good fits. For these stiff materials, EI estimates are of the same order of magnitude than those calculated for the loading cycle.

Discussion

The proposed uniaxial experimental setup has a major advantage over the biaxial setup used in the ROD-m prototype instrument developed in (Sala *et al.*, 2007b): it can be carried out in standard uniaxial universal testing machines, provided special fixtures are mounted to allow the attached knots to freely move in the transverse direction of the netting. Even if such a machine is not available, the experiment can be easily carried out by manual means with a simple and inexpensive setup, as in this work. On the other hand, the uniaxial experimental setup does not provide measurements of transverse data and the knot width a cannot be directly estimated from the experiment. However, the good results obtained with the parameter estimation strategy No. 3, based on simple assumptions about the values of L_{twine} and b , suggest that the knot width a could also be estimated as $a = (L_{mesh} - 2L_{twine})/2$. Note that better approximations could be obtained using the results from (O'Neill, 2003).

The data analysis assumed that all the meshes experience the same deformation. This assumption is not completely true because the panel was held in vertical position during the experiment. Twines at the top of the panel support more weight than twines at the bottom due to the mass of the netting. The ratio of the weight of the netting to the weight of the free bar ranged from 0.34 (PE 100×2.5) to 1.51 (CPE2 80×4). The ratio of

the weight of the netting to the maximum applied force ranged from 1.7% to 2.5%. Hence, the assumption about uniform mesh deformation is plausible except at the beginning of the loading cycle and at the end of the unloading cycle. The assumption would be correct during all the cycle provided the panel was hold in horizontal position.

Regarding the parameter estimation strategies, strategies No. 1 and No. 4 do not offer advantages over the others, and, in fact, have important disadvantages: estimates of EI are inconsistent and estimates of geometrical parameters are often out of physical limits. The other two strategies have their own advantages and disadvantages. Strategy No. 2 (min/max constraints on all parameters) provides slightly better fits, but Strategy No. 3 (fixed constraints on L_{twine} and b and min/max constraints on θ) simplifies the analysis, narrows the confidence intervals and provides EI estimates that are closer across different models. Moreover, the min/max constraint on θ is hardly activated and could be removed, resulting in an even simpler unconstrained regression analysis. The lower computational effort required by Strategy No. 3 can be an advantage when the number of experimental data points is high (e.g. hundreds of points). In these cases, Strategy No. 2 can take hours to analyse the experimental data while Strategy No. 3 can take minutes. The main disadvantage of strategy No. 3 is that it cannot provide good fits for the unloading cycle, except for the very stiff materials. It seems that the large mesh opening applied to PE netting samples before the unloading cycle has introduced permanent deformations in the twines which cause it to not match the idealized netting material described in Figure 1 and Figure 3. On the contrary, the permanent deformations in CPE netting samples seem to be small due to their increased stiffness and strength, and therefore, analysis results for their unloading cycles are still quite acceptable.

Regarding the regression models, the asymptotic model exhibits identifiability problems in the proposed uniaxial experimental setup. Similar problems of correlation between parameters have been already reported in (Sala *et al.*, 2007b). All three of the other models provide similar and very good fits. The exact model seems more reliable due to its narrower confidence intervals. However, this comes at the cost of a very complex computer implementation. The polynomial and spline models are easier to implement, but they provide wider confidence intervals. The variations in estimates provided by different models may seem surprising. However, the estimates are not absolute measurements of the netting properties, but rather calibration parameters for different theoretical models, as observed in (Sala *et al.*, 2007b). Therefore, the model used to analyse the experimental data should be the same model that will be used to make predictions of the netting behaviour. For example, to simulate gear behaviour (Lee *et al.*, 2005; Li *et al.*, 2006; Priour, 1999; Priour *et al.*, 2009; Takagi *et al.*, 2004) or codend selectivity (Herrmann, 2005; O'Neill and Herrmann, 2007).

A detailed analysis of the fits revealed that the estimates given by the exact and spline models are interchangeable. See, for example, the estimates for CPE 80×5 in Table 5. They are very different, but when the exact model is evaluated with the parameters estimated with the spline model, it provides a R^2 value of 0.9987. Conversely, when the spline model is evaluated with the parameters estimated with the exact model, it provides a R^2 value of 0.9988. Visual inspections of the residual plots confirm that both fits are extremely good and virtually identical. On the contrary, estimates from the polynomial model are not interchangeable with other models. This behavior agrees with the numerical experiments in (de la Prada and González, 2014a), which showed that the exact and spline models provide almost identical results. In fact, this also suggests that the narrow confidence intervals of the exact model are not realistic, since very similar

goodness of fits can be obtained with very different parameter values. In this sense, the wide confidence intervals of the spline model seem more realistic.

The *EI* estimates obtained with our best estimation strategies (Figure 8) are smaller than those obtained in (Sala *et al.*, 2007b) for similar materials. It is difficult to compare the results from both works because (Sala *et al.*, 2007b) does not provide qualitative or quantitative indicators of the goodness of fit.

The difference between the loading and the unloading experimental data sets seems a result of the plastic deformations in the netting due to long-term exposure to high stress. Such plastic deformations may be related to viscoelastic creep, which can occur in polymers at room temperatures (McCrum *et al.*, 1997). The available theoretical models for mesh resistance to opening assume a lineal material, and therefore they can only predict the behaviour of netting that operates in the linear range. They cannot be used to predict plastic deformations. For this reason, the loading and the unloading cycles need to be analysed separately, and the data analysis gives different parameter estimates in both cycles. In fact, Figure 5 shows that the mesh resistance to opening is different in both cycles. This result suggests that further research is required to investigate how the loading history affects the mesh resistance to opening of netting during the lifespan of a fishing gear.

Some objections can be made to the experiments presented in this work. In (Sala *et al.*, 2007b), a series of pretension cycles were applied to the netting samples to remove the irreversible part of the elongation and to safeguard against knot slippage (Sala *et al.*, 2004). We applied such pretension by manual means, which obviously cannot achieve the high tensile loads applied in (Sala *et al.*, 2007b). However, we believe that this does not invalidate the excellent results obtained with the proposed combination of

experimental setup, regression models and estimation strategies. Another concern is that several samples of the same material should be tested in order to obtain average estimates of mesh resistance to opening, as in (Sala *et al.*, 2007b). Due to resource limitations, we only tested one sample per material, which means that the obtained estimates may be affected by irregularities or defects in the sample. Nonetheless, as stated in the Introduction, the goal of this work is not to quantify the mesh resistance to opening for a range of netting materials, but rather to investigate the soundness of the presented method.

Conclusions

The method we have presented proved to be a simple yet effective method to quantify the mesh resistance to opening of netting panels. Its main advantage over the method described in (Sala *et al.*, 2007b) is the simplicity of our uniaxial experimental setup, which does not require complex and specially designed measuring instruments. In fact, our experiment can be carried out by manual means or in standard universal testing machines with inexpensive modifications of clamps and fixtures. The advantage over the method described in (Priour and Cognard, 2011) is that the presented method takes into account the knot size and can estimate the angle θ .

We recommend starting the data analysis assuming that $L_{twine} = L_{mesh}/2 - 2D_{twine}$ and $b = D_{twine}$, in order to estimate EI and θ with an unconstrained nonlinear regression. This kind of analysis is simple and fast, and often provides excellent results when the netting material has not suffered permanent plastic deformations due to large mesh opening. If this analysis fails to provide a good fit, a second analysis should be carried out to estimate the four parameters EI , L_{twine} , b , and θ with a min/max constrained nonlinear regression using the parameter limits listed in Table 2. This approach always provides

good fits and parameter estimates within physical limits. Our method does not allow one to estimate the knot width a from experimental data, although it could be estimated as $a = (L_{mesh} - 2L_{twine})/2$. Better approximations might be obtained using the results from (O'Neill, 2003).

The three theoretical models – exact, polynomial and spline – for mesh resistance to opening provide very similar goodness of fit. We recommend analysing the experimental data with the same model that will be used to predict netting deformations. It was found that the loading history can modify the mesh resistance to opening of a netting panel. Further research is required to investigate this issue.

References

- De la Prada, A., and González, M. 2014a. Nonlinear stiffness models of a net twine to describe mesh resistance to opening of flexible net structures. Proceedings of the Institution of Mechanical Engineers, Part M: Journal of Engineering for the Maritime Environment, In press.
- De la Prada, A., and González, M. 2014b. Assessing the suitability of gradient-based energy minimization methods to calculate the equilibrium shape of netting structures. Computers & Structures, 135: 128–140.
- Herrmann, B. 2005. Effect of catch size and shape on the selectivity of diamond mesh cod-ends: I. Model development. Fisheries Research, 71: 1–13.
- Herrmann, B., and O'Neill, F. G. 2006. Theoretical study of the influence of twine thickness on haddock selectivity in diamond mesh cod-ends. Fisheries Research, 80: 221–229.
- Herrmann, B., Wienbeck, H., Moderhak, W., Stepputtis, D., and Krag, L. A. 2013. The influence of twine thickness, twine number and netting orientation on codend selectivity. Fisheries Research, 145: 22–36.
- Lee, C.-W., Lee, J.-H., Cha, B.-J., Kim, H.-Y., and Lee, J.-H. 2005. Physical modeling for underwater flexible systems dynamic simulation. Ocean Engineering, 32: 331–347.
- Li, Y.-C., Zhao, Y.-P., Gui, F.-K., and Teng, B. 2006. Numerical simulation of the hydrodynamic behaviour of submerged plane nets in current. Ocean Engineering, 33: 2352–2368.
- Lowry, N., and Robertson, J. H. B. 1996. The effect of twine thickness on cod-end selectivity of trawls for haddock in the North Sea. Fisheries Research, 26: 353–363.

- McCrum, N. G., Buckley, C. P., and Bucknall, C. B. 1997. *Principles of Polymer Engineering*. Oxford University Press. 464 pp.
- O'Neill, F. G. 2002. Bending of twines and fibres under tension. *Journal of the Textile Institute*, 93: 1–8.
- O'Neill, F. G. 2003. A theoretical study of the factors which influence the measurement of fishing netting mesh size. *Ocean Engineering*, 30: 2053–2063.
- O'Neill, F. G. 2004. The Influence of Bending Stiffness on the Deformation of Axisymmetric Networks. *In ASME 2004 23rd International Conference on Offshore Mechanics and Arctic Engineering*, pp. 749–754. ASME.
- O'Neill, F. G., and Herrmann, B. 2007. PRESEMO - A predictive model of codend selectivity - A tool for fishery managers. *ICES Journal of Marine Science*, 64: 1558–1568.
- O'Neill, F. G., and Priour, D. 2009. Comparison and validation of two models of netting deformation. *Journal of Applied Mechanics, Transactions ASME*, 76: 1–7.
- PREMECS: Development of predictive model of cod-end selectivity. 2000. European Project FAIR Programme CT96 1555. http://www.ifremer.fr/web-com/dpriour/web/papers/2000_premecs_final_report.pdf.
- Priour, D. 1999. Calculation of net shapes by the finite element method with triangular elements. *Communications in Numerical Methods in Engineering*, 15: 755–763.
- Priour, D. 2001. Introduction of mesh resistance to opening in a triangular element for calculation of nets by the finite element method. *Communications in Numerical Methods in Engineering*, 17: 229–237.
- Priour, D., and Cognard, J.-Y. 2011. Investigation of Methods for the Assessment of the Flexural Stiffness of Netting Panels. *In Proceedings of the 10th DEMaT Workshop*, October 26th-29th. Split.
- Priour, D., Herrmann, B., and O'Neill, F. G. 2009. Modelling axisymmetric cod-ends made of different mesh types. *Proceedings of the Institution of Mechanical Engineers Part M: Journal of Engineering for the Maritime Environment*, 223: 137–144.
- Sala, A., Lucchetti, A., and Buglioni, G. 2004. The change in physical properties of some nylon (PA) netting samples before and after use. *Fisheries Research*, 69: 181–188.
- Sala, A., Lucchetti, A., and Buglioni, G. 2007a. The influence of twine thickness on the size selectivity of polyamide codends in a Mediterranean bottom trawl. *Fisheries Research*, 83: 192–203.
- Sala, A., O'Neill, F. G., Buglioni, G., Lucchetti, A., Palumbo, V., and Fryer, R. J. 2007b. Experimental method for quantifying resistance to the opening of netting panels. *ICES Journal of Marine Science*, 64: 1573–1578.
- Seber, G. A. F. 1989. *Nonlinear regression*. Wiley series in probability and mathematical statistics. Wiley, New York. 768 pp.
- Takagi, T., Shimizu, T., Suzuki, K., Hiraishi, T., and Yamamoto, K. 2004. Validity and layout of 'NaLA': A net configuration and loading analysis system. *Fisheries Research*, 66: 235–243.
- Zienkiewicz, O. C. 2000. *The finite element method*. Butterworth-Heinemann, Oxford; Boston.

TABLES

Table 1. Main characteristics of the netting samples: nominal stretched mesh size (L_{mesh}), nominal twine diameter (D_{twine}), external knot width (a_{ext}) and height (b_{ext}), number of meshes in transverse (m_t) and normal (m_n) directions and linear density (Rtex). Material codes: PE is traditional single twine greed-braid polyethylene, CPE is single twine compacted polyethylene and CPE2 is double-twine compacted polyethylene.

Netting	L_{mesh} (mm)	D_{twine} (mm)	a_{ext} (mm)	b_{ext} (mm)	$m_t \times m_n$	Rtex (g/1000m)
PE 80×2.5	80	2.5	8.5	5.5	4×8	2540
PE 100×2.5	100	2.5	8.5	5.5	3×10	2870
PE 80×3	80	3	11.0	6.0	3×12	4225
PE 80×4	80	4	12.5	8.5	3×10	5623
PE 100×4	100	4	12.5	8.5	3×8	6474
CPE 80×5	80	5	16.0	12.0	3×8	11423
CPE2 80×4	80	4	25.0	14.0	2×5	12310

Table 2. Constraints that can be applied to the parameters in the regression analysis. $D_{twine}^* = D_{twine}$ for single twine netting and $D_{twine}^* = 2D_{twine}$ for double twine netting.

Constraint	EI	L_{twine}	b	θ
Fixed	-	$L_{mesh}/2 - 2D_{twine}^*$	D_{twine}^*	0°
Min/max	Min	$L_{mesh}/2 - a_{ext}$	0	5°
	Max	$L_{mesh}/2$	b_{ext}	90°

Table 3. Description of the different parameter estimation strategies used in the regression analysis.

Estimation strategy	Constraint applied on parameter		
	L_{twine}	b	θ
1	-	-	-
2	Min/max	Min/max	Min/max
3	Fixed	Fixed	Min/max
4	-	-	Fixed

Table 4. Results of the analysis with unconstrained parameters (parameter estimation strategy No. 1), loading cycle.

Netting	Model	EI (N/mm ²)	L_{twine} (mm)	b (mm)	θ (deg)	R^2
PE 80×2.5	Exact	23 ± 6%	28	9.9	0	0.9995
	Polynomial	58 ± 23%	53	-16.8	22	0.9995
	Spline	10 ± 3%	20	17.9	-21	0.9996
PE 100×2.5	Exact	21 ± 22%	37	9.3	-2	0.9956
	Polynomial	22 ± 39%	32	13.6	4	0.9973
	Spline	10 ± 34%	24	21.8	-17	0.9930
PE 80×3	Exact	28 ± 60%	27	11.4	-1	0.9965
	Polynomial	33 ± 36%	32	5.1	6	0.9984
	Spline	13 ± 9%	19	18.8	-21	0.9969
PE 80×4	Exact	92 ± 66%	32	3	19	0.9995
	Polynomial	107 ± 31%	43	-10.0	25	0.9994
	Spline	50 ± 86%	25	9.7	9	0.9996
PE 100×4	Exact	33 ± 9%	21	23	0	0.9991
	Polynomial	85 ± 38%	41	2.4	22	0.9987
	Spline	19 ± 8%	17	26.7	-12	0.9993
CPE 80×5	Exact	153 ± 7%	22	15.6	1	0.9998
	Polynomial	140 ± 31%	25	10.2	7	0.9974
	Spline	181 ± 6%	23	14.5	4	0.9997
CPE2 80×4	Exact	1001 ± 70%	34	1.7	25	0.9996
	Polynomial	289 ± 32%	24	9.7	10	0.9986
	Spline	238 ± 10%	19	16.3	0	0.9992

Table 5. Results of the analysis with min/max constraints on all the parameters (parameter estimation strategy No. 2), loading cycle.

Netting	Model	EI (N/mm ²)	L_{twine} (mm)	b (mm)	θ (deg)	R^2
PE 80×2.5	Exact	27 ± 2%	35.2	2.0	7	0.9928
	Polynomial	33 ± 37%	36.8	0.0	11	0.9979
	Spline	32 ± 214%	33.7	3.8	8	0.9991
PE 100×2.5	Exact	27 ± 1%	45.4	0.9	5	0.9926
	Polynomial	31 ± 44%	41.5	3.7	12	0.9956
	Spline	30 ± 261%	41.5	3.8	10	0.9872
PE 80×3	Exact	57 ± 1%	35.5	2.8	15	0.9931
	Polynomial	34 ± 36%	32.8	4.6	7	0.9984
	Spline	39 ± 395%	32.4	5.3	8	0.9946
PE 80×4	Exact	119 ± 2%	32.0	3.8	19	0.9949
	Polynomial	66 ± 8%	33.4	0.0	17	0.9987
	Spline	67 ± 98%	27.9	6.3	15	0.9996
PE 100×4	Exact	159 ± 1%	42.0	2.8	29	0.9983
	Polynomial	85 ± 38%	41.0	2.4	23	0.9987
	Spline	111 ± 220%	37.6	6.3	25	0.9986
CPE 80×5	Exact	445 ± 1%	32.4	6.1	18	0.9993
	Polynomial	159 ± 36%	26.5	8.8	9	0.9973
	Spline	244 ± 71%	25.8	11.5	10	0.9997
CPE2 80×4	Exact	683 ± 1%	28.5	7.4	18	0.9993
	Polynomial	294 ± 33%	24.2	9.5	10	0.9986
	Spline	373 ± 111%	22.5	12.4	9	0.9993

Table 6. Results of the analysis with fixed constraints on L_{rvine} and b and min/max constraints on θ (parameter estimation strategy No. 3), loading cycle.

Netting	Model	EI (N/mm ²)	L_{rvine} (mm)	b (mm)	θ (deg)	R^2
PE 80×2.5	Exact	34 ± 1%	35	2.5	10	0.9955
	Polynomial	33 ± 6%	35	2.5	10	0.9938
	Spline	35 ± 6%	35	2.5	10	0.9990
PE 100×2.5	Exact	39 ± 2%	45	2.5	9	0.9814
	Polynomial	56 ± 24%	45	2.5	17	0.9182
	Spline	77 ± 39%	45	2.5	23	0.9464
PE 80×3	Exact	29 ± 2%	34	3	5	0.9765
	Polynomial	35 ± 6%	34	3	9	0.9974
	Spline	37 ± 25%	34	3	9	0.9914
PE 80×4	Exact	126 ± 3%	32	4	19	0.9920
	Polynomial	99 ± 12%	32	4	15	0.9780
	Spline	126 ± 11%	32	4	19	0.9904
PE 100×4	Exact	219 ± 2%	42	4	30	0.9873
	Polynomial	164 ± 14%	42	4	24	0.9759
	Spline	218 ± 13%	42	4	29	0.9852
CPE 80×5	Exact	248 ± 2%	30	5	19	0.9914
	Polynomial	198 ± 5%	30	5	15	0.9958
	Spline	273 ± 6%	30	5	20	0.9946
CPE2 80×4	Exact	310 ± 3%	24	8	18	0.9852
	Polynomial	233 ± 7%	24	8	13	0.9938
	Spline	314 ± 10%	24	8	18	0.9881

Table 7. Results of the analysis with fixed constraint $\theta = 0^\circ$ (parameter estimation strategy No. 4), loading cycle. Low R^2 values are marked in bold font.

Netting	Model	EI (N/mm ²)	L_{pvine} (mm)	b (mm)	R^2
PE 80×2.5	Exact	24 ± 3%	28.4	9.7	0.9995
	Polynomial	20 ± 9%	27.5	9.4	0.9930
	Spline	22 ± 4%	28.1	9.4	0.9992
	Asymptotic	41 ± 10%	-	-	0.9936
PE 100×2.5	Exact	23 ± 17%	37.9	8.7	0.9956
	Polynomial	18 ± 6%	27.9	17.6	0.9969
	Spline	19 ± 13%	32.3	13.2	0.9896
	Asymptotic	37 ± 21%	-	-	0.9812
PE 80×3	Exact	29 ± 8%	27.7	10.7	0.9964
	Polynomial	26 ± 6%	27.4	10.1	0.9979
	Spline	27 ± 10%	27.2	10.6	0.9952
	Asymptotic	49 ± 20%	-	-	0.9876
PE 80×4	Exact	35 ± 4%	20.6	13.9	0.9995
	Polynomial	28 ± 12%	21.1	12.2	0.9929
	Spline	33 ± 4%	20.3	13.8	0.9996
	Asymptotic	39 ± 31%	-	-	0.9574
PE 100×4	Exact	33 ± 5%	21.2	23.2	0.9991
	Polynomial	28 ± 10%	21.8	21.7	0.9934
	Spline	31 ± 5%	20.9	23.1	0.9991
	Asymptotic	41 ± 31%	-	-	0.9656
CPE 80×5	Exact	148 ± 5%	21.2	15.9	0.9998
	Polynomial	97 ± 14%	21.0	13.9	0.9960
	Spline	144 ± 5%	21.0	15.9	0.9998
	Asymptotic	30 ± 56%	-	-	0.7612
CPE2 80×4	Exact	240 ± 11%	18.8	16.1	0.9988
	Polynomial	164 ± 13%	18.8	14.3	0.9968
	Spline	233 ± 11%	18.6	16.1	0.9989
	Asymptotic	32 ± 64%	-	-	0.7161

Table 8. Results of the analysis with min/max constraints on all the parameters (parameter estimation strategy No. 2), unloading cycle.

Netting	Model	EI (N/mm ²)	L_{twine} (mm)	b (mm)	θ (deg)	R^2
PE 80×2.5	Exact	23 ± 0.4%	34.0	0.1	49	0.9897
	Polynomial	17 ± 195%	31.5	2.2	46	0.9798
	Spline	24 ± 219%	31.5	2.3	51	0.9873
PE 100×2.5	Exact	21 ± 1%	41.7	1.7	41	0.9871
	Polynomial	15 ± 85%	41.5	0.3	46	0.9617
	Spline	49 ± 255%	41.6	1.1	56	0.9724
PE 80×3	Exact	31 ± 0.3%	35.1	0.2	50	0.9903
	Polynomial	12 ± 108%	30.6	3.8	44	0.9635
	Spline	12 ± 92%	31.2	3.2	44	0.9637
PE 80×4	Exact	41 ± 0.4%	30.6	1.4	48	0.9860
	Polynomial	22 ± 78%	29.2	2.1	44	0.9907
	Spline	42 ± 137%	27.6	4.0	50	0.9930
PE 100×4	Exact	107 ± 1%	40.0	2.1	53	0.9937
	Polynomial	24 ± 53%	38.0	2.7	41	0.9917
	Spline	65 ± 132%	37.5	3.9	50	0.9947
CPE 80×5	Exact	80 ± 1%	24.3	8.8	35	0.9931
	Polynomial	52 ± 117%	24.2	8.2	32	0.9971
	Spline	78 ± 600%	24.0	8.6	37	0.9963
CPE2 80×4	Exact	234 ± 1%	29.0	2.8	40	0.9987
	Polynomial	93 ± 44%	23.4	7.8	30	0.9993
	Spline	249 ± 254%	31.2	0.1	43	0.9989

Table 9. Results of the analysis with fixed constraints on L_{twine} and b and min/max constraints on θ (parameter estimation strategy No. 3), unloading cycle.

Netting	Model	EI (N/mm ²)	L_{twine} (mm)	b (mm)	θ (deg)	R^2
PE 80×2.5	Exact	264 ± 30%	35	2.5	52	0.8343
	Polynomial	433 ± 18%	35	2.5	50	0.8563
	Spline	279 ± 31%	35	2.5	52	0.8321
PE 100×2.5	Exact	752 ± 37%	45	2.5	55	0.7635
	Polynomial	853 ± 48%	45	2.5	52	0.8490
	Spline	787 ± 37%	45	2.5	55	0.7678
PE 80×3	Exact	239 ± 42%	34	3	56	0.7947
	Polynomial	348 ± 22%	34	3	54	0.8261
	Spline	351 ± 0%	34	3	59	0.8561
PE 80×4	Exact	535 ± 33%	32	4	48	0.8086
	Polynomial	973 ± 26%	32	4	47	0.8482
	Spline	567 ± 35%	32	4	48	0.8054
PE 100×4	Exact	712 ± 27%	42	4	51	0.8513
	Polynomial	1373 ± 22%	42	4	50	0.8415
	Spline	753 ± 28%	42	4	51	0.8485
CPE 80×5	Exact	263 ± 15%	30	5	40	0.9661
	Polynomial	214 ± 15%	30	5	35	0.9764
	Spline	277 ± 16%	30	5	40	0.9614
CPE2 80×4	Exact	171 ± 6%	24	8	35	0.9975
	Polynomial	133 ± 8%	24	8	30	0.9948
	Spline	182 ± 7%	24	8	35	0.9949

FIGURES

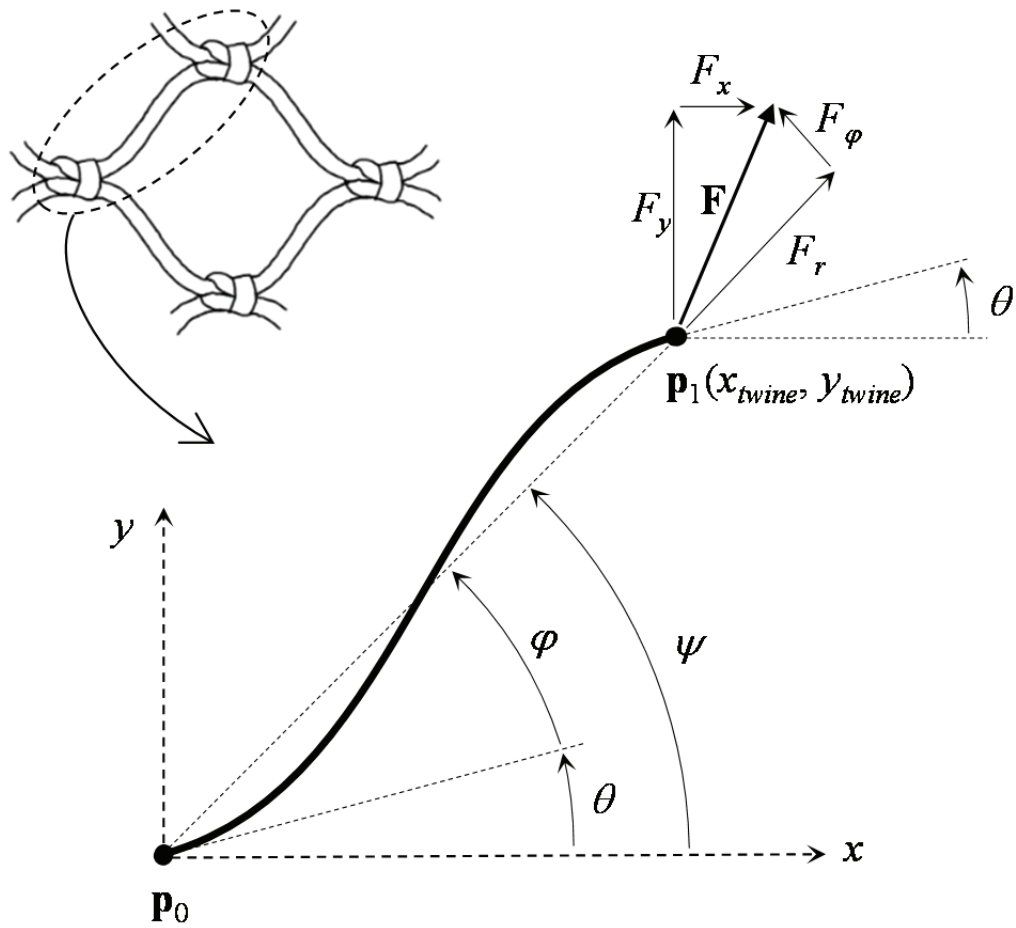


Figure 1. Double-clamped beam model of a mesh twine.

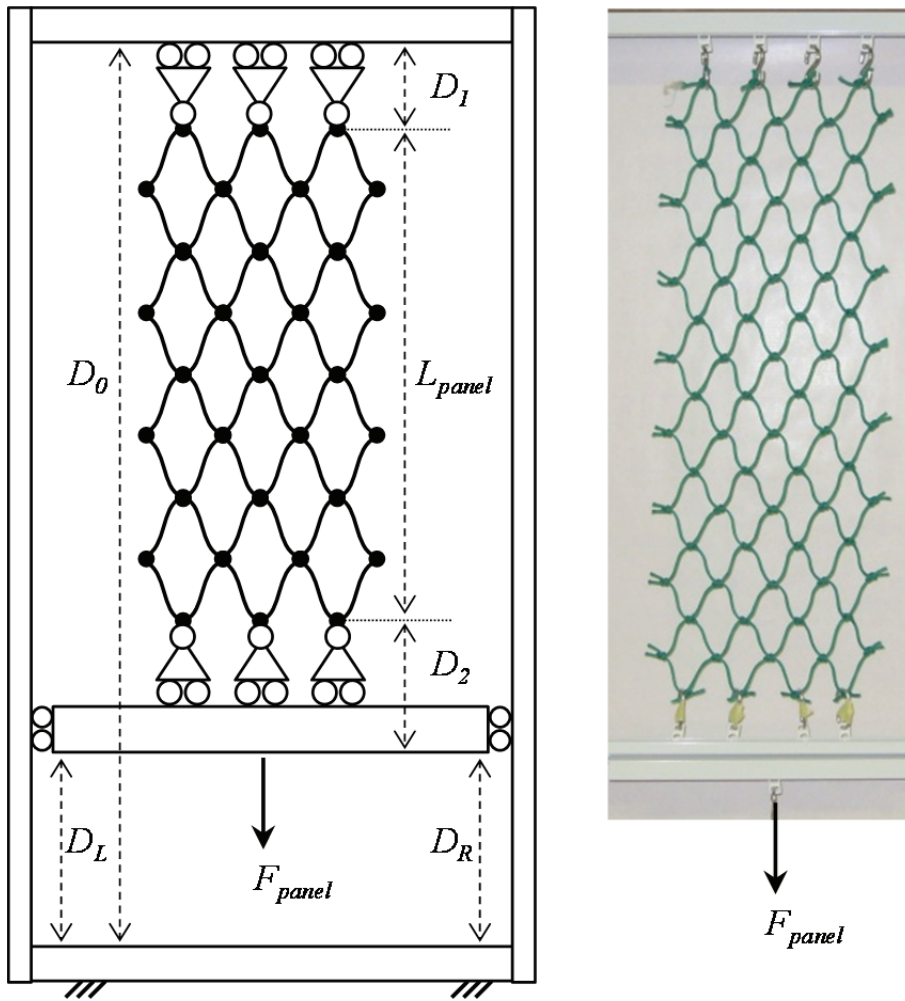


Figure 2. Design of the experimental setup and general view of a netting sample during the test.

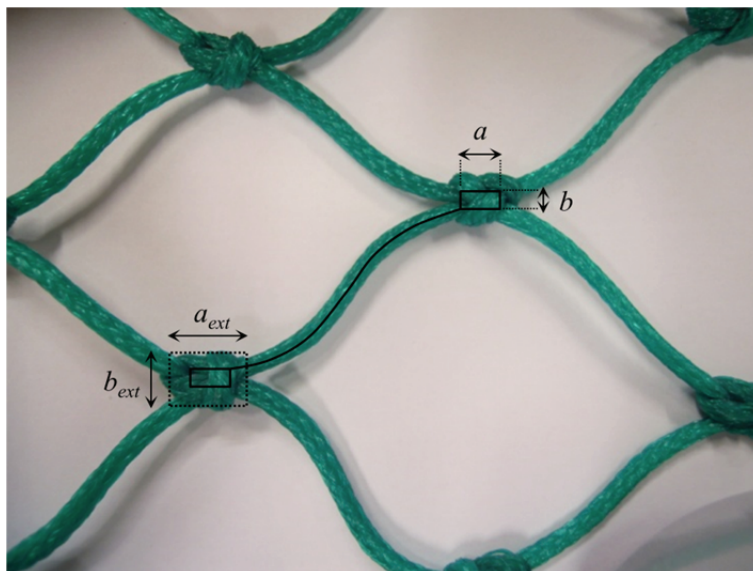


Figure 3. Idealized netting where mesh twines are modelled as beams emerging from the corners of rectangular knots.

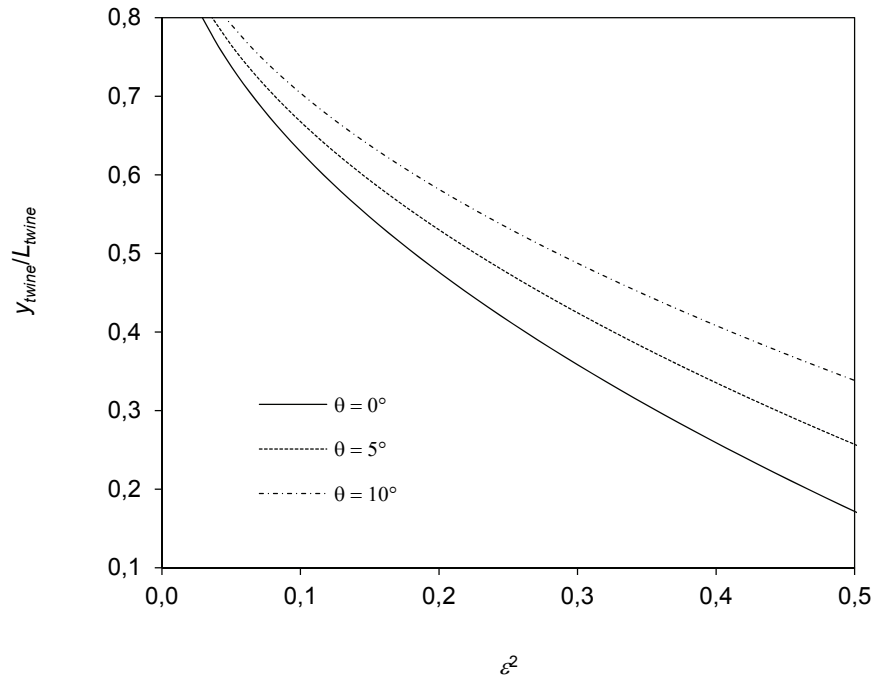


Figure 4. Dimensionless vertical displacement of the twine (y_{twine}/L_{twine}) calculated with the asymptotic solution as a function of $\varepsilon^2 = EI/(FL_{twine}^2)$ for different slope angles θ .

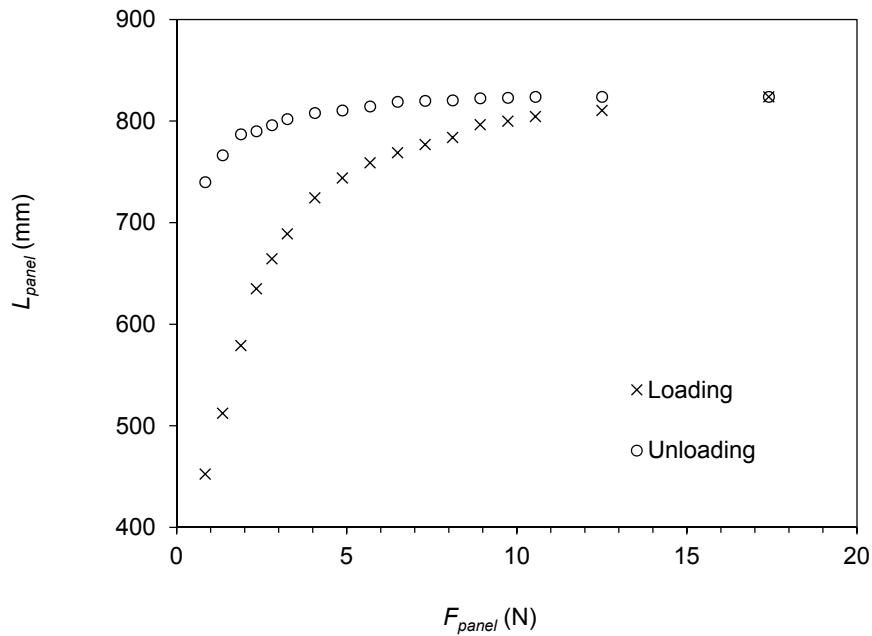


Figure 5. Experimental data obtained for PE 80x3, showing the difference between loading and unloading cycles.

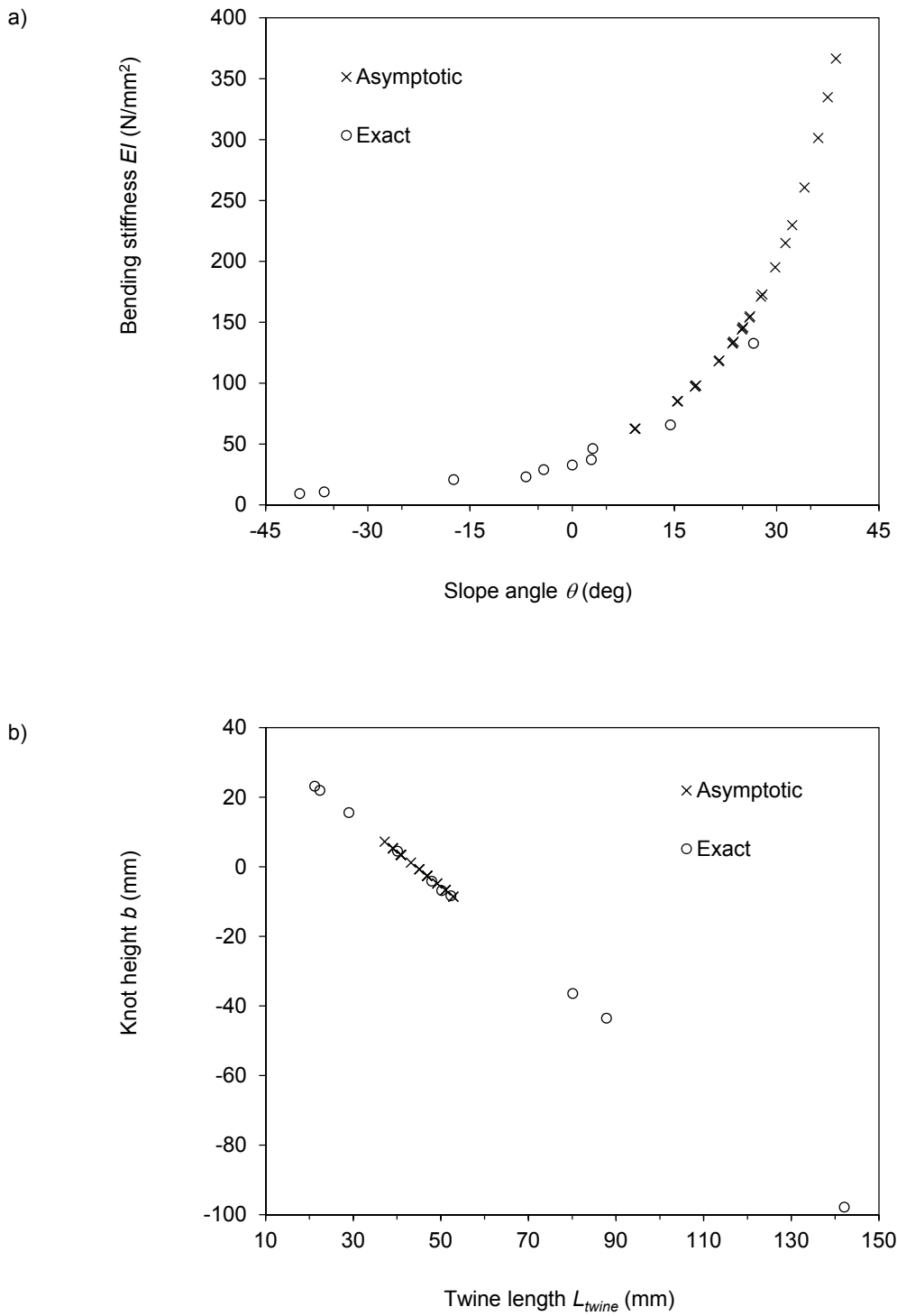


Figure 6. Multiple solutions of the regression with unconstrained parameters for PE 100×4, showing the correlation between parameters in the exact and the asymptotic models: (a) bending stiffness EI versus slope angle θ , (b) knot height b versus twine length L_{twine} .

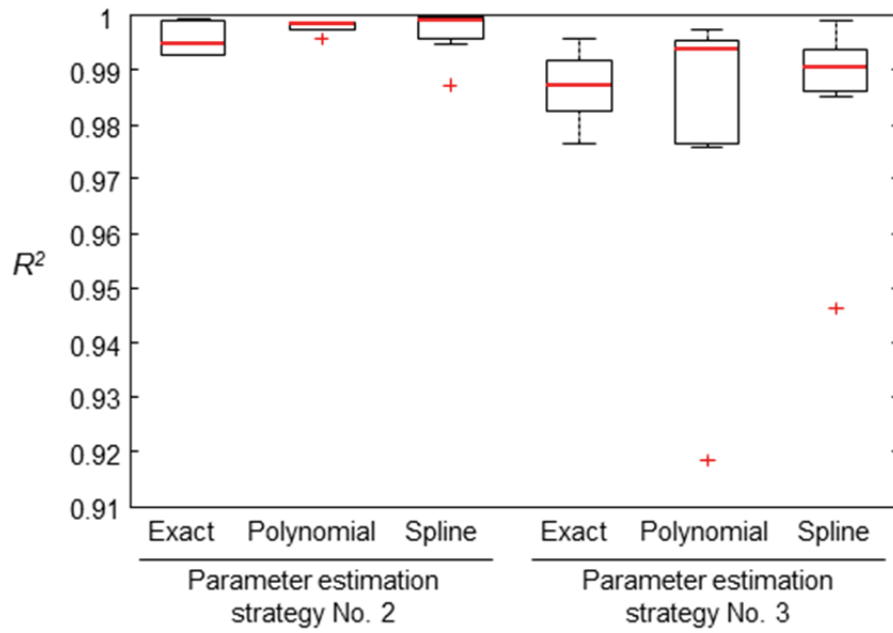


Figure 7. Box plot of the R^2 values from the parameter estimation strategies No. 2 and No. 3, loading cycle.

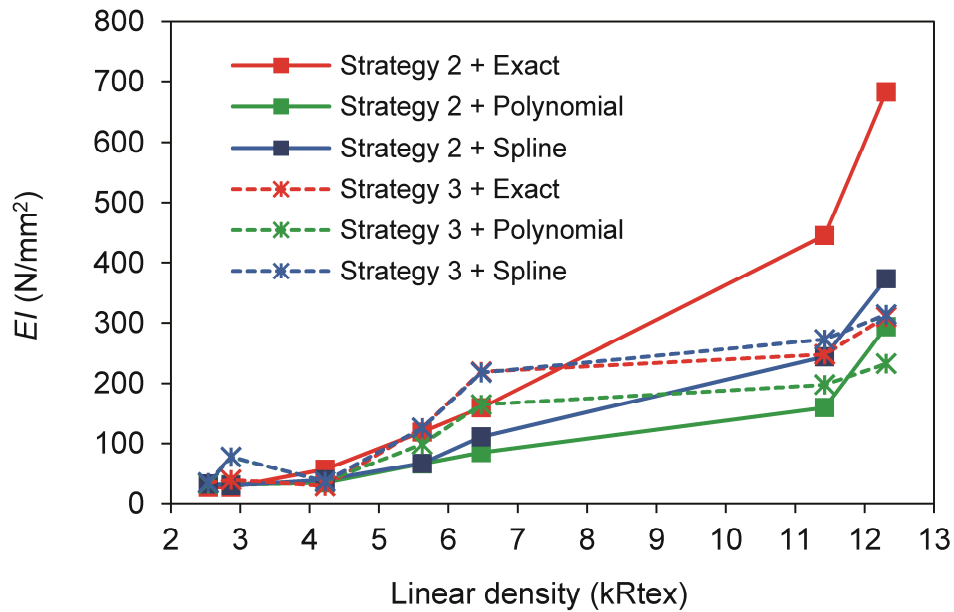


Figure 8. Estimates of EI against the linear density of the netting obtained with parameter estimation strategies No. 2 (Table 5) and No. 3 (Table 6).

Article No. 3

Assessing the suitability of gradient-based energy minimization methods to calculate the equilibrium shape of netting structures

Amelia de la Prada, Manuel González

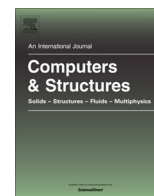
Submitted to *Computers and structures* on 28th April 2013

Revised version submitted on 13th November 2013

Revised version submitted on 29th November 2013

Accepted for publication on 14th January 2014

Published online on 10th February 2014



Assessing the suitability of gradient-based energy minimization methods to calculate the equilibrium shape of netting structures



Amelia de la Prada, Manuel González*

Escuela Politécnica Superior, Universidad de A Coruña, Mendizábal s/n, 15403 Ferrol, Spain

ARTICLE INFO

Article history:

Received 28 April 2013

Accepted 14 January 2014

Keywords:

Netting structures

Equilibrium shape

Energy minimization

Gradient-based optimization

Non-conservative forces

ABSTRACT

This paper assesses the robustness and efficiency of gradient-based energy minimization methods to calculate the equilibrium shape of netting structures, as an alternative to the Newton–Raphson iteration that is normally used for this purpose. A set of benchmark problems is solved to get insight on the behavior of different gradient-based methods and two variants of the Newton–Raphson method, using a finite element model of the structure. Numerical experiments indicate that the limited memory BFGS method is generally more robust, faster, and easier to implement, and therefore it may replace or complement the Newton–Raphson method in this type of analysis.

© 2014 Elsevier Ltd. All rights reserved.

1. Introduction

Netting structures are extensively used in commercial fishing and aquaculture. The increasing concerns about the environmental impact and the energy efficiency in these industries have driven the development of numerical models specially designed for this class of structures. They can be categorized as 1D finite element models [1–3], 2D finite element models [4–6], lumped mass models [7–9] and differential equation models for axisymmetric structures [10,11]. Regarding the type of analysis, some applications require to calculate the dynamic behavior of the structure subjected to water currents, waves and tides, and therefore a direct numerical integration of the equations of motion is used [7,8,12,13]. Other applications only require to calculate the static equilibrium shape of the structure subjected to a constant water current [4,11,14,15], and this work focuses in this kind of analysis.

The robustness and computational efficiency of the equilibrium shape calculation is becoming a key issue due to the recent inception of topology optimization of netting structures [16–18], since it is used to evaluate the objective function in such optimizations. The number of function evaluations is usually high because the number of design variables in netting structures is also high; for example, a recent iterative algorithm to optimize the energy efficiency of fishing gears [17] requires in the order of 10^4 structures which is done in 10–20 h of computing time in modern multi-core computers to

optimize a structure with 134 design variables. Methods based on heuristics (e.g. evolutionary algorithms), better suited to multi-objective optimization of netting structures, will require even more function evaluations and more robust calculations. Furthermore, the design of netting structures for fishing or aquaculture is an iterative optimization process, given the complexity and multidisciplinary nature of these systems: the results of a starting optimization often reveal problems related to factors not included in the numerical model (e.g. environmental impact or fish behavior), and a new optimization must be launched with additional constraints to avoid them; in addition, the uncertainty in the numerical model (ocean currents, friction with sea bottom. . .) also make necessary to launch several optimizations with different model parameters.

The equilibrium shapes of netting structures modeled with finite elements is normally calculated by solving the equilibrium equations of the model with the Newton–Raphson method. The aim of this work is to investigate the robustness and computational performance of gradient-based methods to calculate the equilibrium shape by directly minimizing the total energy, as an alternative to the Newton–Raphson iteration used in the scientific literature. Whereas both approaches are theoretically equivalent, our hypothesis is that some gradient-based optimization methods can outperform Newton–Raphson iteration as they do not require matrix operations and they are not affected by ill-conditioned stiffness matrices which are often present in netting structures. Although energy minimization methods are usually not competitive for the analysis of general structures, they have proved to be a very effective method for some particular kinds of application, such as unstable trusses [19] or hyperelastic membranes [20].

* Corresponding author. Tel.: +34 981337400; fax: +34 981337410.

E-mail addresses: amelia.delaprada@udc.es (A. de la Prada), manuel.gonzalez@udc.es (M. González).

The main contribution of this work is a comprehensive assessment of the robustness and computational performance of both families of methods (gradient-based energy minimization and Newton iteration) to calculate the equilibrium shape of netting structures, in order to get insight on the advantages and disadvantages of each method and identify how they are affected by the particular characteristics of the structure. The assessment is carried out by means of a set of benchmark problems that replicate different challenging features that are present in real world applications of netting structures.

The only reference in the literature to the use of energy minimization methods to calculate the equilibrium shape of netting structures can be found in [3], which briefly mentions the use of the Polak–Ribière version of the nonlinear conjugate gradient method. However, that work assesses neither the computational performance nor the robustness of the method in comparison to the Newton–Raphson iteration normally used in these applications.

The remaining of the paper is organized as follows: Section 2 describes the numerical model of the netting structure and the simulation methods compared in this work. Section 3 describes the set of benchmark problems used to evaluate the performance of the different simulation methods. In Section 4, results from the numerical experiments are presented and discussed. Finally, Section 5 provides conclusions and topics for future work.

2. Methods

2.1. Numerical model

The numerical model used in this work is considered the state-of-the-art for equilibrium shape calculation in netting structures [6,21,14,16–18]; a summarized description is provided here, since details can be found in the references. Without loss of generality, the netting structure is supposed to be made up by panels of diamond mesh, the predominant netting in the fishing and aquaculture industry. The netting surfaces were discretized with the triangular finite element developed in [4]. This element assumes that all twines in each of the two directions of the netting are parallel, and that twines behave as bars made of isotropic and linear elastic material; each node of the element has three translational degrees of freedom. In addition, the mesh resistance to opening is modeled as a torque proportional to the twine angle [22]. Cables and ropes in the structure are modeled as linear bar elements [4], since their bending stiffness is negligible.

Following the same procedure as in the scientific literature [4,22], the direct formulation of the finite element method is used instead of the variation formulation, that is, forces are directly calculated from the position of the nodes in the finite element mesh. The forces applied to the model are:

- (i) Elastic forces in triangular finite elements and bars, through the formulation described in [4,22].
- (ii) Weight and buoyancy.
- (iii) Hydrodynamic drag forces, through the simplified expressions for static analysis based on the drag forces that act on a bar under a uniform current flow [23], without taking into account the fluid–structure interaction and dynamic terms [1]. The fluid velocity is projected in two components \mathbf{v}_n and \mathbf{v}_t , normal and tangential to the netting twine, which generate the normal drag force \mathbf{F}_n and the tangential friction force \mathbf{F}_t , as a function of the twine length L , twine diameter d , fluid density ρ and friction and drag coefficients C_f and C_d . For a triangular finite element, the total hydrodynamic force is the sum of the forces acting on all the twines in the element. The same expressions are used to calculate hydrodynamic forces in cables and ropes discretized by bar elements:

$$\begin{aligned} \mathbf{F}_t &= \frac{1}{2} \rho C_d L d |\mathbf{v}_t| \mathbf{v}_t \\ \mathbf{F}_n &= \frac{1}{2} \rho C_f L d |\mathbf{v}_n| \mathbf{v}_n \end{aligned} \quad (1)$$

Fluid–structure interaction is not considered because this topic is still an open problem in underwater netting structures [24]. Therefore, the velocity field of the fluid is not affected by the shape of the netting structure.

2.2. Newton iteration

The equilibrium shape of the netting structure can be obtained by solving the equilibrium equations in the deformed configuration of the structure, in order to account for the large displacements and rotations:

$$\mathbf{F}(\mathbf{q}) = 0 \quad (2)$$

where \mathbf{q} is the nodal coordinate vector and \mathbf{F} is the nodal force vector which accumulates the contributions of the aforementioned forces. This non-linear system of equations can be solved with the well-known Newton–Raphson (NR) iteration:

$$\mathbf{d}_i = -\mathbf{J}^{-1}(\mathbf{q}_i) \mathbf{F}(\mathbf{q}_i) \quad (3)$$

$$\mathbf{q}_{i+1} = \mathbf{q}_i + \lambda \mathbf{d}_i \quad (4)$$

where \mathbf{J} is the Jacobian matrix of \mathbf{F} , \mathbf{d} is the search direction and λ is the step length. The classic NR method ($\lambda = 1$) is not a globally convergent algorithm, and unfortunately the initial position of the netting is often numerically far from the solution. In addition, the Jacobian matrix is often ill-conditioned with respect to inversion, because the in-plane stiffness of the net is several orders of magnitude higher than the bending stiffness and the mesh opening stiffness; as a consequence, some iterations make a vast change in the variables and the method does not converge. The scientific literature about equilibrium shape calculation in netting structures does not provide details about the techniques used by other authors to overcome these issues [6,21,14,16–18]. In this work we have followed two different approaches:

The first approach is to globalize the NR iteration with a line search and the Armijo Rule [25,26]: for a search direction \mathbf{d}_i , a succession of steps lengths λ_j are tested until the sufficient decrease condition is satisfied (typically $\alpha = 10^{-4}$):

$$|\mathbf{F}(\mathbf{q}_i + \lambda_j \mathbf{d}_i)| < (1 - \alpha) |\mathbf{F}(\mathbf{q}_i)| \quad (5)$$

The values for λ_j are calculated using the three-point safeguarded parabolic model described in [25]. In addition, after five rejected steps (which in practice means stagnation in the iteration), the iteration is finished with a step length calculated with the second approach. This variant of the NR method will be referred to as *NR line search*.

The second approach calculates the step length at each iteration with

$$\lambda_i = \begin{cases} \lambda_{\max} / \max(\mathbf{d}_i) & \text{if } \max(\mathbf{d}_i) > \lambda_{\max} \\ 1 & \text{otherwise} \end{cases} \quad (6)$$

where the maximum step length per coordinate λ_{\max} is selected as a fraction of the characteristic length of the netting structure; our experience suggests that a value about 1% is appropriated in most situations. We have not found references to this method in the literature, but according to our experience, it often works better than the line search in netting structures. This variant of the NR method will be referred to as *NR step limit*.

2.3. Gradient-based optimization methods

As an alternative to the NR method used in the literature, the authors propose the use of gradient-based energy minimization methods to find the steady-state equilibrium position by minimizing of the total energy of the system. The principle of minimum total potential energy can be extended to system with nonconvex nonsmooth forces [27] leading to the unconstrained minimization problem

$$\min_{\mathbf{q}} f(\mathbf{q}) \quad (7)$$

where the objective function is defined as

$$f(\mathbf{q}) = E_p - W_{nc} \quad (8)$$

where E_p represents the potential energy due to conservative forces (deformation in netting and cables, mesh opening resistance, weight and buoyancy) and W_{nc} represents the work carried out by non-conservative forces acting on the system (e.g. hydrodynamic forces and friction). W_{nc} is calculated using a path-following method [27] which allows to find the equilibrium position of non-conservative systems using energy minimization methods. With this approach, the gradient \mathbf{g} of the objective function is the opposite of the nodal force vector \mathbf{F} :

$$\mathbf{g} = \nabla f(\mathbf{q}) = -\mathbf{F}(\mathbf{q}) \quad (9)$$

2.3.1. Short-listing of optimization methods

Given the large number of existing unconstrained optimization methods [28,29], a selection process was applied in order to narrow the scope. Optimization methods that need second-order derivatives of the objective function (Hessian) were rejected, since their evaluation would have a computational cost similar to the evaluation of the search direction \mathbf{d}_i in the Newton–Raphson method. Therefore, the scope was limited to methods that only need first-order derivative information, that is, gradient-based methods. In addition, only methods that show good performance with medium-large problems were selected, since problem sizes in our target application are usually in the order of 10^2 to 10^4 variables.

Ten different gradient-based optimization methods were prescreened (see Table 1), including line search methods, trust region methods and methods for noisy objectives. They were used to solve the test case No. 1 described in Section 3, which is an undemanding numerical problem. In order to reduce the development time of this prescreening process, publicly available implementations in Matlab programming language were used [28,30,31]; Table 1 also lists the function name of the implementation tested for each

Table 1
Shortlisted gradient-based optimization methods, the implementation refers to the function name in the cited reference.

Optimization method	Implementation	Succeed
<i>Smooth objective:</i>		
Steepest descent	Steep [28]	
Nonlinear conjugate gradient	ncg [30]	X
BFGS	lbfgs [30]	X
	bfgswopt [28]	
	fminunc [31]	
Dogleg-Trust region	ntrust [28]	
Newton-CG Trust region	cgtrust [28]	X
Truncated Newton	tn [30]	
<i>Non smooth objective:</i>		
Implicit filtering	imfil [28]	
Nelder–Mead simplex	nelder [28]	
	fminsearch [31]	
Multidirectional search	mds [28]	
Hooke–Jeeves	hooke [28]	

method. While these Matlab implementations may not deliver the best computational performance, they can be used to compare the number of function and gradient evaluations carried out to solve the problem. Most of the methods could not solve the problem in a reasonable number of function evaluations due to very poor convergence or stagnation in the iteration, and tuning the algorithm parameters did not improve the behavior. The only three methods that succeeded in solving the problem are described in the next subsections.

2.3.2. Nonlinear conjugated gradient method

The nonlinear conjugated gradient method (CG) belongs to the family of line search methods, where each iteration i determines a search direction \mathbf{s}_i and then minimizes $f(\mathbf{q}_i + \alpha_i \mathbf{s}_i)$ with respect to the step length α_i to generate a new iterate $\mathbf{q}_{i+1} = \mathbf{q}_i + \alpha_i \mathbf{s}_i$. CG methods calculate the search direction using conjugacy properties [29]. The implementation used by the authors follows the algorithm described in [28]:

1. Initial position: \mathbf{q}_0
2. Evaluate $f_0 = f(\mathbf{q}_0)$, $\mathbf{g}_0 = -\mathbf{F}(\mathbf{q}_0)$
3. Initial approximation: $\mathbf{s}_0 = -\mathbf{g}_0$, $i = 0$
4. While $\|\mathbf{g}_i\| > 0$
5. Compute step length α_i , set $\mathbf{q}_{i+1} = \mathbf{q}_i + \alpha_i \mathbf{s}_i$
6. Evaluate $\mathbf{g}_{i+1} = -\mathbf{F}(\mathbf{q}_{i+1})$
7. Compute β_{i+1}
8. $\mathbf{s}_{i+1} = -\mathbf{g}_{i+1} + \beta_{i+1} \mathbf{s}_i$
9. $i = i + 1$
10. End while
11. Solution: $\mathbf{q}^* = \mathbf{q}_i$

β_{i+1} in Step 7 is computed with the Polak–Ribière method, since it proved to be more efficient than other methods in this application:

$$\beta_{i+1} = \frac{\mathbf{s}_{i+1}^T (\mathbf{s}_{i+1} - \mathbf{s}_i)}{\mathbf{s}_i^T \mathbf{s}_i} \quad (10)$$

2.3.3. Limited memory BFGS method

Quasi-Newton optimization methods also follow the line search strategy but they evaluate the search direction \mathbf{s} for each iteration i according to the formula

$$\mathbf{s}_i = -\mathbf{H}_i^{-1} \mathbf{g}_i \quad (11)$$

where \mathbf{H}^{-1} is the inverse of the second-order derivative of f (the Hessian matrix). Quasi-Newton methods estimate \mathbf{H} with information of the gradient \mathbf{g} and the position \mathbf{q} . The BFGS method (Broyden–Fletcher–Goldfarb and Shanno) estimates \mathbf{H} with the expression

$$\mathbf{H}_{i+1}^{BFGS} = \mathbf{H} + \left(1 + \frac{\gamma^T \mathbf{H} \gamma}{\delta^T \gamma} \right) \frac{\delta \delta^T}{\delta^T \gamma} - \frac{\delta \gamma^T \mathbf{H} + \mathbf{H} \gamma \delta^T}{\delta^T \gamma} \quad (12)$$

$$\gamma_i = \mathbf{g}_{i+1} + \mathbf{g}_i \quad (13)$$

$$\delta_i = \mathbf{q}_{i+1} - \mathbf{q}_i \quad (14)$$

Note that sub-index (i) has been omitted on the right-hand side of Eq. (12). Results have demonstrated that BFGS is generally the most robust and efficient of quasi-Newton's methods [29]. To avoid matrix operations and the large memory storage of the classic BFGS method, we selected the limited memory BFGS variant (LBFGS), that uses the history of the iteration to compute the step without matrix operations [28,30]; our implementation follows the algorithm described in [30].

2.3.4. Newton-CG Trust region

Line search methods and trust-region methods both generate steps with the help of a quadratic model of the objective function, but they use it in different ways. Line search methods generate a search direction, and then find a suitable step length along this direction. Trust-region methods work in the opposite way: they define a region around the current iteration within which they trust the model to be an adequate representation of the objective function, and then choose a suitable direction; in practice, the size of the region and the length of the step are chosen simultaneously.

The Newton-CG Trust described in [28] combines the trust region ideas with the Truncated Newton CG method, which approximates the search direction of the Newton method using CG. The implementation used by the authors follows the algorithm detailed in [28]:

1. Initial position: \mathbf{q}_0
2. Evaluate $f_0 = f(\mathbf{q}_0)$, $\mathbf{g}_0 = -\mathbf{F}(\mathbf{q}_0)$
3. $i = 0$
4. While $\|\mathbf{g}_i\| > 0$
5. Compute \mathbf{s}_i by solving $\nabla^2 f(\mathbf{q}_i)\mathbf{s}_i = -\mathbf{g}_i$ using a CG method
6. Compute step length α_i , set $\mathbf{q}_{i+1} = \mathbf{q}_i + \alpha_i\mathbf{s}_i$
7. Evaluate $\mathbf{g}_{i+1} = -\mathbf{F}(\mathbf{q}_{i+1})$
8. $i = i + 1$
9. End while
10. Solution: $\mathbf{q}^* = \mathbf{q}_i$

3. Benchmark setup

3.1. Description of the test cases

A small set of simple test cases has been defined to measure the ability of gradient-based energy minimization methods to deal with the challenges arising in the calculation of equilibrium shapes of netting structures. In the literature, the performance of numerical models and simulation methods for netting structures is usually demonstrated with real world problems, like fishing gears or aquaculture cages. On the other hand, small and simple test cases offer advantages over complex problems [32]: they can isolate a specific characteristic of netting structures, and therefore evaluate the response of a model or method that particular characteristic. In addition, comprehensive model descriptions can be provided and other authors are encouraged to reuse them because they need to invest little time in the modelization, thus making easier to compare results of different research works.

Table 2 list the test cases proposed in this work. Each test features a particular characteristic (see Table 3) and it is usually based on a previous, simpler test. Some tests are available in two variants, with different initial positions or stiffness values. Each test

Table 2 List of test cases.

Test no.	Based on	Description	Variant
1	-	Base test	
2	1	Large displacements	2A Far initial position
			2B Near initial position
3	2B	Low stiffness in compression	3A Low stiffness
			3B Very low stiffness
4	3A	Cables in the structure	4A Medium stiffness
			4B High stiffness
5	3A	Rope with ground contact	
6	-	Panel with ground contact	6A Far initial position
			6B Near initial position

Table 3 Relevant features of each test case.

Feature	Test case									
	1	2A	2B	3A	3B	4A	4B	5	6A	6B
Large displacements	-	✓	✓	✓	✓	✓	✓	✓	✓	✓
High initial stress	-	✓	-	-	-	-	-	-	-	-
Far initial position	-	✓	-	-	-	-	-	-	✓	-
Netting with low compression stiffness	-	-	-	✓	-	✓	✓	✓	✓	✓
Netting with very low compression stiffness	-	-	-	-	✓	✓	✓	✓	✓	✓
Cables	-	-	-	-	-	✓	✓	-	✓	✓
Cables, high stiffness	-	-	-	-	-	-	✓	-	-	-
Ground contact	-	-	-	-	-	-	-	✓	✓	✓
Panel parallel to flow	-	-	-	-	-	-	-	-	✓	✓

will be described with a figure of the netting structure showing the coordinate system and the position and numbering of representative points in the structure, whose initial coordinates (SI) are provided in a table. Fixed points are marked with a bold dot in the figures and with an “(f)” symbol in the tables. Figures also show the initial position of the structure and a wireframe representation of the finite element mesh in the equilibrium position. In all tests, the structure is exposed to a constant water current of 2 m/s in y direction, which is a representative value of the operation conditions in fishing and aquaculture applications.

Test 1 consists on a square netting panel with its four corners fixed, as shown in Fig. 1. The dimensions, configuration and mechanical properties of the panel are listed in Table 4; note that the couple due to mesh opening stiffness is zero for a twine angle of 30° instead of 0° as in [22], which explains why the resistance to opening is much higher than in [22]. Mesh coordinates [4] of points 0–3 are (0,0), (100,0), (100,100) and (0,100) respectively. In the

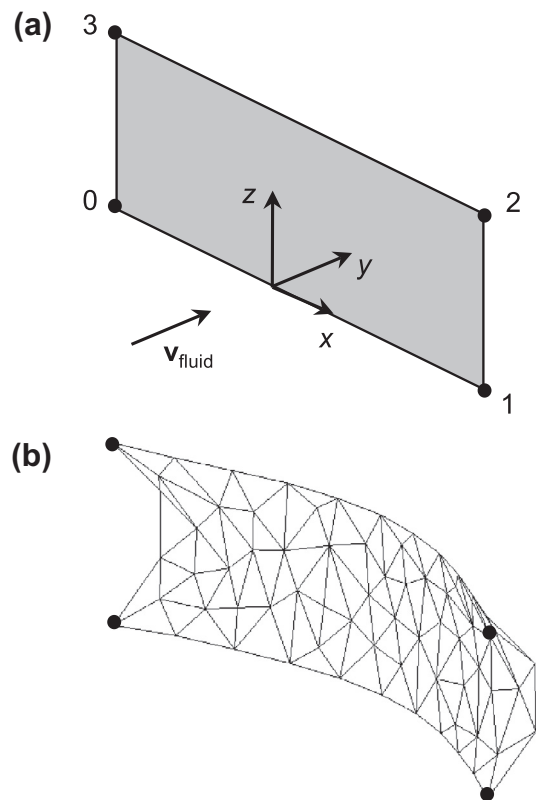


Fig. 1. Test 1, base test: (a) initial position, (b) equilibrium position.

Table 4
Properties of the netting panel in test 1.

Property	Value
Number of meshes	100 × 100
Mesh size	80 mm (diamond type)
Mesh orientation	Normal direction along z
Twine diameter	2.5 mm
Twine angle	30 deg
Panel density	0.29 kg/m ²
Twine axial stiffness (EA)	2000 N
Resistance to opening	35 Nm/rad

initial position (Table 5), the fixed points form a rectangle of 7.72 × 2.07 m, which corresponds to the undeformed dimensions of the netting panel, and therefore the net has no initial stress and the initial position of the static analysis is numerically close to the equilibrium position. This test is not a challenging problem, but it is included in the benchmark setup since it is the foundation for the following tests, which share most of the properties of the netting panel. In addition, it can be used to easily detect simulation methods not suited for netting structures, since methods that show a bad performance with this undemanding test will not be able to cope with any of the next tests. Test 1 was used in the short-listing of optimization methods described in Section 2.3.1.

Test 2 is based on test 1, but the corner points of the netting panel are fixed closer to each other to generate a bag-shaped equilibrium position (Fig. 2(c)). Two variants are provided for the initial position, defined in Table 6. In test 2A (Fig. 2(a)) the panel starts from a flat initial position, which is numerically quite far from the equilibrium position and generates a very high initial compression stress; solving this tests with a method with good global convergence properties requires in the order of 10 more iterations than test 1. On the other hand, in test 2B (Fig. 2(b)) the initial position is closer to the equilibrium position, since the coordinates of points 4–9 correspond to the solution in Fig. 2(c); in this test variant, the position of the mesh nodes is interpolated from the position of points 0–9 using NURBS (non-uniform rational basis splines). Mesh coordinates [4] of points 4–9 are (50,0), (100,100/3), (100,200/3), (50,100), (0,200/3) and (0,100/3) respectively.

In test 1 and test 2, the twine axial stiffness has the same value in tension and compression. While this material behavior may be representative of some metallic netting structures used in aquaculture cages, most of the netting materials in fishing and aquaculture applications have a negligible bending stiffness, hence they are assumed to take no compression [33,34]. Test 3 is based on test 2B but introduces this non-linear material behavior when subjected to either tension or compression. Since a zero value of axial stiffness in compression often generates numerical problems in an equilibrium shape calculation, in practice a small positive value is used: higher values improve convergence, but they introduce more error in the solution. This test has two variants with different values of axial stiffness in compression, defined as a percentage of the axial stiffness in tension: 1.25% (test 3A) and 0.001% (test 3B). According to the authors' experience, the value in test 3A is approximately the minimum value to achieve good convergence using the NR-line search method. The value in test 3B is virtually

Table 5
Initial position for test 1.

Point	x	y	z
0 (f)	-3.86	0	0
1 (f)	3.86	0	0
2 (f)	3.86	0	2.07
3 (f)	-3.86	0	2.07

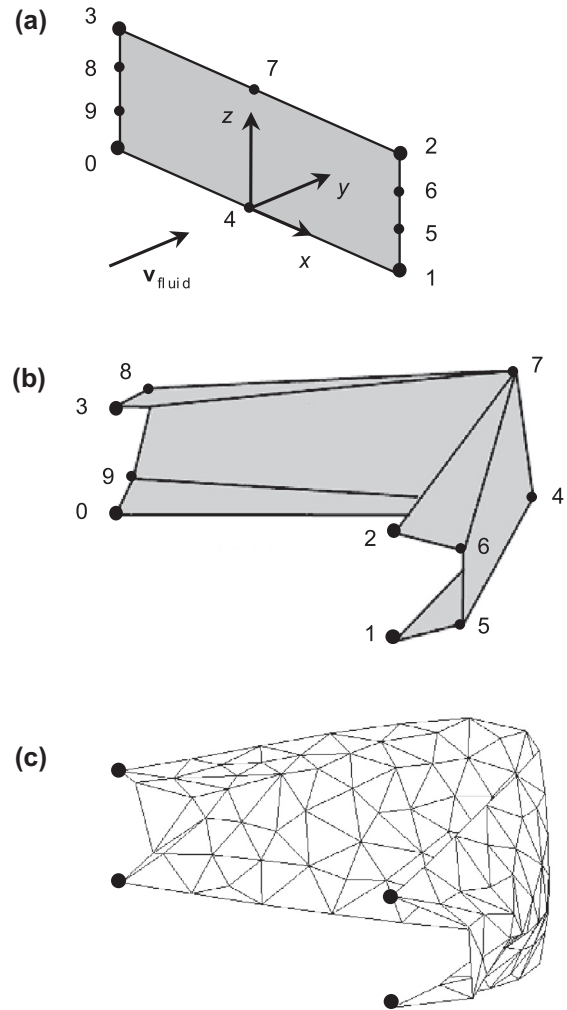


Fig. 2. Test 2, panel undergoing large displacements: (a) initial position for test 2A, (b) initial position for test 2B, (c) equilibrium position.

Table 6
Initial position for test 2.

Point	Test 2A			Test 2B		
	x	y	z	x	y	z
0 (f)	-2.36	0	0	-2.36	0	0
1 (f)	2.36	0	0	2.36	0	0
2 (f)	2.36	0	1.07	2.36	0	1.07
3 (f)	-2.36	0	1.07	-2.36	0	1.07
4	0	0	0	0	2.92	-0.47
5	2.36	0	0.35	2.84	0.60	0.06
6	2.36	0	0.71	2.84	0.44	0.73
7	0	0	1.07	0.2	2.83	1.01
8	-2.36	0	0.71	-2.88	0.50	0.81
9	-2.36	0	0.35	-2.74	0.66	0.14

identical to the assumption of no compression, and therefore generates more accurate results for this kind of netting materials. Fig. 3 shows the equilibrium position for both test variants; note the different shape in the lateral sides.

Cables are often present in netting structures. Test 4 adds four cables to test 3A, as shown in Fig. 4. The cables, with a natural length of 1 m and a diameter of 26 mm, connect the netting corner points 0–3 (which are free in this test) to the fixed points 10–13. In the initial position, the coordinates of points 10–13 are displaced 1 m in the -y direction with respect to points 0–3. Two test

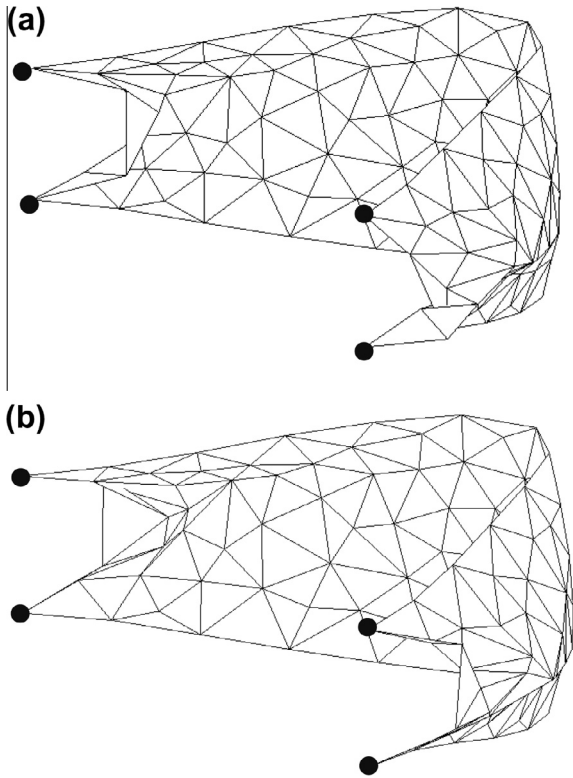


Fig. 3. Test 3, panel with low compression stiffness, equilibrium positions for: (a) test 3A and (b) test 3B.

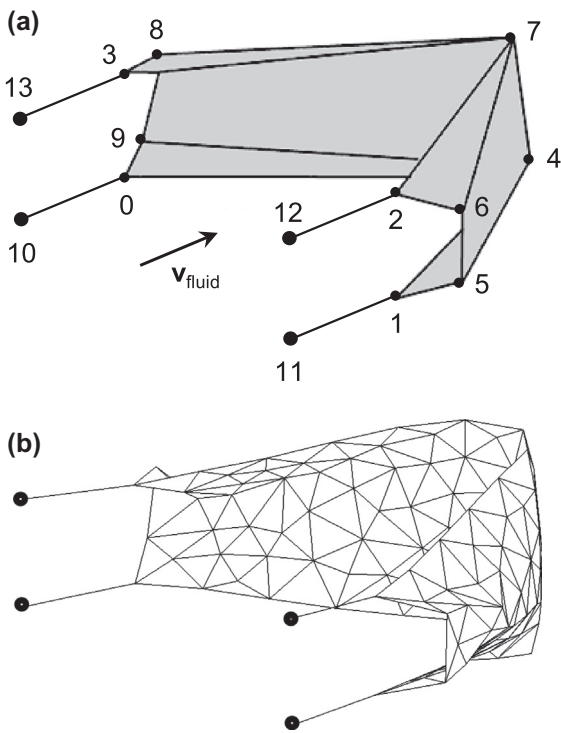


Fig. 4. Test 4, panel with cables: (a) initial position, (b) equilibrium position.

variants are provided, with different values of cable stiffness. Cables in test 4A have an axial stiffness (EA) of 10^4 N, characteristic of synthetic ropes or wire ropes of small diameter. In test 4B the axial stiffness is 10^7 N, a value characteristic of wire ropes of large

diameter; this test variant is more challenging, due to the large differences in stiffness in the model. The initial position and solution is the same for both tests variants, since the cable elongation is negligible.

Trawling is a method of fishing that involves pulling a bag-shaped fishing net through the sea behind one or more boats. Due to its importance for the commercial fishing industry and its environmental impacts, numerical simulation and optimization of fishing trawls is an active topic of research [3,16–18]. The next tests introduce two features present in trawl gears.

Bottom trawling is a sort of trawling where the net is pulled along the seafloor: a weighted foot rope is attached to the lower mouth of the net in order to keep it close up to the seafloor. This feature is modeled in test 5, which adds a footrope with ground contact to test 3A. Although this netting structure is moving with a constant velocity through the sea, the usual modeling practice is to locate the system of reference on the structure, fix the points which are connected to the boat by cables, and apply a water velocity opposite to the boat velocity. With this model, the boundary conditions and initial position of test 3A can also be used for this test. The footrope is modeled with bar elements and represented as a dotted line in Fig. 5; it has a natural length of 7.72 m, a diameter of 26 mm, a weight of 10 kg and an axial stiffness of 10^4 N. To model the contact with the sea bottom ($z_i < z_i^{ground}$), a normal contact force F_n proportional to the indentation is applied

$$F_n = k_{ground}(z_i - z_i^{ground})\hat{z} \quad (15)$$

and a tangential drag force F_t is calculated as

$$F_t = \eta F_n \hat{v} \quad (16)$$

where \hat{z} is a unit vector normal to the sea bottom (assumed constant in this test), \hat{v} is a unit vector in the direction of the relative velocity between node i and the water, projected to the sea bottom surface. k_{ground} and η depend on the characteristics of the sea floor and the design of the footrope. In this test case, the sea bottom is located at $z = 0$, $k_{ground} = 10^5$ N/m and $\eta = 1.0$ (coefficients of friction equal or greater than 1 are used to model friction in sandy or muddy seafloor). The initial position for this test is the same used for test 3A and test 2B, with the exception of points 4 and 7, which are

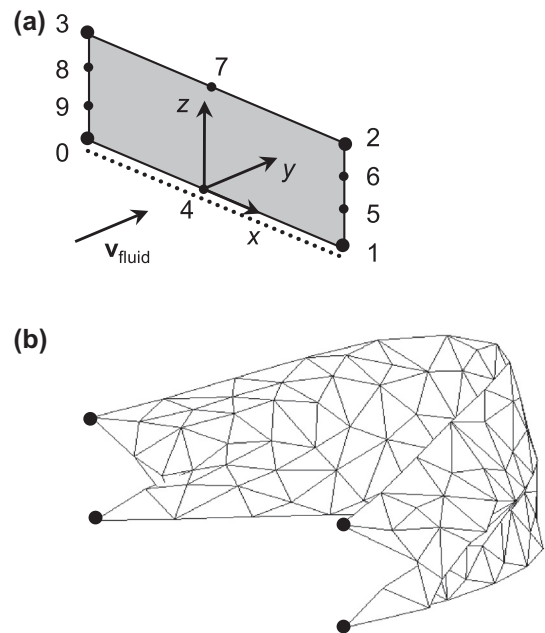


Fig. 5. Test 5, panel with footrope and ground contact: (a) initial position, (b) equilibrium position.

located at the new equilibrium position for this test (differences are caused by the contact with the sea bottom at $z = 0$): point 4 is placed at $(0, 2.96, 0)$ and point 7 at $(0, 2.73, 1.97)$.

Test 6 features another characteristic of trawling: the presence of large pieces of netting parallel to the water current. In this test (Fig. 6), the netting panel is pulled along the seafloor by two cables connected to the moving points 4–5; using the same modeling technique as in the previous tests, moving points become fixed, and a water velocity opposite to the pull velocity is applied. Cables have a natural length of 10 m, a diameter of 26 mm and an axial stiffness of 10^4 N (a low value is used to avoid too large variation of stiffness in the structure, as in test 4B). A footrope is placed in the front side of the netting (between points 0 and 1) to keep it in contact with the seafloor; it has a natural length of 2.07 m, a weight of 100 kg, a diameter of 26 mm and an axial stiffness of 10^4 N. The sea bottom is located at $z = -3$ m, and contact is modeled with the same expressions and parameters as in Test 5. Two variants are provided for this test, with far (6A) and near (6B) initial positions: coordinates are provided in Table 7. In the equilibrium position, the rear part of the panel is located about 30 cm above the sea bottom (Fig. 6(c)).

3.2. Numerical experiments

Three numerical experiments were carried out to evaluate the robustness and computational efficiency of the selected gradient-

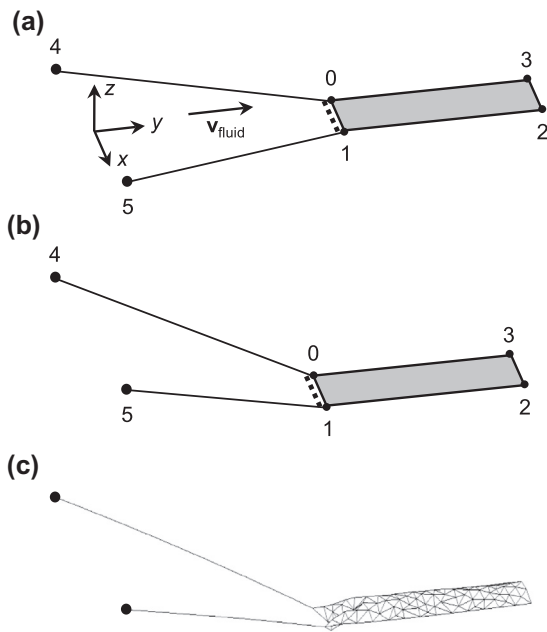


Fig. 6. Test 6, panel aligned with flow current: (a) initial position for test 6A, (b) initial position for test 6B, (c) equilibrium position.

Table 7
Initial position for test 6.

Point	Test 6A			Test 6B		
	x	y	z	x	y	z
0	-1.03	10	0	-0.82	8.68	-2.70
1	1.03	10	0	0.82	8.62	-2.70
2	1.03	17.72	0	1.00	16.42	-2.73
3	-1.03	17.72	0	-1.00	16.42	-2.73
4 (f)	-5.03	0	0	-5.03	0	0
5 (f)	5.03	0	0	5.03	0	0

based optimization methods, and to compare them with the Newton–Raphson methods normally used for the equilibrium shape calculation of netting structures. The first one consisted on a comparison of the three gradient-based optimization methods selected in Section 2.3. Test 1 was used to carry out this comparison, since it is an undemanding problem and can be used to easily detect simulation methods not suited for netting structures. The second numerical experiment consisted on a comparison of the best optimization method in the previous experiment against the two variants of the Newton–Raphson iteration described in Section 2.2. All the test cases described in Section 3 were used in this comparison. Finally, the third numerical experiment investigated the effect of the problem size on the computational performance of the three methods tested in the second experiment.

The numerical model and simulation methods have been implemented in C/C++ programming language and optimized to achieve the best computational performance by using state-of-the-art linear algebra implementations [35]. In the case of the Newton–Raphson iteration, the Jacobian was evaluated with analytical expressions and it was stored in a compressed column sparse matrix; Eq. (3) was reordered and solved with the KLU sparse linear equation solver, since it proved to be the most efficient among the solvers described in [35] for problems with similar size and structure. A sequential, single-core version of the algorithms was used, since parallelization of the simulation methods is out of the scope of this work. The codes were compiled with Microsoft Visual C++ 2010 and all numerical experiments were carried out on an Intel Core i7 CPU 2.67 GHz running Windows 7 64.

Reference solutions for each test case were obtained by running a dynamic simulation of the model until it reached a steady state; a very low stopping tolerance $|g|/N$ of 10^{-12} was used in order to obtain highly accurate equilibrium positions. The implicit single-step Newmark method was used as numerical integration scheme. While dynamic simulation requires exceptionally long CPU times to reach steady state (between 1 and 5 h with the abovementioned stopping tolerance, depending on the test case), it is a very reliable method to perform equilibrium shape calculation of netting structures, since it can find the equilibrium position even for the most complex and demanding problems.

Table 8 shows the size of the finite element mesh for each test case, and the resulting number of variables N . Since the likelihood of getting folded or tangled mesh configurations during the iteration process increases with the number of 2D triangular elements in the finite element mesh, the authors decided to use models with a small number of triangular elements: in this way, failures in the equilibrium shape calculation are hardly caused by a tangled mesh. The number of finite elements will be increased in the third numerical experiment to investigate the effect of the problem size.

4. Results and discussion

4.1. Comparison of optimization methods

The three gradient-based optimization methods short-listed and described in Section 2.3 were applied to solve test 1: nonlinear

Table 8
Size of the finite element mesh in each test case.

Test	2D elements	1D elements	Nodes	Variables
1	208	0	121	363
2	196	0	114	342
3	196	0	114	342
4	196	52	166	498
5	202	12	117	351
6	208	269	387	1161

conjugated gradient method (CG), limited memory BFGS (LBFGS) and Newton-CG Trust region (CGTRUST). The three optimization methods were run with a gradient norm stopping tolerance $\|g\|/N$ of 5×10^{-2} and converged to the reference solution calculated by dynamic simulation (Fig. 1(b)).

Fig. 7 shows the iteration history for the three methods: objective function and gradient norm $\|g\|$ divided by the number of variables N . The number of function calls (evaluation of objective function and gradient) is used as a measurement of the computational effort since it is nearly proportional to the CPU-time in the three compared methods, due to the similar internal structure of their algorithms. The iteration history shows that LBFGS achieves a steeper descent in the objective function, especially at the beginning of the optimization process; it also achieves a more sustained, less noisy reduction of the gradient norm.

Table 9 summarizes the computational effort needed to attain two levels of gradient norm stopping tolerance $\|g\|/N$, corresponding to medium precision (0.5) and high precision (0.05) solutions. Medium precision solutions are usually adequate to evaluate the performance of netting structures used in fishing and aquaculture, because the level of uncertainty in the numerical model is high (mechanical properties of the netting, drag coefficients...) [18]. High precision solutions may only be used as a final validation in the design cycle. Results in the table show that LBFGS is almost twice as efficient as CG or CGTRUST, both for medium and high precision.

4.2. LBFGS versus Newton–Raphson iteration

The second numerical experiment compares the NR line search and NR step limit methods described in Section 2.2 with the best optimization method in the first numerical experiment (LBFGS). The three methods were used to solve all the test cases described

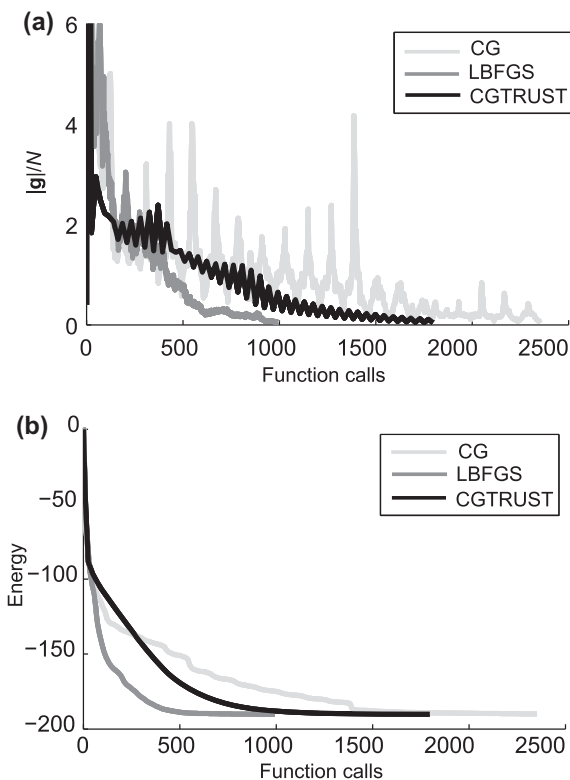


Fig. 7. Iteration history for different optimization methods applied to test 1: (a) norm of the gradient g divided by the size of the problem N , (b) objective function.

Table 9

Computational effort (function calls) and precision of different optimization methods applied to test 1.

Precision	Method	Function calls	$\ g\ /N$
Medium $\ g\ /N \leq 0.5$	CG	967	0.4989
	LBFGS	521	0.4405
	CGTRUST	881	0.3413
High $\ g\ /N \leq 0.05$	CG	2353	0.0408
	LBFGS	993	0.0469
	CGTRUST	1717	0.0439

in Section 3 with a gradient norm stopping tolerance $\|g\|/N \leq 10^{-2}$. In this experiment, the CPU time was used as a measurement of the computational effort instead of the number of function calls, since NR function calls include the evaluation of the Jacobian and therefore they are not comparable with LBFGS function calls. The presented CPU times do not include the preprocessing time before starting the analysis, which is higher in NR methods due to the assembling and symbolic factorization of the sparse Jacobian.

Fig. 8 shows the iteration history of the three methods for all the test cases, representing the evolution of the log of the gradient norm $\|g\|/N$. Table 10 shows the computational effort (CPU-time) required to attain a medium precision solution $\|g\|/N \leq 0.5$. The table also provides the value of $\|g\|/N$ in the last iteration and the error in position, measured as the norm of the difference between the solution q provided by the method and the reference solution q_{ref} calculated by dynamic simulation, divided by N . Position errors in the order of 10^{-2} m are a sign of an incorrect solution, which often shows tangled 2D elements in the mesh. Position errors of 10^{-3} m or less generally correspond to good quality solutions, where the difference between the deformed shapes of the structure q and q_{ref} is hardly noticeable in a visual comparison. Finally, Fig. 9 displays the computational performance in a bar chart to compare methods at a glance.

Regarding the behavior of NR methods, they successfully solve all test cases except 2A and 3B. In test 2A (netting undergoing large displacements, far initial position), despite NR methods converge to the stopping tolerance, they generate solutions with tangled meshes, as indicated by the high position error in Table 10. In test 3B (netting material with very low compression stiffness), although they can eventually attain the medium precision solution $\|g\|/N \leq 0.5$ (and the corresponding CPU-time is shown in Table 10 and Fig. 9), they cannot converge to the prescribed stopping gradient norm tolerance $\|g\|/N \leq 10^{-2}$ because the iteration enters in a never-ending oscillation loop: the Jacobian approaches singularity due to the presence of elements in compression, and therefore the generated search directions have very poor quality. A visual inspection of the solution shows some regions with tangled elements, but a good overall shape as indicated by the position error in Table 10. Note that these corroboration methods (visual inspection and comparison with a reference solution) cannot be used in many applications, such as automatic optimization of netting structures. In the remaining of the test cases, the iteration history shows two characteristic stages of the Newton iteration: an initial stage where the gradient norm is high and decreases slowly with frequent peaks, and a final stage where the method enters in the local convergence region and the gradient is severely reduced in few iterations. The initial stage is present in all the test cases, which means that a globally convergent algorithm is needed even if the initial position is fairly close to the equilibrium position (e.g. test 2B and specially test 6B). The NR line search method often reaches stagnation points, followed by a step calculated by the NR step limit method (as described in Section 2.2) that causes a peak in the gradient norm curve. The NR step limit method is not affected by stagnation, and in fact it performs better than NR line search in all test cases except 2A.

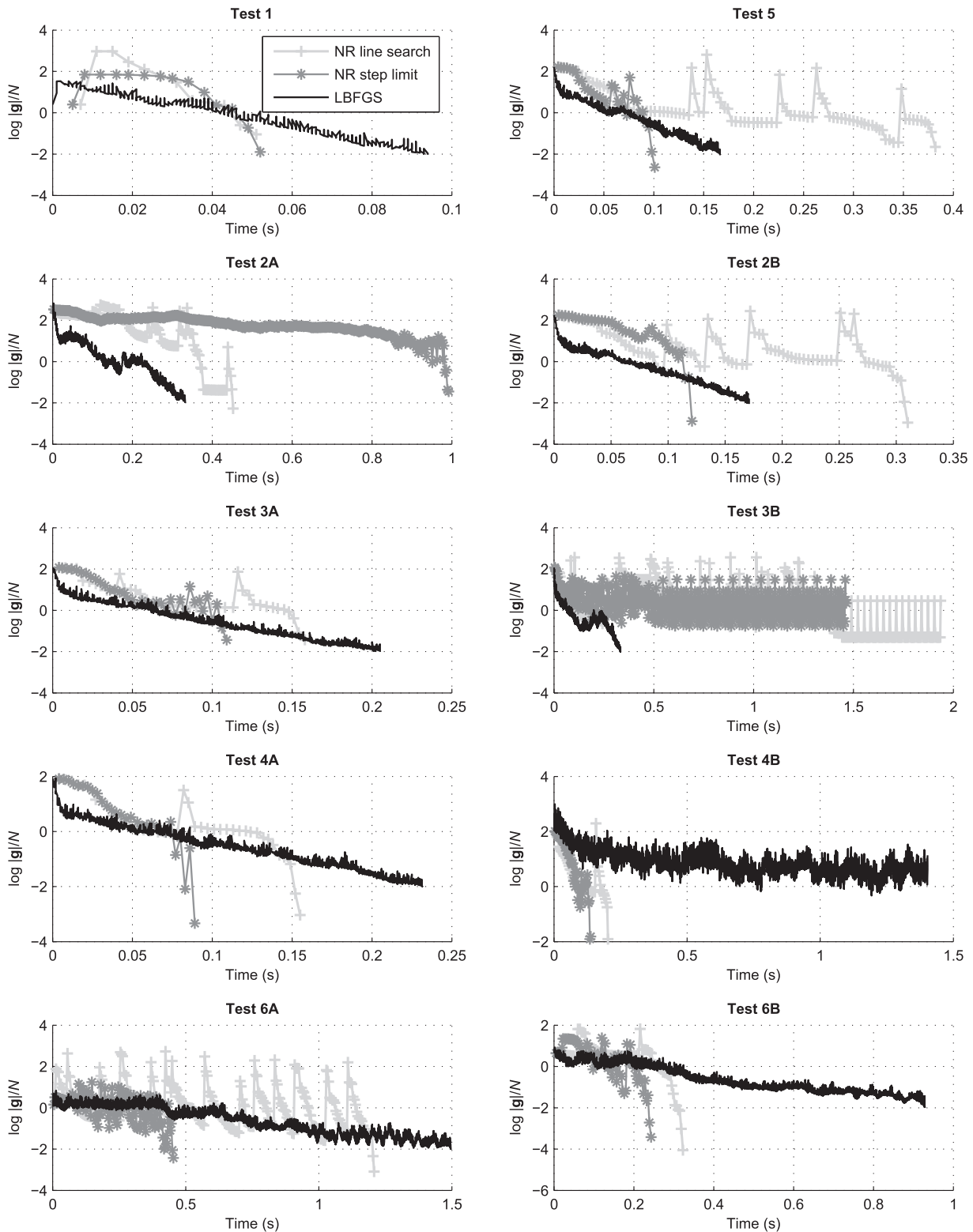


Fig. 8. Iteration history of different solution methods: log of the norm of the gradient \mathbf{g} divided by the size of the problem N .

Regarding the LBFGS method, it successfully solves all test cases except 4B (cables with a stiffness four orders of magnitude higher than the netting stiffness). Its behavior in test 4B is similar to those of NR methods in test case 3B: the convergence is very slow, and although it can eventually attain the medium precision solution, it cannot converge to the prescribed stopping gradient norm tolerance. Despite the overall position error is not high, a visual inspection

of the solution shows some 2D elements in a wrong position. Additional tests were carried out to verify that the convergence of LBFGS gets worse as the difference in stiffness values increases. Table 10 also shows a high position error for LBFGS in test 6A for a tolerance $|\mathbf{g}|/N \leq 0.5$, but it can eventually reach the correct solution at the stopping tolerance $|\mathbf{g}|/N \leq 10^{-2}$. The poor computational performance of LBFGS in test 6 can only be explained by

Table 10

Precision and computational effort of NR line search (NR-LS), NR step limit (NR-SL) and LBFGS methods, for a stopping tolerance of $\|g\|/N \leq 0.5$.

Test	Method	Function calls	$\ g\ /N$	$\ q - q_{ref}\ /N$	Time (s)
1	NR-LS	11	0.248	5.000×10^{-6}	0.047
	NR-SL	13	0.189	1.000×10^{-6}	0.049
	LBFGS	174	0.494	2.890×10^{-4}	0.046
2A	NR-LS	96	0.455	1.570×10^{-2}	0.376
	NR-SL	335	0.293	1.552×10^{-2}	0.994
	LBFGS	522	0.483	5.229×10^{-3}	0.131
2B	NR-LS	81	0.206	9.500×10^{-5}	0.299
	NR-SL	39	0.154	1.000×10^{-5}	0.116
	LBFGS	291	0.462	1.425×10^{-3}	0.074
3A	NR-LS	40	0.411	3.900×10^{-5}	0.151
	NR-SL	34	0.312	6.700×10^{-5}	0.100
	LBFGS	287	0.471	1.560×10^{-3}	0.073
3B	NR-LS	37	0.482	2.752×10^{-3}	0.140
	NR-SL	64	0.344	3.249×10^{-3}	0.188
	LBFGS	361	0.457	2.238×10^{-3}	0.092
4A	NR-LS	36	0.322	1.550×10^{-4}	0.138
	NR-SL	25	0.141	1.510×10^{-4}	0.077
	LBFGS	284	0.491	1.921×10^{-3}	0.080
4B	NR-LS	49	0.471	1.450×10^{-4}	0.189
	NR-SL	29	0.323	1.695×10^{-3}	0.089
	LBFGS	4247	0.472	4.353×10^{-3}	1.193
5	NR-LS	46	0.395	1.903×10^{-3}	0.178
	NR-SL	30	0.333	1.467×10^{-3}	0.092
	LBFGS	317	0.500	6.130×10^{-4}	0.084
6A	NR-LS	24	0.472	2.659×10^{-3}	0.117
	NR-SL	37	0.410	1.542×10^{-3}	0.144
	LBFGS	1070	0.452	1.213×10^{-2}	0.431
6B	NR-LS	54	0.495	7.007×10^{-4}	0.278
	NR-SL	39	0.295	1.100×10^{-3}	0.146
	LBFGS	702	0.486	4.268×10^{-3}	0.284

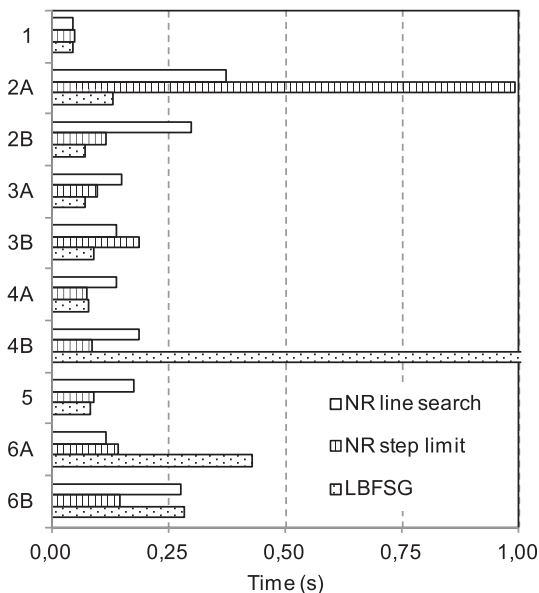


Fig. 9. Computational effort of NR line search, NR step limit and LBFGS methods, for a stopping tolerance of $\|g\|/N \leq 0.5$.

the presence of netting parallel to the water current, because cables of medium stiffness and ground contact were already present in tests 4A and 5. In this configuration, vertical forces on the rear part of the panel are small and more or less independent of the vertical position of the netting, and therefore LBFGS has trouble in finding the equilibrium position in the vertical direction; we still

do not fully understand all the mechanisms that cause this deficient behavior of LBFGS. In the remaining of the test cases, the iteration history of LBFGS shows a consistent reduction of the gradient norm, with small bounces in tests 2A and 3B. In general, the gradient norm curve fits very well with a straight line; the noise in the curve has a frequency of 4–5 iterations and a small amplitude. This means that the convergence ratio of the LBFGS method is practically independent on how far the initial position is from the solution, which makes LBFGS more robust than NR methods. Furthermore, users can easily predict the additional computational effort required to enhance the accuracy in the solution.

Results in Table 10 indicate that NR methods obtain a better precision than LBFGS: the error in position with respect to the reference position is, on average, one order of magnitude smaller. The main reason is that NR iterations in the local convergence region reduce the gradient norm in large steps, and therefore the final value of $\|g\|/N$ is usually a fraction of the 0.5 stopping value required to achieve a medium precision solution. On the other hand, LBFGS reduces the gradient norm in small steps, and its final value of $\|g\|/N$ is only slightly below the stopping value.

With respect to the computational effort required to attain a medium precision solution $\|g\|/N \leq 0.5$, LBFGS is equal or faster than the best NR method (usually NR line search) in all of the test cases except tests 6A–6B and obviously test 4B, despite it requires in the order of 10 times more function evaluations. This is because LBFGS only requires vector operations, and therefore its iterations are considerably faster than NR iterations, which require the solution of a linear equation system. LBFGS spends most of the time in function evaluations, while NR methods spend it in factorizations and back-substitutions to solve Eq. (3).

If a very high precision was required, for example the stopping tolerance in this experiment ($\|g\|/N \leq 10^{-2}$), the iteration history shows that NR methods would be faster than LBFGS in all the test cases. However, in this situation the best approach would be to solve the problem with a hybrid method: start with LBFGS to attain medium precision, and then continue the iteration with a classic Newton iteration to improve the solution with quadratic convergence in a few iterations; this combination of the two methods can generate high precision solutions with a computational effort smaller than NR methods.

In the case of shape optimization for netting structures that require the calculation of the equilibrium shape to carry out the evaluation of the objective function, the suitability of NR and LBFGS depends on the type of optimization strategy. In shape optimization methods that modify just one design variable at each iteration [17,18], the initial position for the equilibrium shape calculation (taken from the solution of the previous optimization iteration) is nearly identical to the solution, and therefore NR methods or even a classic Newton iteration will be more convenient. On the other hand, more advanced optimization methods that modify all the design variables at every iteration, or heuristic methods that can make large modifications in the design variables (e.g. mutation operators in genetic algorithms), will generate initial positions that are numerically far from the solution, and therefore LBFGS will be more suitable.

4.3. Effect of problem size

The size of the finite element models used in the previous numerical experiments is small, in the order of hundreds of variables (Table 8), to avoid tangled up mesh configurations in the iteration procedure. Since real world applications of netting structures require larger models, it is interesting to investigate how the problem size affects the computational performance of the assessed methods.

In this numerical experiment, the three methods compared in the previous experiment were applied to solve test case 1 using a numerical model of increasing size: the size of the triangular finite elements in the mesh was reduced progressively to increase the number of variables N from 363 (initial value in Table 8) to approximately 5000.

Results from this experiment are summarized in Fig. 10, which plots the computational effort (CPU-time) as a function of the problem size (number of variables N). Despite the three methods have a similar performance for very small problems, the advantage of the LBFGS method over NR methods increases noticeably with the problem size: for 5000 variables, LBFGS is 4 times faster than the best NR method. If this ratio is applied to scale the relative performances shown in Fig. 9 for small problems, LBFGS is estimated to be between 2 and 8 times faster than NR methods for problems of medium size ($N \sim 5000$), depending on the test case. For models with $N \sim 10^4$ variables, which can be considered as large models in the numerical simulation of netting structures [18], the trend on the right side of the figure suggests that the advantage of LBFGS can be even higher.

These results are explained by the fact that LBFGS only requires vector operations, while NR methods require the solution of a linear equation system. Despite a high-performance sparse solver was used in the implementation of NR, it is clearly outperformed by LBFGS for medium and large problem sizes. It is important to mention that LBFGS was implemented using the reference implementation of the Basic Linear Algebra Subprograms (BLAS) to evaluate the vector operations; if a hardware-optimized implementation were used, the performance of LBFGS in large problems could increase by a 30–40% [35]. However, the effect of the BLAS implementation in the performance of the direct sparse solver used in NR methods is negligible [35].

Fig. 10 also shows interesting behaviors of the two methods. For $N < 3000$, the LBFGS curve fits nearly exactly with a straight line of slope 1.5×10^{-4} , while NR curves have a worse linear fitting and a slope three times higher. For $N > 3000$ the slopes of the three methods are reduced, probably due to effects in the cache memory of the CPU hardware. However, the performance of NR methods gets more irregular as the problem size increases: this is caused by tangled mesh configurations generated occasionally during the iteration process, which increase the number of iterations required to converge to the solution. On the other hand, LBFGS does not generate tangled meshes because iterations advance at very small steps. Note that the test case used in this numerical experiment (test 1) is an easy, undemanding problem where the starting position is close

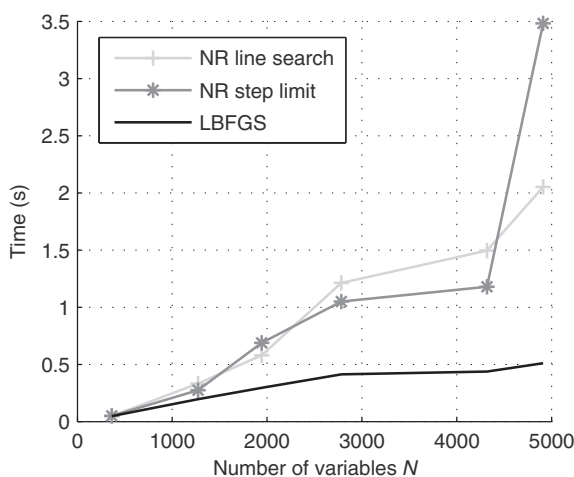


Fig. 10. Effect of problem size N on the computational efficiency of different methods applied to Test 1.

to the solution and mesh elements undergo small displacements; in problems where the mesh displacements are larger (e.g. test cases 2–5), the chances of getting tangled meshes are increased, and therefore the performance of NR methods will get even more irregular. According to the authors' experience, tangled mesh configurations are among the major causes of failure of NR methods in medium and large problems.

4.4. Implementation issues

Besides the results of the three numerical experiments presented in this section, the authors' experience with the different solution methods has also provided results related to their implementation.

The implementation of gradient-based optimization methods, and in particular the LBFGS method, is easier and more straightforward than NR methods, because the algorithms only require vector computations and avoid any kind of matrix operation. On the other hand, an efficient implementation of NR methods require the use of compressed sparse matrices, reordering algorithms and sparse linear equation solvers, which appreciably increments the complexity of the code.

Another disadvantage of NR methods is the need of analytical expressions (for the sake of efficiency) to evaluate the contribution of the different force terms to the Jacobian, which may have singularities that cause a failure in the method. For example, our implementation of the Jacobian of the hydrodynamic force model used in this work presents singularities when any of the two twine directions in a triangular finite element is parallel to the fluid velocity, since the cross product of both vectors is used during the evaluation; the workaround used by the authors was to make a momentary small change in the orientation of the triangular element during the Jacobian evaluation. These problems are hard to detect and require extensive debugging of the Jacobian terms. Conversely, gradient-based energy minimization methods only require energy terms, which can be easily calculated and do not present singularities. The implementation of material nonlinearity is also easier in energy minimization methods [19].

The LBFGS method also seems to be more suited to parallelization, because it spends most of the CPU time in evaluating energy and force in each finite element. Since these evaluations can be carried out in parallel with a low synchronization cost, the theoretical speedup of a parallel implementation is high. On the contrary, NR methods spend most of the CPU time in the solution of Eq. (3): numerical factorization of the Jacobian and back-substitution. A parallel linear equation solver could be used, but their speedups for the typical problem sizes in this application field are low [36], and therefore the theoretical speedup of a parallel NR implementation is also low.

5. Conclusions and future work

The aim of this paper has been to assess the robustness and computational efficiency of gradient-based energy minimization methods to calculate the equilibrium shape of netting structures, as an alternative to the Newton–Raphson iteration that is normally used in this kind of analysis. For this purpose, the authors used a set of benchmarks problems that replicate different challenging features that are present in real world applications of netting structures. Orientation-dependent non-conservative forces (e.g. drag) were included in the numerical model.

Ten gradient-based optimization methods were preselected for evaluation, and three of them were suitable for netting structures: nonlinear conjugated gradient, limited memory Broyden–Fletcher–Goldfarb and Shanno (LBFGS) and Newton–CG trust

region. Numerical experiments show that LBFGS is nearly twice as efficient as the other methods.

LBFGS was compared with two globalized variants of the Newton–Raphson (NR) iteration: the well-known *NR line search* method, which uses a line search and the Armijo rule as sufficient decrease condition, and the *NR step limit* method that limits the step length by a fraction of the characteristic length of the netting structure.

Regarding the behavior of NR methods, the following conclusions can be established:

- The NR step limit method performs better than the NR line search method in most of the problems, since it is not affected by stagnation.
- Both methods exhibit poor convergence in netting materials with very low compression stiffness (equal or less than 1% of the tension stiffness).
- Both methods have difficulty with initial positions that are far from the solution, since their iteration process usually generates tangled meshes which increase the computation time and may converge to an invalid (e.g. tangled) solution.
- Their performance gets more irregular as the problem size increases, since the chances of generating a tangled mesh configuration during the iteration are also increased.

Regarding the LBFGS method, it has been found that it has the following advantages over Newton–Raphson methods:

- It is usually faster in achieving medium precision solutions, and its advantage increases with the problem size. For problems of medium size ($N \sim 5 \times 10^3$ variables), LBFGS is estimated to be between 2 and 8 times faster, depending on the type of problem. In the unusual cases where a high precision solution is required, the use of LBFGS followed by a classic Newton iteration is presumably faster than a globalized NR method. Only problems with a starting position that is nearly identical to the solution make LBFGS slower than NR methods.
- It is more robust, since it often converges to the solution at a constant rate regardless of the goodness of the initial position, the magnitude of the displacements in the structure or the size of the finite element mesh. LBFGS does not suffer from stagnation and it avoids the generation of tangled meshes.
- It is significantly easier to implement: its algorithm avoids matrix operations, and it does not require the error-prone evaluation of analytical Jacobians. The lack of Jacobians also makes easier to implement and test new force models.
- It offers more opportunities for parallelization, since it spends most of the computing time in function evaluations, which can be parallelized with high theoretical speedups.

On the other hand, LBFGS also has drawbacks. It shows very poor convergence in problems with elements of very different stiffness (four orders of magnitude or more), such as soft netting structures attached to wire ropes of medium or large diameter. Problems where netting panels are towed parallel to the water flow, such in the case of bottom trawl fishing gears, also reduce the convergence ratio of the method.

The advantages of the LBFGS method suggest that it is a good candidate to replace or complement Newton–Raphson methods currently used in the equilibrium shape calculation of netting structures. Further research must be carried out to diminish its drawbacks and to verify that it also exhibits good performance when applied to real world applications in fishing and aquaculture. Results also show that both LBFGS and NR are several orders of magnitude faster than dynamic simulation methods used by some

authors to find the equilibrium shape of netting structures [1,7,9,23].

In addition, the proposed set of test cases has demonstrated to be a useful tool to assess the performance of simulation methods for netting structures, since it has revealed the advantages and shortcomings of the tested methods. Its simplicity also encourages its reuse in future research, making easier to compare results from different works.

References

- [1] Bessonneau JS, Marichal D. Study of the dynamics of submerged supple nets (Applications to trawls). *Ocean Eng* 1998;25:563–83.
- [2] Tsukrov I, Eroshkin O, Fredriksson D, Swift MR, Celikkol B. Finite element modeling of net panels using a consistent net element. *Ocean Eng* 2003;30:251–70.
- [3] Le Dret H, Lewandowski R, Priour D, Chagneau F. Numerical simulation of a cod end net. Part 1: Equilibrium in a uniform flow. *J Elast* 2004;76:139–62.
- [4] Priour D. Calculation of net shapes by the finite element method with triangular elements. *Commun Numer Methods Eng* 1999;15:755–63.
- [5] Nicoll RS, Steinke DM, Attia J, Roy A, Buckham BJ. Simulation of a high-energy finfish aquaculture site using a finite element net model. In: Proceedings of the international conference on offshore mechanics and arctic engineering – OMAE; 2011; p. 35–44.
- [6] Priour D. Analysis of nets with hexagonal mesh using triangular elements. *Int J Numer Methods Eng* 2003;56:1721–33.
- [7] Takagi T, Shimizu T, Suzuki K, Hiraishi T, Yamamoto K. Validity and layout of “NaLA”: a net configuration and loading analysis system. *Fish Res* 2004;66:235–43.
- [8] Li Y-C, Zhao Y-P, Gui F-K, Teng B. Numerical simulation of the hydrodynamic behaviour of submerged plane nets in current. *Ocean Eng* 2006;33:2352–68.
- [9] Lee C-W, Lee J-H, Cha B-J, Kim H-Y, Lee J-H. Physical modeling for underwater flexible systems dynamic simulation. *Ocean Eng*. 2005;32:331–47.
- [10] O'Neill FG. Axisymmetric trawl cod-ends made from netting of a generalized mesh shape. *IMA J Appl Math (Inst Math Appl)* 1999;62:245–62.
- [11] Priour D, Herrmann B, O'Neill FG. Modelling axisymmetric cod-ends made of different mesh types. *Proc IMechE Part M: J Eng Maritime Env* 2009;223:137–44.
- [12] DeCew J, Tsukrov I, Risso A, Swift MR, Celikkol B. Modeling of dynamic behavior of a single-point moored submersible fish cage under currents. *Aquacult Eng* 2010;43:38–45.
- [13] Lee C-W, Kim Y-B, Lee G-H, Choe M-Y, Lee M-K, Koo K-Y. Dynamic simulation of a fish cage system subjected to currents and waves. *Ocean Eng* 2008;35:1521–32.
- [14] O'Neill FG, Priour D. Comparison and validation of two models of netting deformation. *J Appl Mech Trans ASME* 2009;76:1–7.
- [15] O'Neill FG, Herrmann B. PRESEMO – A predictive model of codend selectivity – a tool for fishery managers. *ICES J Mar Sci* 2007;64:1558–68.
- [16] Priour D. Numerical optimisation of trawls design to improve their energy efficiency. *Fish Res* 2009;98:40–50.
- [17] Khaled R, Priour D, Billard J-Y. Numerical optimization of trawl energy efficiency taking into account fish distribution. *Ocean Eng* 2012;54:34–45.
- [18] Khaled R, Priour D, Billard J-Y. Cable length optimization for trawl fuel consumption reduction. *Ocean Eng* 2013;58:167–79.
- [19] Toklu Y. Nonlinear analysis of trusses through energy minimization. *Comput Struct* 2004;82:1581–9.
- [20] Bouzidi R, van AL. Numerical solution of hyperelastic membranes by energy minimization. *Comput Struct* 2004;82:1961–9.
- [21] Herrmann B, Priour D, Krag LA. Theoretical study of the effect of round straps on the selectivity in a diamond mesh cod-end. *Fish Res* 2006;80:148–57.
- [22] Priour D. Introduction of mesh resistance to opening in a triangular element for calculation of nets by the finite element method. *Commun Numer Methods Eng* 2001;17:229–37.
- [23] Vincent B. A new generation of tools for trawls – dynamic numerical simulation. In: Proceedings of the fourth DEMaT workshop, Rostock; 1999.
- [24] Pichot G, Germain G, Priour D. On the experimental study of the flow around a fishing net. *Eur. J. Mech. B/Fluids* 2009;28:103–16.
- [25] Kelley CT. Iterative methods for linear and nonlinear equations. Philadelphia: SIAM; 1995.
- [26] Kelley CT. Solving nonlinear equations with Newton's method. Philadelphia: SIAM; 2003.
- [27] Mistakidis ES. Nonconvex optimization in mechanics: algorithms, heuristics, and engineering applications by the F.E.M. Dordrecht; Boston: Kluwer Academic Publishers; 1998.
- [28] Kelley CT. Iterative methods for optimization. Philadelphia: SIAM; 1999.
- [29] Fletcher R. Practical methods of optimization. Chichester, New York: Wiley; 1987.
- [30] Dunlavy DM, Kolda TG, Acar E. Poblano v1.0: A matlab toolbox for gradient-based optimization. Sandia national laboratories, Albuquerque, NM and Livermore, CA; 2010.
- [31] Matlab. The MathWorks Inc; 2013.
- [32] González M, González F, Luaces A, Cuadrado J. A collaborative benchmarking framework for multibody system dynamics. *Eng Comput* 2010;26:1–9.

- [33] Moe H, Olsen A, Hopperstad OS, Jensen Ø, Fredheim A. Tensile properties for netting materials used in aquaculture net cages. *Aquacult Eng* 2007;37:252–65.
- [34] Sala A, O'Neill FG, Buglioni G, Lucchetti A, Palumbo V, Fryer RJ. Experimental method for quantifying resistance to the opening of netting panels. *ICES J Mar Sci* 2007;64:1573–8.
- [35] González M, González F, Dopico D, Luaces A. On the effect of linear algebra implementations in real-time multibody system dynamics. *Comput Mech* 2008;41:607–15.
- [36] González F, Luaces A, Luján U, González M. Non-intrusive parallelization of multibody system dynamic simulations. *Comput Mech* 2009;44:493–504.

Article No. 4

An efficient and accurate model for netting structures with mesh resistance to opening

Amelia de la Prada, Manuel González

Submitted to the *International Journal of Solids and Structures*
on 25th April 2014

An efficient and accurate model for netting structures with mesh resistance to opening

Amelia de la Prada, Manuel González*

Laboratorio de Ingeniería Mecánica
Escola Politécnica Superior, Universidade da Coruña
Mendizábal s/n, 15403 Ferrol, Spain

E-mail address: amelia.delaprada@udc.es, manuel.gonzalez@udc.es

* Corresponding author.

E-mail address: manuel.gonzalez@udc.es tel.: (+34) 981337400 fax: (+34) 981337410

Abstract

Netting structures are extensively used in industrial fishing and aquaculture. In recent years, there is a trend towards the use of netting materials manufactured with thicker and stiffer twines. The increased mesh resistance to opening of such materials has a notable impact in the structural response and performance of the structures. Several models exist to simulate this behaviour, but they do not combine efficiency and accuracy. This work describes a new lumped mass model for netting structures with mesh resistance to opening. It is designed to be used in applications that only require calculating the shape of the structure but not the stress field in the material, a common case in marine applications. The model combines a non-linear twine beam model for small axial deformations, a twine spring model for large axial deformations and a sphere model for netting knots. Results of numerical and experimental validations are presented. The model is robust, accurate and very efficient: its computational performance is similar to linear models that do not consider mesh resistance to opening. It shows an excellent agreement with experimental data, significantly better than previous models described in the literature. Furthermore, it can be easily implemented in existing computer codes for netting structures based on lumped mass methods.

Keywords: netting, resistance to opening, elastic behavior, lumped mass, equilibrium

1. Introduction

Flexible netting structures are extensively used in marine applications such as industrial fishing gears and aquaculture cages. The increasing concerns about the energy efficiency and environmental impact of these structures have driven the development of numerical models specially designed for them. They can be categorized as 1D finite element models (Tsukrov et al., 2003; Wan et al., 2002), 2D finite element models (Nicoll et al., 2011; Priour, 2003, 1999), lumped mass models (Bessonneau and Marichal, 1998; Le Dret et al., 2004; Lee et al., 2005, 2008; Li et al., 2006; Takagi et al., 2004; Theret, 1993) and differential equation models for axisymmetric structures (O'Neill, 1999; Priour et al., 2009). Such models have been successfully applied to solve real-life design and optimization problems in fishing and aquaculture (DeCew et al., 2010; Lee et al., 2011, 2011; Priour, 2009; Shimizu et al., 2007; Xu et al., 2011).

In most marine applications, the performance of a netting structure is mainly determined by its equilibrium shape under static or quasi-static conditions. Stress or vibrations under dynamics loads are not important in this kind of structures. For example, the shape of a fishing trawl affects its hydrodynamic drag and its energy efficiency (Priour, 2009), and individual mesh shapes determine the size selectivity of a fishing gear (O'Neill and Herrmann, 2007). In addition, the computational performance of the models is becoming an important issue due to the recent inception of topology optimization of netting structures (Khaled et al., 2012; Priour, 2009). Therefore, most netting models focus on calculating the equilibrium position in an efficient and accurate way, and they do not calculate stress fields in the material.

In recent years there is a trend towards the use of netting materials manufactured with thicker and stiffer twines in order to increase the durability of the fishing gears (Sala et

al., 2007b). The increased mesh resistance to opening of such materials has a notable impact in the structural response and performance of the gears. Fig. 1 illustrates the effect of the resistance to opening in netting of diamond-oriented mesh (Fig. 1a), the predominant material in marine applications: thicker and stiffer twines hinder mesh opening in normal direction (Fig. 1b) compared with transverse direction (Fig. 1c). The mesh resistance to opening is mainly characterized by the twine bending stiffness EI (Herrmann and O'Neill, 2006; O'Neill, 2004). Theoretical and experimental studies demonstrate that mesh resistance to opening plays a major role in the reduction of selective performance of fishing trawls (Herrmann and O'Neill, 2006; Herrmann et al., 2013; Lowry and Robertson, 1996; Sala et al., 2007a): an increased resistance to opening hampers mesh opening in the codend (the aft end of fishing trawls where fish is retained), which affects the escapement of small fish. An increased twine bending stiffness also changes the overall shape of the fishing gear during fishing operations (O'Neill, 2004; Priour, 2001), which has an impact on the hydrodynamic drag and thus affects the energy efficiency of the gear (Priour, 2009). Therefore, methods to incorporate mesh resistance to opening in numerical models of netting materials are becoming fundamental to accurately simulate the structural response and performance of modern flexible netting structures.

Most of the numerical models for netting materials ignore mesh resistance to opening because they assume that twines are completely flexible and easily bent without resistance. Only two models have been adapted to take into account this mechanical property. Priour proposed a model based on the assumption that the couple created by the twines on the knots varies linearly with the angle between twines (Priour, 2001). Although this linear model can be easily included in numerical formulations, it is not derived from any physical law and the twine bending stiffness EI is not a parameter of

the model. O'Neill described the equations governing the bending stiffness of a twine and found an exact analytical solution and an asymptotic analytical solution (O'Neill, 2002). The exact solution is far too complex for practical applications. The asymptotic solution expresses the position of the end points of the twine as an explicit function of the tensile forces acting on it. It is only valid when the tensile forces are very high compared to the twine bending stiffness, and it is used in the differential equation models by the same author (O'Neill and Herrmann, 2007), which are limited to axisymmetric structures. This asymptotic solution has drawbacks when used in more general numerical formulations (i.e., not limited to axisymmetric structures) that need to evaluate elastic forces in twines as a function of mesh deformation: it does not consider twine axial elongation and it needs to be numerically inverted for every mesh element in the model at every simulation iteration, causing a significant computational overhead.

We have recently developed a nonlinear stiffness model for a twine (de la Prada and González, 2014a) that overcomes the drawbacks of the two abovementioned models for mesh resistance to opening: it takes into account both axial and bending stiffness of the twines, it is very accurate and it has a low computational overhead. This work uses that twine stiffness model to develop an efficient and accurate model to calculate the equilibrium position of flexible netting structures with mesh resistance to opening. The main contributions of this work are:

(i) The twine stiffness model developed in (de la Prada and González, 2014a) is only valid for small axial deformations. However, twines can experience very large and unrealistic axial deformations in numerical simulations due to iterations that lead the model through positions very far from the equilibrium (de la Prada and González, 2014b). Here we extend our twine stiffness model in order to be able to deal with such large axial deformations.

(ii) Previous numerical models of netting represent knots as points and therefore neglect their size and structure. A preliminary research with analytical axisymmetric models in (O'Neill, 1999) demonstrate that taking into account the structure of the knots is essential to get a good agreement between numerical and experimental results. The numerical model presented here represents knots as spheres instead of points, and therefore the average knot radius is taken into account in the simulations.

(iii) Previous models of netting based on the lumped mass method require eight point masses to represent a numerical mesh: four at the knots and four at the midpoint of the twines. The twine stiffness model used in this work avoids the need of the point masses at the centres of the twines, thus reducing the number of degrees of freedom of the models.

The remaining of the paper is organized as follows: Section 2 describes the numerical model for netting structures; Section 3 presents a numerical validation, comparing the model with a detailed finite element model and assessing its robustness and accuracy; Section 4 presents an experimental validation of the model; Section 5 assesses the computational efficiency of the model and compares it with a traditional formulation which does not consider mesh resistance to opening. Finally, Sections 6 and 7 present the discussion and the conclusions.

2. Model

2.1. Twine model for small axial deformations

The twine stiffness model used in this work was developed by the authors in (de la Prada and González, 2014a). Based in the approach proposed in (O'Neill, 2002), a twine is modelled as the bi-dimensional double-clamped beam shown in Fig. 2, where

\mathbf{p}_0 and \mathbf{p}_1 are the points where the beam attaches to the knots and φ_0 is the slope angle between the twine and the knots at the insertion points. The x -axis and the y -axis are aligned with the transverse direction and the normal direction of the mesh, respectively. The novelty of this model is the method used to obtain the force-displacement response of the twine. Point \mathbf{p}_0 was fixed and an enforced displacement constraint was applied to \mathbf{p}_1 to calculate the reaction force \mathbf{f}^{beam} at that point by nonlinear static finite element analysis (Zienkiewicz, 2000). The displacement constraint placed \mathbf{p}_1 on the vertices of a rectangular curvilinear grid of size $[r_{min}, r_{max}] \times [\varphi_{min}, \varphi_{max}] = [0.92, 1.05] \times [0, \pi/2]$, where $r = (x_{twine}^2 + y_{twine}^2)^{0.5} / L_{twine}$ is the dimensionless distance between \mathbf{p}_0 and \mathbf{p}_1 , L_{twine} is the length of the twine, $\varphi = \psi - \varphi_0$ and $\psi = \tan^{-1}(y_{twine}/x_{twine})$. This grid spans all the deformed positions that a twine can undergo in bending and moderate compression or tension. A static analysis was run for each vertex of the grid, and dimensional analysis and fitting techniques were applied to the obtained results to find a dimensionless model that expresses the reaction force \mathbf{f}^{beam} as an explicit function of the twine deformation. The best compromise between simplicity and accuracy consists on a polynomial surface fitting of the polar components of the force $\mathbf{f}^{beam} = (F_r^{beam}, F_\varphi^{beam})$ as a function of the coordinates (r, φ) of \mathbf{p}_1 , resulting in a polynomial degree (m, n) of (2,3) for the radial component and (1,4) for the tangential component:

$$F_r^{beam}(r, \varphi) = \left(\frac{EI}{L_{twine}^2} \right) \sum_{0 < i+j < m+n} c_{ij} r^i (\cos \varphi)^j \quad (1)$$

$$F_\varphi^{beam}(r, \varphi) = \left(\frac{EI}{L_{twine}^2} \right) \sum_{0 < i+j < m+n} c_{ij} r^i (\cos \varphi)^j \quad (2)$$

Coefficient values of both polynomial surfaces are provided in Table 1 and Table 2 for three representative values of the twine axial stiffness EA in netting materials: 500 N, 1000 N and 2000 N. It was shown in (de la Prada and González, 2014a) that the effect of EA is negligible for moderate vertical deformations of the twine ($\varphi < 48^\circ$). For larger deformations, forces can be evaluated using three-point parabolic interpolation for a given EA . The resulting twine stiffness model has a high goodness of fit with respect to the finite element model, with a coefficient of determination R^2 above 0.98 and a relative error below 7%.

2.2. Twine model for large axial deformations

The twine model described in the previous subsection is only valid for deformations within the boundaries of the rectangular curvilinear grid $[r_{min}, r_{max}] \times [\varphi_{min}, \varphi_{max}]$ used to generate the fitting. This grid size spans all of the deformed positions that a mesh twine can undergo in real applications of netting structures, but twines can experience larger, unrealistic axial deformations in a numerical simulation due to iterations that lead the model through positions very far from the equilibrium (de la Prada and González, 2014b). This is often the case when Newton iteration is used to find the equilibrium position of the structure, particularly at the first iterations. In order to overcome this problem, the beam model is replaced by a translational spring between \mathbf{p}_0 and \mathbf{p}_1 when the dimensionless distance r between both points is outside the interval $[r_{min}, r_{max}]$. In this way, if the twine reaches a very large axial deformation, the spring model is activated to bring it close to the equilibrium position in a few iterations.

The translational spring force is expressed in polar components as $\mathbf{f}^{spring} = (F_r^{spring}, 0)$, and two models for F_r^{spring} are considered in this work. The first one corresponds to an ideal mechanical linear spring of natural length L_{twine} :

$$F_r^{spring}(r) = EA(r-1) \quad (3)$$

while the second model corresponds to a spring with variable natural length, thus taking into account the reduction in the distance between \mathbf{p}_0 and \mathbf{p}_1 as the twine bends:

$$F_r^{spring}(r, \cos \varphi) = EA(r - r_{eq}(\cos \varphi)) \quad (4)$$

where the length $r_{eq}(\cos \varphi)$ is the dimensionless radial coordinate of the trajectory described by \mathbf{p}_1 when F_r^{beam} is zero. This trajectory was calculated in (de la Prada and González, 2014a) as $r_{eq}(\cos \varphi) = a \cdot \cos \varphi + b$, and the coefficients $a = 0.202$ and $b = 0.798$ are nearly independent of the twine axial stiffness EA .

To achieve a smooth transition between the beam model and the spring model, a piecewise linear blending function $\alpha(r)$ is defined. Hence, the total force in the twine $\mathbf{f}(r, \varphi) = (F_r, F_\varphi)$ can be expressed as a composition of the forces derived from the beam model \mathbf{f}^{beam} (Eq. 1 and Eq. 2) and the spring model \mathbf{f}^{spring} (Eq. 3 or Eq. 4):

$$\mathbf{f}(r, \varphi) = \alpha \mathbf{f}^{beam} + (1 - \alpha) \mathbf{f}^{spring} \quad (5)$$

Fig. 3 shows the shape of the function $\alpha(r)$ defined in Eq. 6. The parameter ε determines the width of the transition region.

$$\alpha(r) = \begin{cases} 0 & \text{if } r < (r_{min} - \varepsilon) \\ (r - r_{min} + \varepsilon) / \varepsilon & \text{if } (r_{min} - \varepsilon) < r < r_{min} \\ 1 & \text{if } r_{min} < r < r_{max} \\ (-r + r_{max} + \varepsilon) / \varepsilon & \text{if } r_{max} < r < (r_{max} + \varepsilon) \\ 0 & \text{if } r > (r_{max} + \varepsilon) \end{cases} \quad (6)$$

When $r < (r_{min} - \varepsilon)$ or $r > (r_{max} + \varepsilon)$, the twine is highly stressed, $\alpha = 0$ and the model behaves as a spring. When $r_{min} \leq r \leq r_{max}$, the model behaves as a beam.

In the unusual applications where the netting structure in equilibrium position may have twines with large compression that affect the overall shape of the structure, the axial stiffness EA in Eqs. (3) and (4) can be replaced by a lower value when $r < r_{min}$.

2.3. Mesh model

Most models for marine netting structures are based on the lumped mass method: the netting is modelled as a series of lumped point masses that are interconnected with massless force elements (Bessonneau and Marichal, 1998; Le Dret et al., 2004; Lee et al., 2005, 2008; Li et al., 2006; Takagi et al., 2004; Theret, 1993). We chose this modelling method because it is very efficient when the stress fields in the material are not required and it allows introducing new force elements in an easy way.

For the sake of clarity, the following description assumes that (i) the netting material has a diamond-mesh configuration (Fig. 1), the most common netting in marine applications; and (ii) a numerical mesh represents a physical mesh. These assumptions do not limit the applicability of the formulation. The mesh model presented in this work can be easily adapted to other mesh geometries, for instance, square and hexagonal meshes. Mesh grouping techniques can be used to model a group of physical meshes by a single equivalent numerical mesh in order to reduce the number of variables in the model (Theret, 1993).

A numerical mesh (Fig. 4) is made up of four nodes $\{\mathbf{p}_0, \mathbf{p}_1, \mathbf{p}_2, \mathbf{p}_3\}$ placed at the centre of the knots. Each node \mathbf{p}_i has three translational degrees of freedom (x, y, z) and an associated lumped mass that represents $\frac{1}{4}$ of the total mass of the numerical mesh.

Nodes are numbered in clockwise order: nodes \mathbf{p}_0 and \mathbf{p}_2 are aligned with the transverse direction of the mesh (Fig. 1) and nodes \mathbf{p}_1 and \mathbf{p}_3 are aligned with the normal direction.

In this way, the transverse direction \mathbf{t} of the mesh is calculated as:

$$\mathbf{t} = (\mathbf{p}_2 - \mathbf{p}_0) / |\mathbf{p}_2 - \mathbf{p}_0| \quad (7)$$

Netting knots are modelled as spheres of diameter D centred at the nodes. The knots are connected by four massless twine elements $\{T_{01}, T_{21}, T_{23}, T_{03}\}$. The ending points of the twines \mathbf{p}_{ij} and \mathbf{p}_{ji} are located at the surface of the knot spheres and aligned with the nodes \mathbf{p}_i and \mathbf{p}_j :

$$\begin{aligned} \mathbf{p}_{ij} &= \mathbf{p}_i + (D/2)(\mathbf{p}_j - \mathbf{p}_i) / |\mathbf{p}_j - \mathbf{p}_i| \\ \mathbf{p}_{ji} &= \mathbf{p}_j - (D/2)(\mathbf{p}_j - \mathbf{p}_i) / |\mathbf{p}_j - \mathbf{p}_i| \end{aligned} \quad (8)$$

The following paragraphs describe how to evaluate the elastic forces on nodes \mathbf{p}_0 and \mathbf{p}_1 due to twine element T_{01} . The procedure for twines T_{21} , T_{23} and T_{03} is analogous.

A local basis $\{\mathbf{u}_r, \mathbf{u}_\varphi, \mathbf{u}_z\}$ is defined for each twine T_{ij} . Fig. 4 shows the local basis of twine T_{01} (\mathbf{u}_z is not shown since it is normal to the plane of the figure). The origin of coordinates is located on point \mathbf{p}_{01} , and the directions are defined as:

$$\begin{aligned} \mathbf{u}_r &= (\mathbf{p}_1 - \mathbf{p}_0) / |\mathbf{p}_1 - \mathbf{p}_0| \\ \mathbf{u}_z &= \mathbf{t} \times \mathbf{u}_r \\ \mathbf{u}_\varphi &= \mathbf{u}_r \times \mathbf{u}_z \end{aligned} \quad (9)$$

The dimensionless polar coordinates r and φ of the twine are evaluated as

$$\begin{aligned} r &= |\mathbf{p}_{01} - \mathbf{p}_{10}| / L_{twine} \\ \varphi &= \psi - \varphi_0 = a \cos(\mathbf{t} \cdot \mathbf{u}_r) - \varphi_0 \end{aligned} \quad (10)$$

and they are used to evaluate the twine force $\mathbf{f}^{twine}(r, \varphi) = (F_r, F_\varphi)$ according to Eq. 5.

The force applied by twine T_{01} on its ending nodes \mathbf{p}_0 and \mathbf{p}_1 can be expressed in the local basis of the twine as

$$\begin{aligned} \bar{\mathbf{f}}_0^{twine} &= (-F_r, -F_\varphi, 0) \\ \bar{\mathbf{f}}_1^{twine} &= (F_r, F_\varphi, 0) \end{aligned} \quad (11)$$

These local forces are transformed to the global coordinate system by the twine transformation matrix \mathbf{T} :

$$\mathbf{T}_{01} = [\mathbf{u}_r \quad \mathbf{u}_\varphi \quad \mathbf{u}_z] \quad (12)$$

$$\begin{aligned} \mathbf{f}_0^{twine} &= \mathbf{T}_{01} \cdot \bar{\mathbf{f}}_0^{twine} \\ \mathbf{f}_1^{twine} &= \mathbf{T}_{01} \cdot \bar{\mathbf{f}}_1^{twine} \end{aligned} \quad (13)$$

The total force on each node also includes the contribution of all the usual forces that act on marine netting structures, which can be calculated with well-known methods (Priour, 2013): hydrodynamic drag \mathbf{f}^{hydro} , weight \mathbf{f}^{weight} , buoyancy $\mathbf{f}^{buoyancy}$ and bottom contact with the seafloor $\mathbf{f}^{contact}$:

$$\mathbf{f}_i = \mathbf{f}_i^{twine} + \mathbf{f}_i^{hydro} + \mathbf{f}_i^{weight} + \mathbf{f}_i^{buoyancy} + \mathbf{f}_i^{contact} \quad (14)$$

Previous lumped mass models of netting structures use eight nodes per mesh: four at the knots and four at the midpoint of the twines. The nodes at the midpoint of the twines are required to simulate twine bending, because such models represent twines as bar elements articulated in the nodes. Our model avoids the nodes in the twines because our twine element takes into account twine bending, thus reducing the number of degrees of freedom in the model.

As far as the knot shape is concerned, experimental methods to measure mesh resistance to opening (Sala et al., 2007b) assume that knots are rigid rectangles of size $a \times b$ and that twines emerge from the rectangle corners (Fig. 5). Note that the rectangle size does not match with the knot external size $a_{ext} \times b_{ext}$ because in the numerical model the twine is modelled as the central line of the real twine. This work models knots as

spheres of diameter D , and D can be estimated from the rectangle size $a \times b$ estimated from experimental measurements. We have found that $D = (a + b) / 2$ works well.

3. Numerical validation

Three numerical experiments were carried out to evaluate the accuracy and the robustness of the numerical model described in the previous section. The test problem used in the three experiments is based on the experimental procedure used in (Sala et al., 2007b) to measure the mesh resistance to opening of netting panels. It consists on a 3×3 mesh netting panel that is stretched by applying simultaneous transverse and normal loads F_t and F_n to its edges, while the transverse L_t and normal L_n mesh openings are measured (Fig. 6). The loads and the properties of the netting panel are taken from (Sala et al., 2007b) for traditional green-braided polyethylene 7270 Rtex: mesh size $L_{mesh} = 92$ mm, knot size $a \times b = 2 \times 2.1$ mm, $EI = 345$ N/mm² and $\varphi_0 = 15^\circ$. The applied loads $F_t = F_n$ range from 0 to 15 kg.

3.1. Comparison with a detailed finite element model

A detailed finite element model (FEM) of the test problem was built with a commercial software (ANSYS, 2007). Each twine was discretized with 20 BEAM189 elements, a quadratic 3D element based on Timoshenko beam theory suited for large rotation and large strain linear applications. Knots were modelled as rigid rectangles using four MPC184-Rigid-Beam elements. The model has 2220 nodes and 13320 degrees of freedom. A geometric nonlinear static analysis was used to calculate the mesh openings L_t and L_n for each value of the applied load. The test problem was also modelled with the formulation described in the previous Section. This lumped mass model has 24 nodes and 74 degrees of freedom. The optimization method described in (de la Prada

and González, 2014b) was used to find the equilibrium shape of the panel for each value of the applied load.

Fig. 7 compares the solutions of the two models: it plots the values of L_t and L_n (Fig. 7a) and the relative errors in both variables calculated with the lumped mass model using the FEM solution as reference (Fig. 7b). Both models generate very similar solutions, and the relative error of the lumped mass model is below 5% in most of the load range. This error is a result of two simplifications: (i) the approximation introduced in the twine stiffness model described by Eqs. (1) and (2), and (ii) the approximation of knots as spheres instead of rectangles. The relative error in L_n reaches 12% when the applied load is close to zero, but this situation does not happen in real-life applications.

3.2. Robustness to bad initial positions

Numerical methods to find the equilibrium shape of netting structures start from an initial position provided by the user. In real marine applications (e.g. complex designs of fishing gears), it is difficult to estimate a good initial position. Hence, the netting model and the solution method should be robust enough to converge to the right solution despite of starting from bad initial positions. In this numerical experiment, the equilibrium shape of the test problem (Fig. 6) is calculated for a load of 3 kg starting from different initial positions, in order to evaluate the robustness of our formulation.

The initial position is obtained by applying a stretching factor β to the shape of the unstretched panel. That is, the transverse and normal dimensions of the panel in the initial position are βL_t^{panel} and βL_n^{panel} , where L_t^{panel} and L_n^{panel} are the dimensions of the unstretched panel. These unstretched dimensions are calculated as

$$L_t^{panel} = m_t L_{mesh} \cos \varphi_0 \quad (13)$$

$$L_n^{panel} = m_n L_{mesh} \sin \varphi_0 \quad (14)$$

where m_t and m_n are number of meshes in transverse and normal direction (3 in the test problem) and L_{mesh} is the nominal mesh size. The stretching factor β ranges from 0.1 to 10, and therefore the panel can be highly compressed (panel area 10 times smaller) or stretched (panel area is 10 times larger) in the initial position, compared with the unstretched shape. The optimization method described in (de la Prada and González, 2014b) was used to find the equilibrium position of the panel. The two twine models for large axial deformations described in Section 2 were used: the linear spring model in Eq. (3) and the variable natural length spring model in Eq. (4).

Fig. 8 plots the number of function calls required to achieve the equilibrium as a function of the stretching factor β . Both spring models were able to converge to the right solution even for the minimum and maximum values of β . Both models present a quite similar behaviour for $\log_{10}(\beta) < 0.3$, but the linear spring model is more efficient for higher stretching factors. The high number of function calls shown in the figure is caused by the high accuracy required to the solution and the optimization method used to solve the problem, which does not use the Jacobian of the forces. Experiments with a lower level of accuracy result in a lower number of function calls but confirm the trend shown in Fig. 8. We have also confirmed that a twine model for large axial deformations is required to solve the problem even when β is close to 1.

3.3. Influence of the transition region of the blending function

The blending function $\alpha(r)$ defined in Eq. 6 depends on the parameter ε , which determines the width of the transition region between the beam model and the spring model. This parameter affects the convergence ratio of the model. Fig. 9 plots the number of function calls required to reach the equilibrium as a function of ε for three

different initial positions (stretching factor $\beta = 1, 2, 3$). Numerical experiments for higher values of β were carried out, but results are not shown since they follow the trend in Fig. 9. The influence of ε becomes noticeable when $\beta > 2$: the number of function calls always increases for $\varepsilon < 0.03$ and $\varepsilon > 0.05$, regardless of the value of β . Therefore, a value of $\varepsilon = 0.04$ is recommended.

4. Experimental validation

A simple experiment (Fig. 10) was carried out to verify that the model presented in this work can predict the mesh resistance to opening of a real netting material. A 3×8 mesh polyethylene panel was hold between an upper fixed bar and a bottom free bar. The panel was stretched in the normal direction of the meshes by applying a growing force F^{panel} to the bottom bar and the resulting length of the panel L^{panel} was measured. The experimental data was analyzed with the method proposed in (Sala et al., 2007b) to estimate the mechanical and dimensional parameters of the netting sample. The method uses nonlinear least squares regression to fit a theoretical model for mesh resistance to opening to the experimental data. In this example, the model function used in the regression analysis was a computer implementation of the netting model described in Section 2, particularized for a 3×8 mesh panel to match the dimensions of the sample used in the experiment. Four parameters of the model were estimated: the twine bending stiffness EI , the twine length L_{twine} , the diameter D of the knot spheres and the angle φ_0 .

The nonlinear regression provides the following estimates and confidence intervals for the parameters: $EI = 74.9 \pm 8.7 \% \text{ N/mm}^2$, $L_{twine} = 41.5 \pm 2.6 \% \text{ mm}$, $D = 2.1 \pm 0.7\% \text{ mm}$ and $\varphi_0 = 22.7^\circ \pm 0.4\%$. Fig. 11 plots the length of the panel L^{panel} as a function of the applied force F^{panel} . The values of L^{panel} predicted by the fitted model are

superimposed to the experimental data. The quality of the fitting is quantified by coefficient of determination $R^2 = 0.997$. A visual inspection of the residuals in Fig. 11 and the narrow confidence intervals of the parameter estimates confirm that the fitting is excellent. Therefore, the netting model presented in this work can predict the mesh resistance to opening of netting materials with high accuracy.

Note that this experimental validation was done with a full model of the netting panel simulated with a computer implementation of the numerical model described in Section 2, including the use of spherical knots. A similar experiment was presented by the authors in (de la Prada and González, 2014a), but in that case we only used the measurements in a twine to validate Eqs. (1) and (2) and the knots were considered as rigid rectangles. Hence, the experimental validation presented here is far more complete.

5. Computational efficiency

In this section, the computational efficiency of the presented netting model is compared with a classical linear spring model that does not take into account mesh resistance to opening. The test problem is a 100×100 mesh panel hold by its two upper corners (Fig. 12). The properties of the netting are: $EI = 345 \text{ Nmm}^2$, $L_{\text{twine}} = 43.95 \text{ mm}$, $D = 2.05 \text{ mm}$ and $\varphi_0 = 15^\circ$. A vertical force of 10 N per knot is applied to the bottom edge of the panel to simulate the weight of a rope attached to it. The panel is exposed to a constant water current of 2 m/s normal to the panel, and hydrodynamic forces are calculated using the well-known method described in (Vincent, 1999).

The problem is modelled with two formulations. First, with the formulation described in Section 2. Second, with a simpler formulation that models knots as points and twines as

linear springs, ignoring the effect of mesh resistance to opening and the knot structure. This second formulation is very similar to the lumped mass netting models developed by other authors (Bessonneau and Marichal, 1998; Le Dret et al., 2004; Lee et al., 2005, 2008; Li et al., 2006; Takagi et al., 2004; Theret, 1993), but in this case we do not use nodes in the midpoints of twines in order to be able to share the numerical mesh grid between both models. For simplicity, each physical mesh is modelled with a numerical mesh in both models: the problem has 10^4 numerical meshes, 20604 nodes and 61812 variables.

The equilibrium position shown in Fig. 12 was calculated with the same optimization method used in Section 3 (de la Prada and González, 2014b), imposing a stopping tolerance of 10^{-3} to achieve a highly accurate solution. The results obtained with the two models are visibly different. Table 3 summarizes the computational performance of both models. The solution time and the number of force evaluations are high because the initial position was far from the equilibrium, a very fine mesh grid was used and a small tolerance was required. In practical applications, a coarse mesh grid would be used in the first iterations, thus reducing the total computing time in about two orders of magnitude. The key performance indicator is the time per force evaluation in a numerical mesh (the last row in Table 3), which includes the evaluation of all non-constant forces (twine elastic forces and hydrodynamic drag). The model presented in this work does not affect the number of iterations, but it is twice as slow as the classical linear spring model without mesh resistance to opening.

A clarification is necessary to interpret this result. The classical linear spring model used in this comparison does not have nodes in the midpoints of twines, as explained before. But such nodes are used in all lumped mass models for netting structures (Bessonneau and Marichal, 1998; Le Dret et al., 2004; Lee et al., 2005, 2008; Li et al.,

2006; Takagi et al., 2004; Theret, 1993) to describe the curvature of the twine. The midpoint nodes duplicate the number of linear springs in a numerical mesh (from 4 to 8), and therefore they increase the time per force evaluation in a mesh in a factor about two. This means that the computational efficiency of the model presented in this work is similar to previous lumped mass models that do not consider mesh resistance to opening. Note that the presented model does not need nodes in the midpoints of the twines to take into account twine bending, since it is already considered in the beam model described by Eqs. (1) and (2).

6. Discussion

The results of the numerical validation show that the presented model is robust and has a good accuracy compared to a detailed finite element model. The differences with the finite element model (relative errors below 5%) are not important due to the high uncertainty in the mechanical properties of netting materials for marine applications, which change during use (Sala et al., 2004). Moreover, the detailed finite element model used in Section 3 is an approximation of the real structure of the netting: real twines are likely to have a very complex behavior due to the structure its polymer fibers, and real knots are not completely rigid structures.

The results of the experimental validation are far better than the results presented in (Sala et al., 2007b), which used a similar experiment to quantify the mesh resistance to opening of netting panels. The asymptotic model developed in (O'Neill, 2002) was used in that work to analyze experimental data, and the authors reported a systematic lack of fit of their model to the experimental data and identifiability problems in the parameters of the model. On the contrary, our model provides an excellent goodness of fit and parameter estimates with narrow confidence intervals. This suggests that the model

presented in this work could be also used to quantify the mesh resistance to opening of netting panels in a more reliable way than in (Sala et al., 2007b).

The approximation of knots as spheres instead of rectangles seems to have little effect in the experimental validation presented in this work. However, knots in other kind of netting materials may have the shape of a rectangle with a large aspect ratio, and therefore the sphere approximation may provide worse agreement with experimental data in such materials. More research is required to get insight about this topic. If required, the presented netting model could be easily modified to consider knots as rectangular parallelepipeds.

A major objection to the netting model presented in this work is that it does not consider the twine flexion outside the plane of the netting. This is the usual practice in all the netting models for marine applications, since the curvature of marine netting structures is small and therefore the moment generated by the out-of-plane bending can be neglected. In our netting model, this simplification is present in the mesh model described in Section 2, which implicitly assumes that twines are contained in the plane defined by its ending knots and the transverse direction of the mesh. However, out-of-plane bending modifies the shape of the twines and hence it may modify the resistance to opening of the netting. This issue has not been investigated yet in the literature. Further experimental work is required to verify the accuracy of the presented netting model when out-of-plane bending is present. This matter is out of the scope of this article due to the complexity of the required experimental work.

7. Conclusions

A lumped mass model for netting structures with mesh resistance to opening is presented. It is designed to be used in applications that only require calculating the shape of the structures but not the stress fields in the material. This is the case of many marine applications of netting structures (e.g. fishing gears). The model combines a twine beam model for small axial deformations, a twine spring model for large axial deformations and a sphere model for netting knots. The model has significant advantages over previous methods to simulate the resistance to opening in netting materials. Numerical experiments confirmed that it is very robust. It also shows an excellent agreement with experimental data. Despite the higher non-linearity of this model, its computational performance is similar to other models that do not consider mesh resistance to opening because it avoids nodes in the midpoints of twines. The model can be easily implemented in existing computer codes that use other lumped mass models for netting structures.

The presented model will be very useful to improve the designs of certain marine netting structures. For example, the design of selective fishing gears is a very active research field that requires predicting the selectivity of the gear using behavioral models of fish and structural models of netting (O'Neill and Herrmann, 2007). Accurate simulation of mesh opening in the gear is essential for these methods, and the model presented in this work can achieve such accuracy when thicker and stiffer twines are used. Another application of the presented model is the experimental quantification of the mesh resistance to opening of netting materials, as an alternative to the method described in (Sala et al., 2007b): the model can be fitted to experimental data using non-

linear regression in order to obtain an accurate estimation of the mechanical and dimensional parameters that govern the resistance to opening.

Finally, further research is needed to verify that the model is still valid with out-of-plane bending is present in the netting material. Despite out-of-plane bending is neglected in netting models for marine applications due to the low curvature of the netting structures, it may affect the resistance to opening of the netting.

References

- ANSYS, 2007. . ANSYS, Inc.
- Bessonneau, J.S., Marichal, D., 1998. Study of the dynamics of submerged supple nets. (Applications to trawls). *Ocean Eng.* 25, 563–583.
- De la Prada, A., González, M., 2014a. Nonlinear stiffness models of a net twine to describe mesh resistance to opening of flexible net structures. *Proc. Inst. Mech. Eng. Part M J. Eng. Marit. Environ.* In press. doi:10.1177/1475090214530876, proof available at <http://lim.ii.udc.es/tmp/PIM530876.pdf>
- De la Prada, A., González, M., 2014b. Assessing the suitability of gradient-based energy minimization methods to calculate the equilibrium shape of netting structures. *Comput. Struct.* 135, 128–140. doi:10.1016/j.compstruc.2014.01.021
- DeCew, J., Tsukrov, I., Risso, A., Swift, M.R., Celikkol, B., 2010. Modeling of dynamic behavior of a single-point moored submersible fish cage under currents. *Aquac. Eng.* 43, 38–45.
- Herrmann, B., O'Neill, F.G., 2006. Theoretical study of the influence of twine thickness on haddock selectivity in diamond mesh cod-ends. *Fish. Res.* 80, 221–229.
- Herrmann, B., Wienbeck, H., Moderhak, W., Stepputtis, D., Krag, L.A., 2013. The influence of twine thickness, twine number and netting orientation on codend selectivity. *Fish. Res.* 145, 22–36.
- Khaled, R., Priour, D., Billard, J.-Y., 2012. Numerical optimization of trawl energy efficiency taking into account fish distribution. *Ocean Eng.* 54, 34–45.
- Le Dret, H., Lewandowski, R., Priour, D., Chagneau, F., 2004. Numerical simulation of a cod end net part 1: Equilibrium in a uniform flow. *J. Elast.* 76, 139–162.
- Lee, C.-W., Lee, J.-H., Cha, B.-J., Kim, H.-Y., Lee, J.-H., 2005. Physical modeling for underwater flexible systems dynamic simulation. *Ocean Eng.* 32, 331–347.
- Lee, J., Lee, C.-W., Choe, M.-Y., Lee, G.-H., 2011. Applying fishing-gear simulation software to better estimate fished space as fishing effort. *Fish. Aquat. Sci.* 14, 138–147.
- Lee, J.H., Karlsen, L., Lee, C.W., 2008. A method for improving the dynamic simulation efficiency of underwater flexible structures by implementing non-active points in modelling. *ICES J. Mar. Sci.* 65, 1552–1558.
- Li, Y.-C., Zhao, Y.-P., Gui, F.-K., Teng, B., 2006. Numerical simulation of the hydrodynamic behaviour of submerged plane nets in current. *Ocean Eng.* 33, 2352–2368.
- Lowry, N., Robertson, J.H.B., 1996. The effect of twine thickness on cod-end selectivity of trawls for haddock in the North Sea. *Fish. Res.* 26, 353–363.
- Nicoll, R.S., Steinke, D.M., Attia, J., Roy, A., Buckham, B.J., 2011. Simulation of a high-energy finfish aquaculture site using a finite element net model, in: *Proceedings of the International Conference on Offshore Mechanics and Arctic Engineering - OMAE*. pp. 35–44.
- O'Neill, F.G., 1999. Axisymmetric trawl cod-ends made from netting of a generalized mesh shape. *IMA J. Appl. Math. Inst. Math. Its Appl.* 62, 245–262.
- O'Neill, F.G., 2002. Bending of twines and fibres under tension. *J. Text. Inst.* 93, 1–8.
- O'Neill, F.G., 2004. The Influence of Bending Stiffness on the Deformation of Axisymmetric Networks, in: *ASME 2004 23rd International Conference on Offshore Mechanics and Arctic Engineering*. ASME, pp. 749–754. doi:10.1115/OMAE2004-51421
- O'Neill, F.G., Herrmann, B., 2007. PRESEMO - A predictive model of codend selectivity - A tool for fishery managers. *ICES J. Mar. Sci.* 64, 1558–1568. doi:10.1093/icesjms/fsm101
- Priour, D., 1999. Calculation of net shapes by the finite element method with triangular elements. *Commun. Numer. Methods Eng.* 15, 755–763.
- Priour, D., 2001. Introduction of mesh resistance to opening in a triangular element for calculation of nets by the finite element method. *Commun. Numer. Methods Eng.* 17, 229–237.
- Priour, D., 2003. Analysis of nets with hexagonal mesh using triangular elements. *Int. J. Numer. Methods Eng.* 56, 1721–1733.
- Priour, D., 2009. Numerical optimisation of trawls design to improve their energy efficiency. *Fish. Res.* 98, 40–50.
- Priour, D., 2013. *A finite element method for netting*. Springer, New York.
- Priour, D., Herrmann, B., O'Neill, F.G., 2009. Modelling axisymmetric cod-ends made of different mesh types. *Proc. Inst. Mech. Eng. Part M J. Eng. Marit. Environ.* 223, 137–144.
- Sala, A., Lucchetti, A., Buglioni, G., 2004. The change in physical properties of some nylon (PA) netting samples before and after use. *Fish. Res.* 69, 181–188.

- Sala, A., Lucchetti, A., Buglioni, G., 2007a. The influence of twine thickness on the size selectivity of polyamide codends in a Mediterranean bottom trawl. *Fish. Res.* 83, 192–203. doi:10.1016/j.fishres.2006.09.013
- Sala, A., O'Neill, F.G., Buglioni, G., Lucchetti, A., Palumbo, V., Fryer, R.J., 2007b. Experimental method for quantifying resistance to the opening of netting panels. *ICES J. Mar. Sci.* 64, 1573–1578.
- Shimizu, T., Takagi, T., Korte, H., Hiraishi, T., Yamamoto, K., 2007. Application of NaLA, a fishing net configuration and loading analysis system, to bottom gill nets. *Fish. Sci.* 73, 489–499.
- Takagi, T., Shimizu, T., Suzuki, K., Hiraishi, T., Yamamoto, K., 2004. Validity and layout of “NaLA”: A net configuration and loading analysis system. *Fish. Res.* 66, 235–243.
- Theret, F., 1993. Etude de l'équilibre de surfaces réticulées placées dans le courant uniforme. Application aux chaluts. Université de Nantes.
- Tsukrov, I., Eroshkin, O., Fredriksson, D., Swift, M.R., Celikkol, B., 2003. Finite element modeling of net panels using a consistent net element. *Ocean Eng.* 30, 251–270.
- Vincent, B., 1999. A new generation of tools for trawls - Dynamic numerical simulation, in: Proceedings of the 4th DEMaT Workshop. Presented at the DEMaT, Rostock.
- Wan, R., Hu, F., Tokai, T., 2002. A static analysis of the tension and configuration of submerged plane nets. *Fish. Sci.* 68, 815–823. doi:10.1046/j.1444-2906.2002.00497.x
- Xu, T.-J., Dong, G.-H., Zhao, Y.-P., Li, Y.-C., Gui, F.-K., 2011. Analysis of hydrodynamic behaviors of gravity net cage in irregular waves. *Ocean Eng.* 38, 1545–1554.
- Zienkiewicz, O.C., 2000. *The finite element method*, 5th ed. ed. Butterworth-Heinemann, Oxford; Boston.

TABLES

Table 1. Coefficient values for the radial force of the twine beam model.

c_{ij}	Twine axial rigidity (EA)		
	500 N	1000 N	2000 N
c_{00}	-6.58×10^3	-8.58×10^3	-2.02×10^4
c_{10}	1.18×10^4	1.36×10^4	2.90×10^4
c_{01}	2.74×10^4	5.55×10^4	1.34×10^5
c_{20}	-4.92×10^3	-4.59×10^3	-7.42×10^3
c_{11}	-5.65×10^4	-1.12×10^5	-2.60×10^5
c_{02}	4.34×10^2	-5.95×10^2	-6.67×10^3
c_{21}	2.88×10^4	5.59×10^4	1.22×10^5
c_{12}	-1.63×10^1	1.59×10^3	1.23×10^4
c_{03}	-3.16×10^2	-7.04×10^2	-3.04×10^3

Table 2. Coefficient values for the tangential force of the twine beam model.

c_{ij}	Twine axial rigidity (EA)		
	500 N	1000 N	2000 N
c_{00}	-1.28×10^2	-1.12×10^2	-9.35×10^2
c_{10}	1.76×10^2	1.73×10^2	1.06×10^3
c_{01}	6.79×10^2	4.05×10^2	4.03×10^3
c_{11}	-7.31×10^2	-4.49×10^2	-4.35×10^3
c_{02}	-2.06×10^3	-2.04×10^3	-7.86×10^3
c_{12}	2.09×10^3	1.96×10^3	8.36×10^3
c_{03}	1.54×10^3	1.85×10^3	4.70×10^3
c_{13}	-1.53×10^3	-1.68×10^3	-5.06×10^3
c_{04}	-2.50×10^1	-1.05×10^2	6.55×10^1

Table 3. Computational performance of the presented model compared with a classical linear spring model without mesh resistance to opening.

	Presented model	Classical linear spring model
Numerical meshes	10000	10000
Total solution time (s)	305.3	162.4
Force evaluation calls	10933	10804
Time per call (ms)	27.9	15.0
Time per call per mesh (μ s)	2.79	1.50

FIGURE CAPTIONS

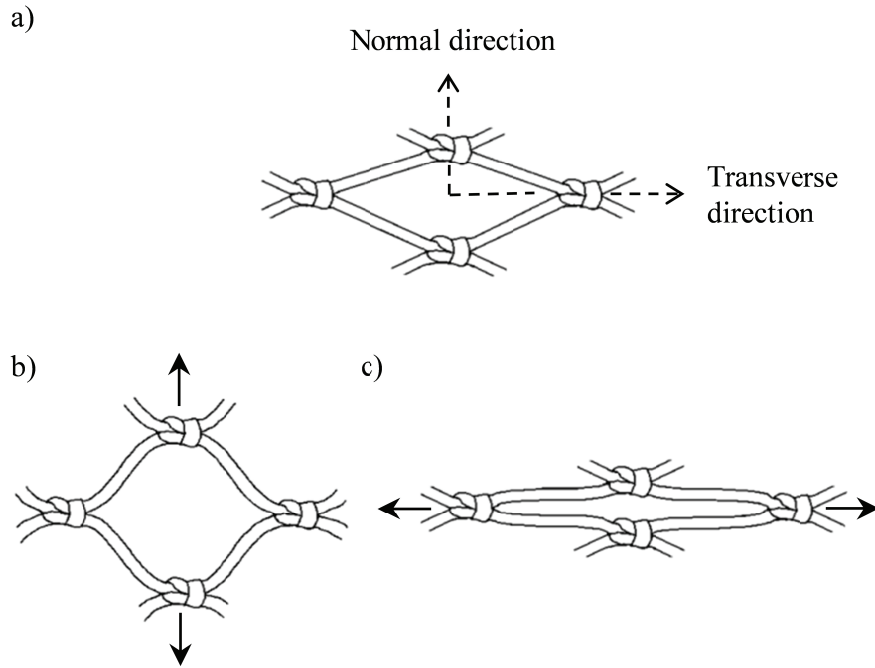


Fig. 1. Diamond-shaped mesh of netting. (a) unstretched, (b) stretched in the transverse direction, (c) stretched in the normal direction.

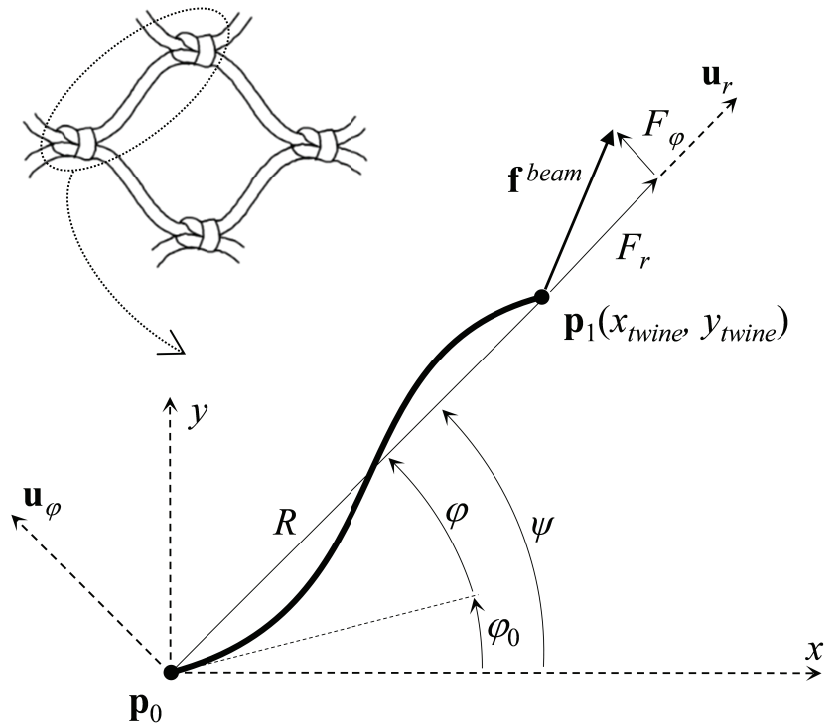


Fig. 2. Bidimensional double-clamped beam model of a mesh twine.

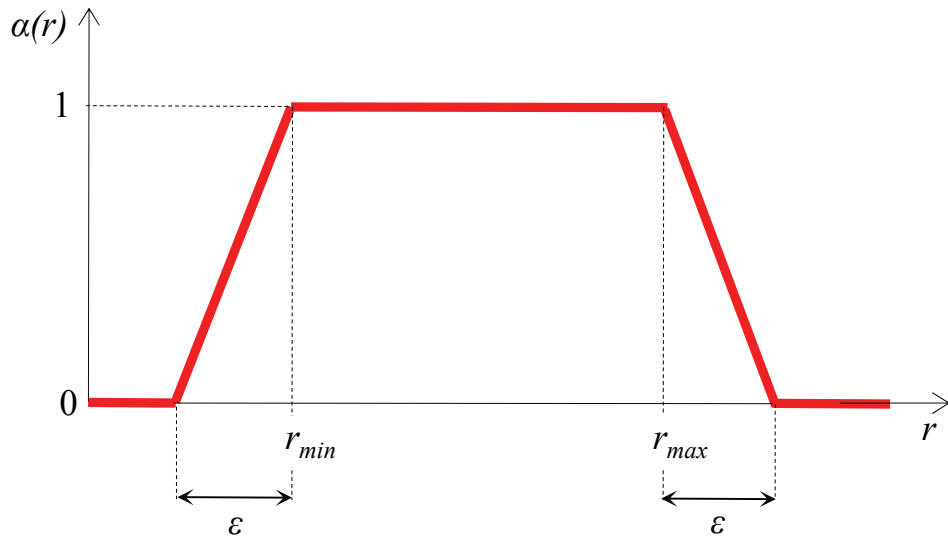


Fig. 3. Plot of the blending function $\alpha(r)$.

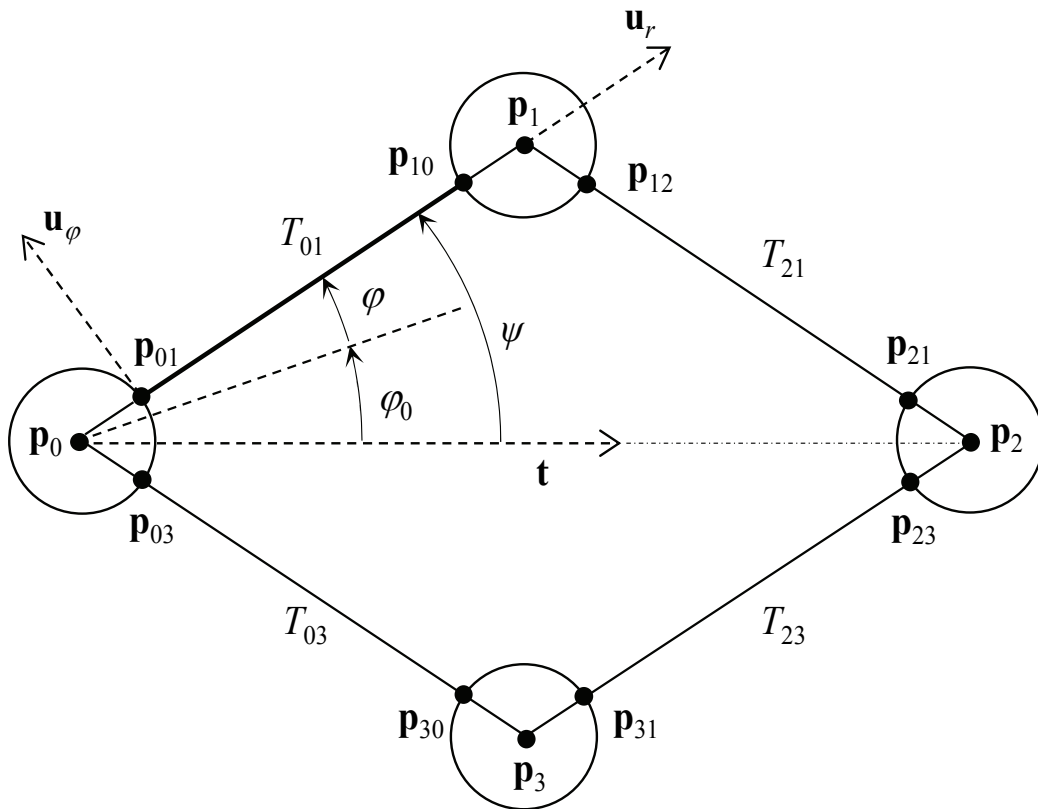


Fig. 4. Modelling of a numerical netting mesh.

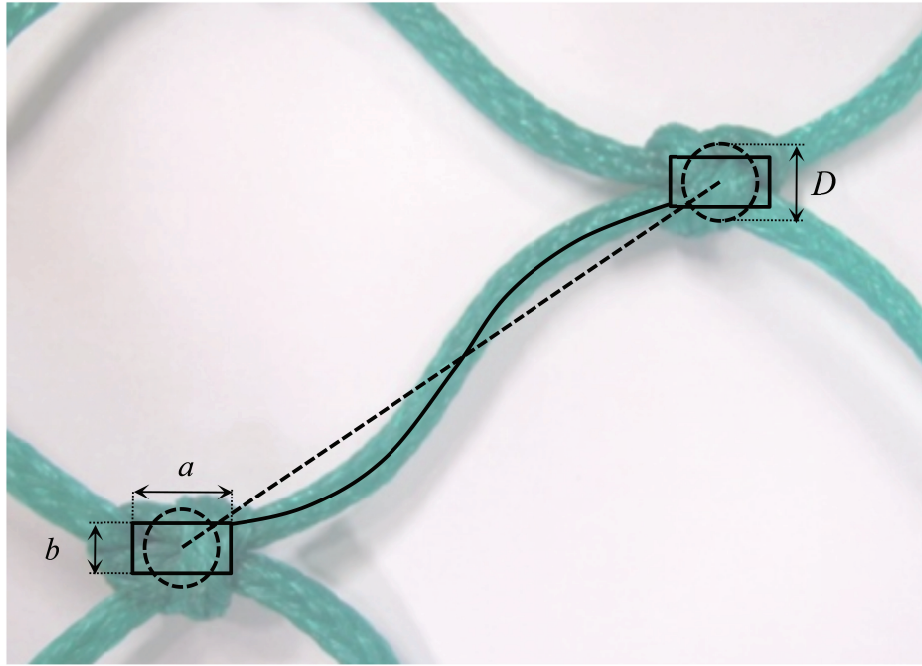


Fig. 5. Comparison between spherical and rectangular knot shapes.

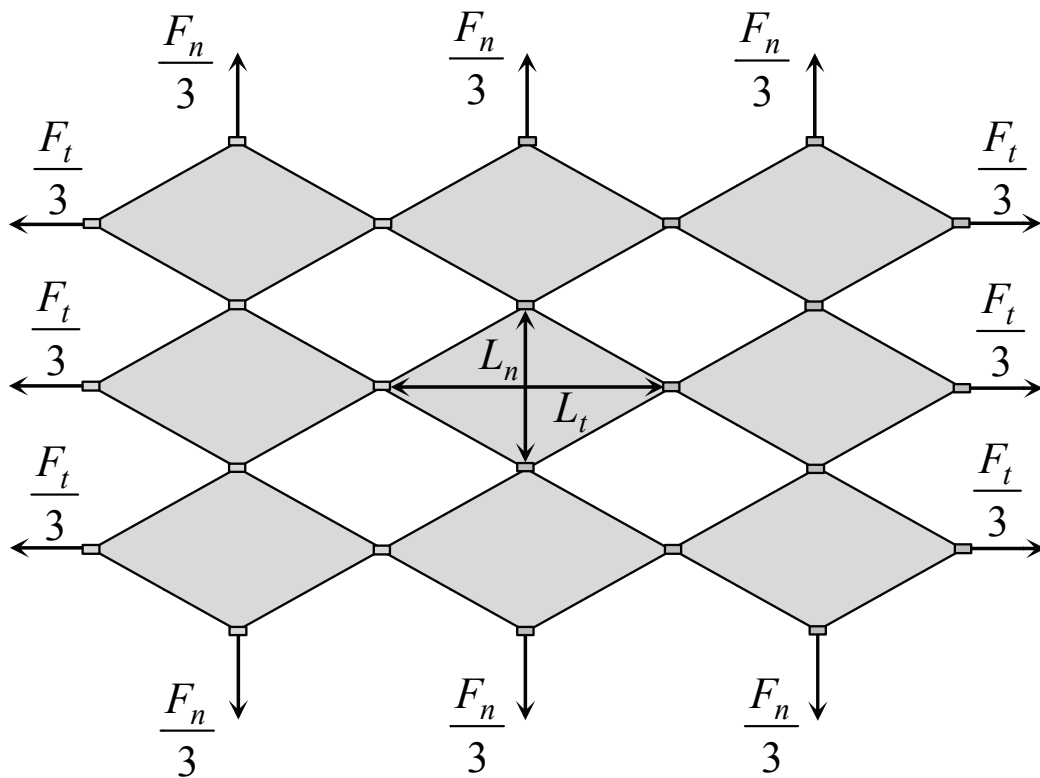


Fig. 6. Test problem used in the numerical experiments. The panel is stretched by transverse and normal loads (F_t and F_n) and the transverse and normal mesh openings (L_t and L_n) are measured.

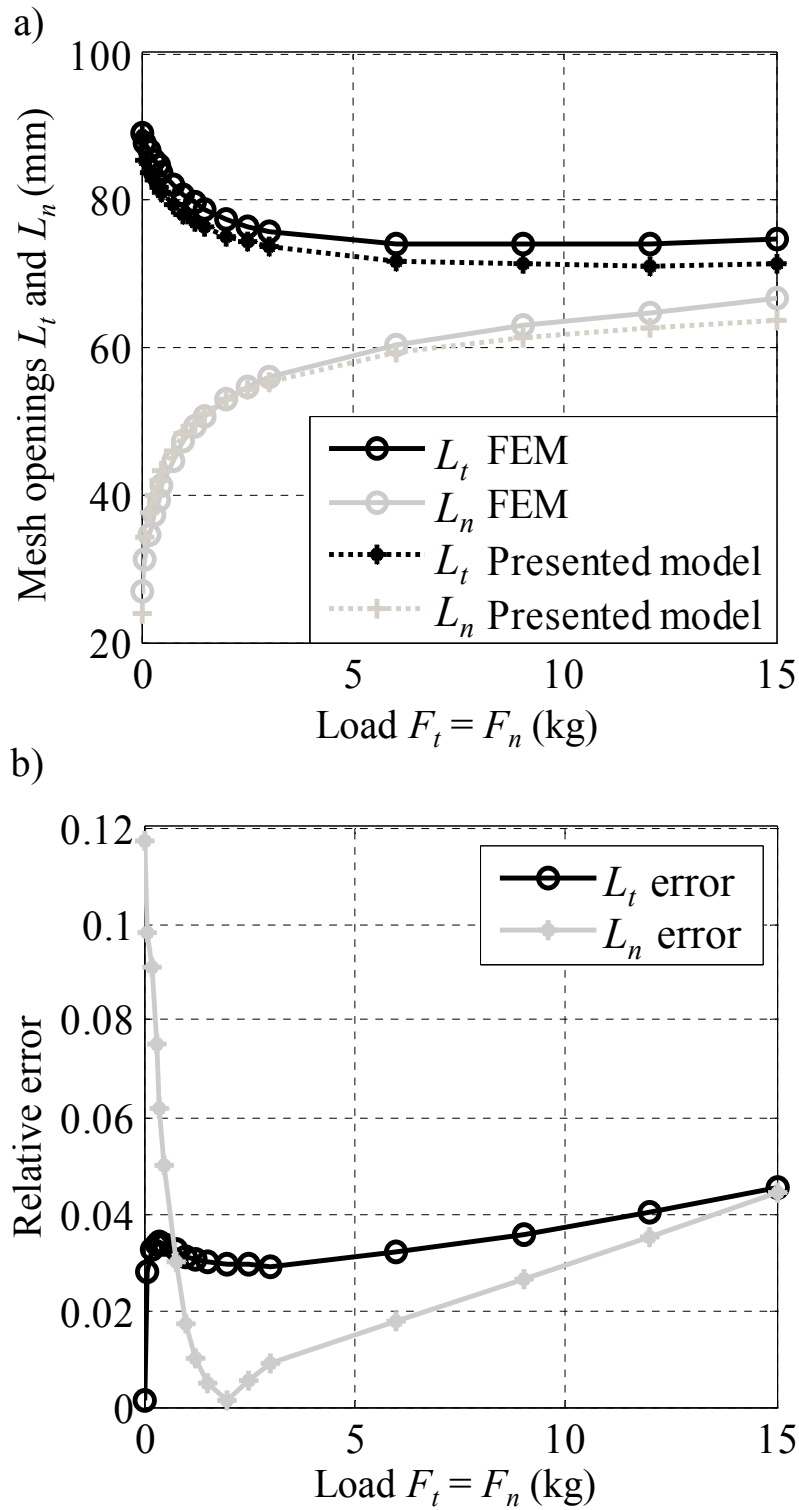


Fig. 7. Comparison of the lumped mass model with a detailed finite element model (FEM). (a) transverse (L_t) and normal (L_n) mesh opening as a function of the applied load $F_t = F_n$, (b) relative error of the lumped mass model.

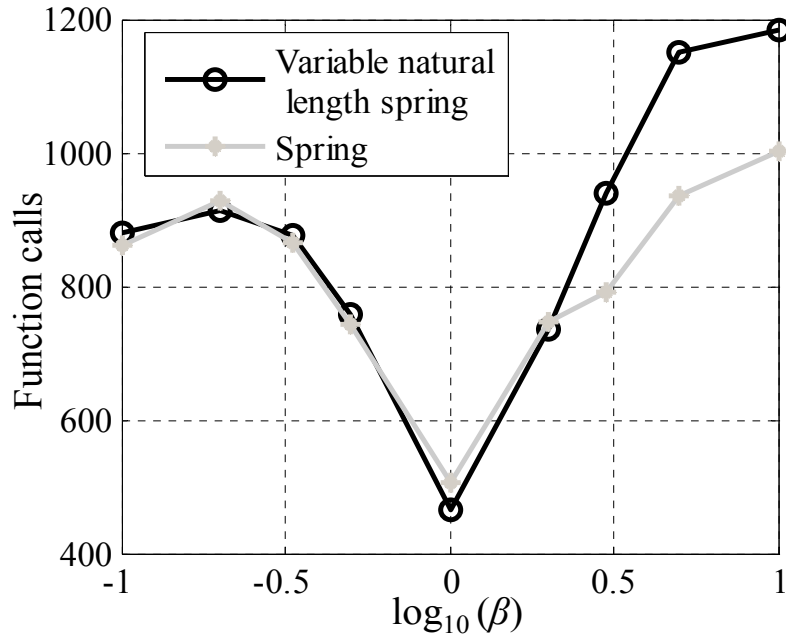


Fig. 8. Robustness to bad initial positions. Number of function calls required to reach the equilibrium as a function of the stretching factor β , for the linear spring model and the variable natural length spring model.

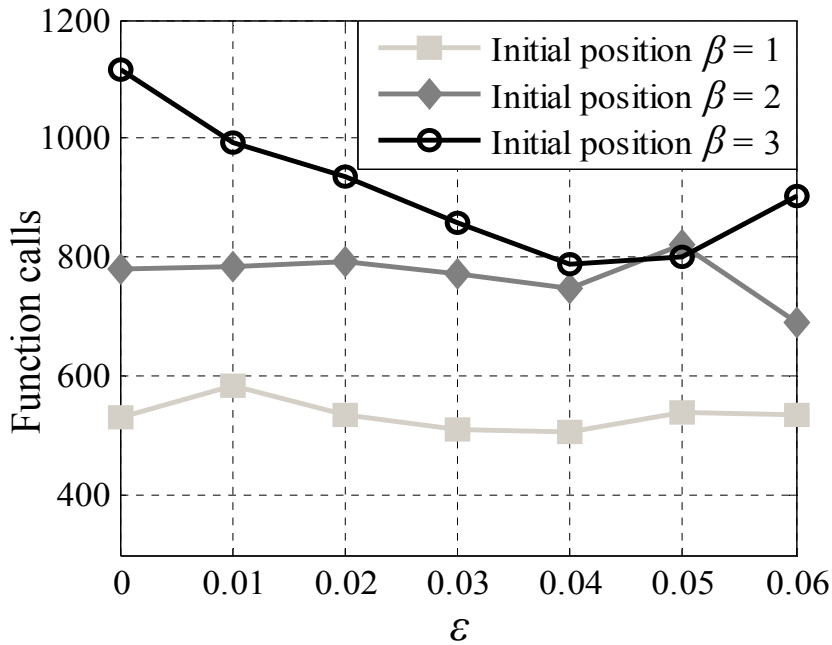


Fig. 9. Effect of the width of the transition region of the blending function. Number of function calls required to reach the equilibrium as a function of the width ϵ for different values of the stretching factor β in the initial position.

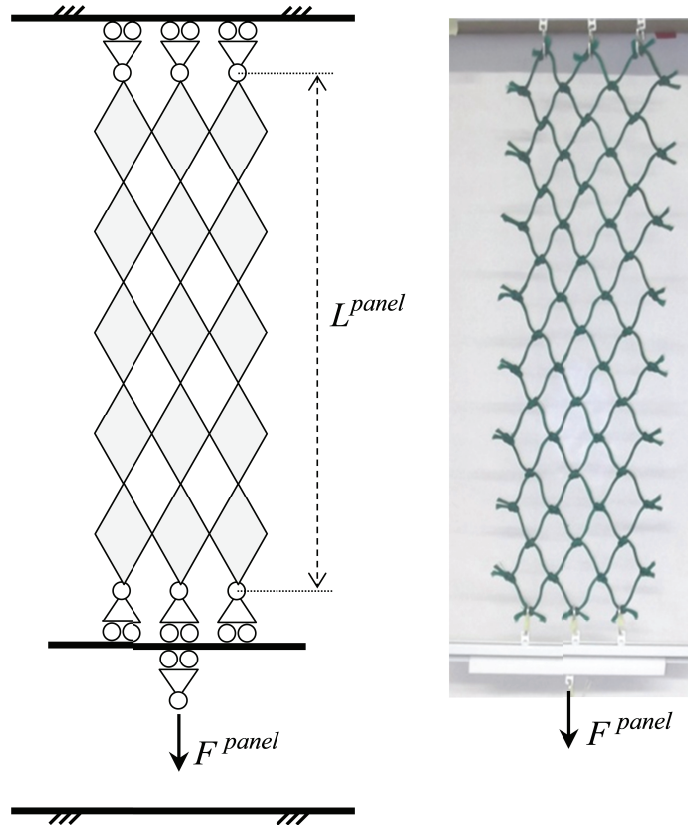


Fig. 10. Design of the experimental setup and general view of the netting panel during the test.

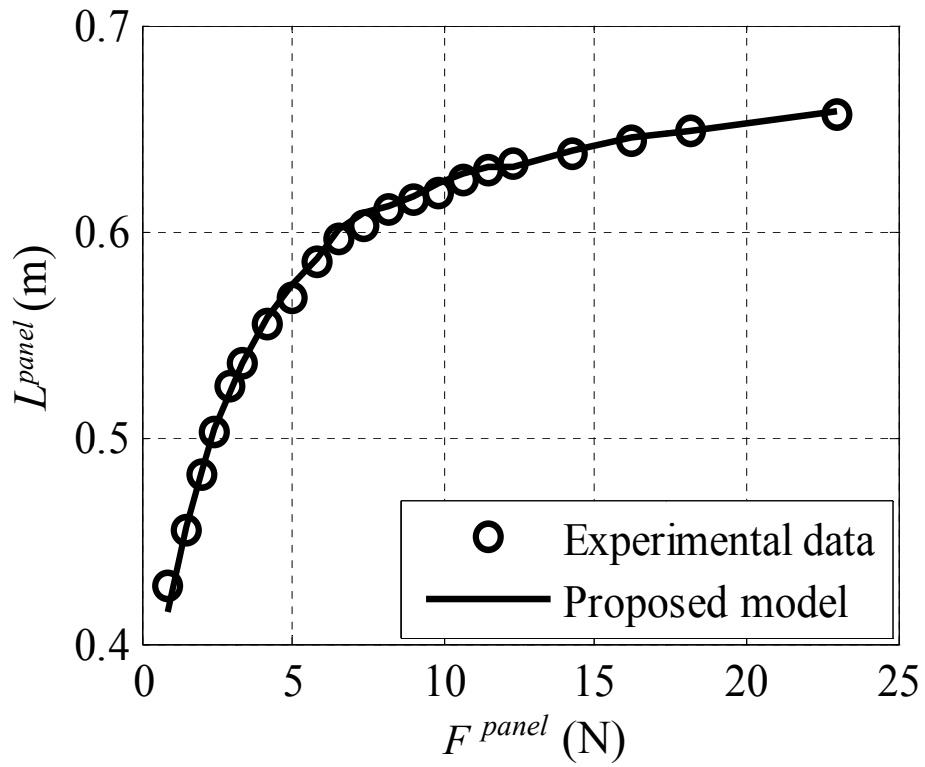


Fig. 11. Experimental data and result of the nonlinear regression.

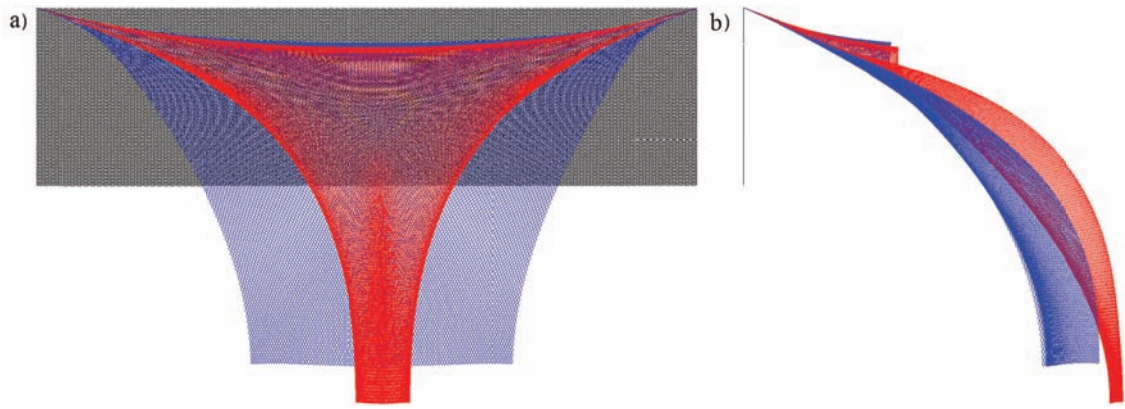


Fig. 12. Test problem to evaluate the computational performance of the presented model. (a) front view, (b) right view. It shows the initial position (grey) and equilibrium position obtained with the presented model (blue) and with a classical linear spring model without mesh resistance to opening (red).

